DIRECTED EVOLUTION OF PHOSPHOTRIESTERASE FOR STEREOSELECTIVE DETOXIFICATION OF ORGANOPHOSPHATE NERVE AGENTS

A Dissertation

by

PING-CHUAN TSAI

Submitted to the Office of Graduate Studies of
Texas A&M University
in partial fulfillment of the requirements for the degree of

DOCTOR OF PHILOSOPHY

December 2009

Major Subject: Chemistry

DIRECTED EVOLUTION OF PHOSPHOTRIESTERASE FOR STEREOSELECTIVE DETOXIFICATION OF ORGANOPHOSPHATE NERVE AGENTS

A Dissertation

by

PING-CHUAN TSAI

Submitted to the Office of Graduate Studies of
Texas A&M University
in partial fulfillment of the requirements for the degree of

DOCTOR OF PHILOSOPHY

Approved by:

Chair of Committee,	Frank M. Raushel
Committee Members,	Paul A. Lindahl
	Marcetta Y. Darensbourg
	Gregory D. Reinhart
Head of Department,	David H. Russell

December 2009

Major Subject: Chemistry

ABSTRACT

Directed Evolution of Phosphotriesterase for Stereoselective Detoxification of Organophosphate Nerve Agents.

(December 2009)

Ping-Chuan Tsai, B.S., National Tsing-Hua University

Chair of Advisory Committee: Dr. Frank M. Raushel

The bacterial phosphotriesterase (PTE) from *Pseudomonas diminuta* possess very broad substrate specificity for organophosphorus compounds. It is capable of hydrolyzing several insecticides including paraoxon and various chemical warfare agents such as sarin (GB), soman (GD), cyclosarin (GF) and VX. The catalytic ability of PTE for the hydrolysis of paraoxon is close to the limit of diffusion of the reactant in solution. However, the catalytic activity of PTE for the organophosphate nerve agents is lower than that for paraoxon. It was reported that the wild-type PTE preferentially catalyze the hydrolysis of the less toxic R_p- enantiomers of organophosphate nerve agents and their analogues than the more toxic S_p- enantiomers. The first generation of PTE mutants that contains a modified substrate binding pocket was identified and it was observed that their catalytic activity towards the more toxic S_p- enantiomers organophosphate nerve agent analogues was enhanced. The H254G/H257W/L303T mutant was shown to have a reversed stereoselectivity. The k_{cat}/K_m values of this mutant towards the hydrolysis of the S_pR_c- and S_pS_c-enantiomers of the GD analogue and the S_p-enantiomer of the GF

analogue were enhanced by 73-, 543-, and 1340-fold relatively to the wile-type enzyme, respectively.

The second generation of PTE mutants were isolated and shown to have higher activity toward the S_p-enantiomers of the GD and GF analogues than the first generation mutants. Saturation mutagenesis, *in vitro* screening and *in vivo* selection were conducted using the gene for the mutants from the first generation. The GWT-d3 mutant was identified as the most active PTE mutant towards the hydrolysis of the S_p-enantiomers of the GD analogue, the k_{cat}/K_m values were 780- and 3530-fold higher than the wild-type enzyme toward the S_pR_c- and S_pS_c-enantiomers of the GD analogues. The GWT-f5 mutant was the best PTE mutant towards the S_p-enantiomer of the GF analogue, the k_{cat}/K_m values were 15500-fold higher than the wild-type enzyme.

The X-ray crystal structures of the wild-type PTE and the G60A mutant were determined in the presence of the hydrolysis product diethyl phosphate and a product analogue cacodylate, respectively. This result supports the reaction mechanism previously proposed by Dr. Sarah Aubert.

DEDICATION

For my parents, Chiao and Hsiu-Chin, and my husband, Kai Yang

ACKNOWLEDGEMENTS

I would like to express my sincere appreciation to my committee chair, Dr. Frank Raushel for his guidance and advice throughout my graduate career. I also would like to thank my committee members, Dr. Paul Lindahl, Dr. Marcetta Darensbourg, and Dr. Gregory Reinhart. I would like to extend my appreciation Dr. David Barondeau and his student, Nicolas Fox, for their endeavor in the crystallography of the second generation of PTE mutants. I would also like to thank my mentor, Dr. Eman Ghanem, for her selfless instruction in the beginning my graduate research.

Thanks to my family for sharing my happiness and difficulties in my life. Thanks to my husband, Kai Yang, for his patience and support in my graduate career and my life. I would like to extend my gratitude to my friends for their encouragement.

TABLE OF CONTENTS

LIST OF FIGURES

FIGURE Page

FIGURE Page

FIGURE Page

LIST OF TABLES

CHAPTER I

INTRODUCTION

Bacterial phosphotriesterase (PTE) belongs to the amidohydrolase superfamily. The enzymes in this superfamily adopt a $(\beta/\alpha)_8$ barrel fold structure with conserved active site residues and one or two divalent cations (*1*). PTE was found in two different soil bacteria, *Pseudomonas diminuta* MG and a strain of *Flavobacterium* sp. (*2*). This enzyme is of significant interest because of its ability to catalyze the detoxification of organophosphate insecticides and chemical warfare agents. PTE detoxifies paraoxon, a known pesticide, at rates close to the diffusion limit of enzymatic reactions. The k_{cat} and k_{cat}/K_m values are $\sim 10^4$ s^{-1} and 10^8 M^{-1} s^{-1}, respectively (*3*). In addition, PTE is the only known enzyme to hydrolyze the most toxic nerve agent, VX (*4*).

It has been shown that the organophosphate nerve agents, such as sarin, soman and VX, are more toxic as the S_p- stereoisomers than the R_p- stereoisomers (*5*). However, the catalytic activity of the wild-type PTE for the more toxic S_p- stereoisomers is not as efficient as the R_p- stereoisomers. Rational design and directed enzyme evolution have been utilized to optimize the activity, stability, or substrate specificity of the enzyme by manipulating the protein structure of this enzyme (*6*). Herein, PTE was subjected to rational design and directed evolution to optimize the active site structure for detoxification of organophosphate nerve agents.

This dissertation follows the style of *Biochemistry*.

Directed Enzyme Evolution

Directed evolution is a valuable tool used in protein engineering to control the power of natural selection in order to evolve proteins with desired properties not found in nature, such as enzymes with improved specificity, activity, stability, etc. Rational design and directed evolution are two approaches currently being used. Rational design involves changing the amino acid sequence using site-directed mutagenesis. This technique requires a good understanding of protein structure, function and reaction mechanism. Directed evolution does not require complete knowledge of the protein structure. As shown in **Figure 1.1**, directed evolution starts from one or multiple genes, and creates a library of mutant genes by random mutagenesis or gene recombination. The resulting library is cloned into an expression vector and transformed into microorganisms for protein expression. The functionally improved enzymes are then selected and identified through a carefully designed selection process or high-throughput screening methods.

There are several strategies that have been used to create randomized libraries of the targeted gene: saturation mutagenesis, error-prone PCR, DNA shuffling and *E. coli* mutator strains. Saturation mutagenesis changes specific amino acids that are selected by mapping the structure of the enzyme active site. This can be accomplished by several methods: cassette insertion (*7*), mutagenic oligonucleotide PCR amplification (*8*), or splicing overlap extension (SOE) of DNA fragments (*9*).

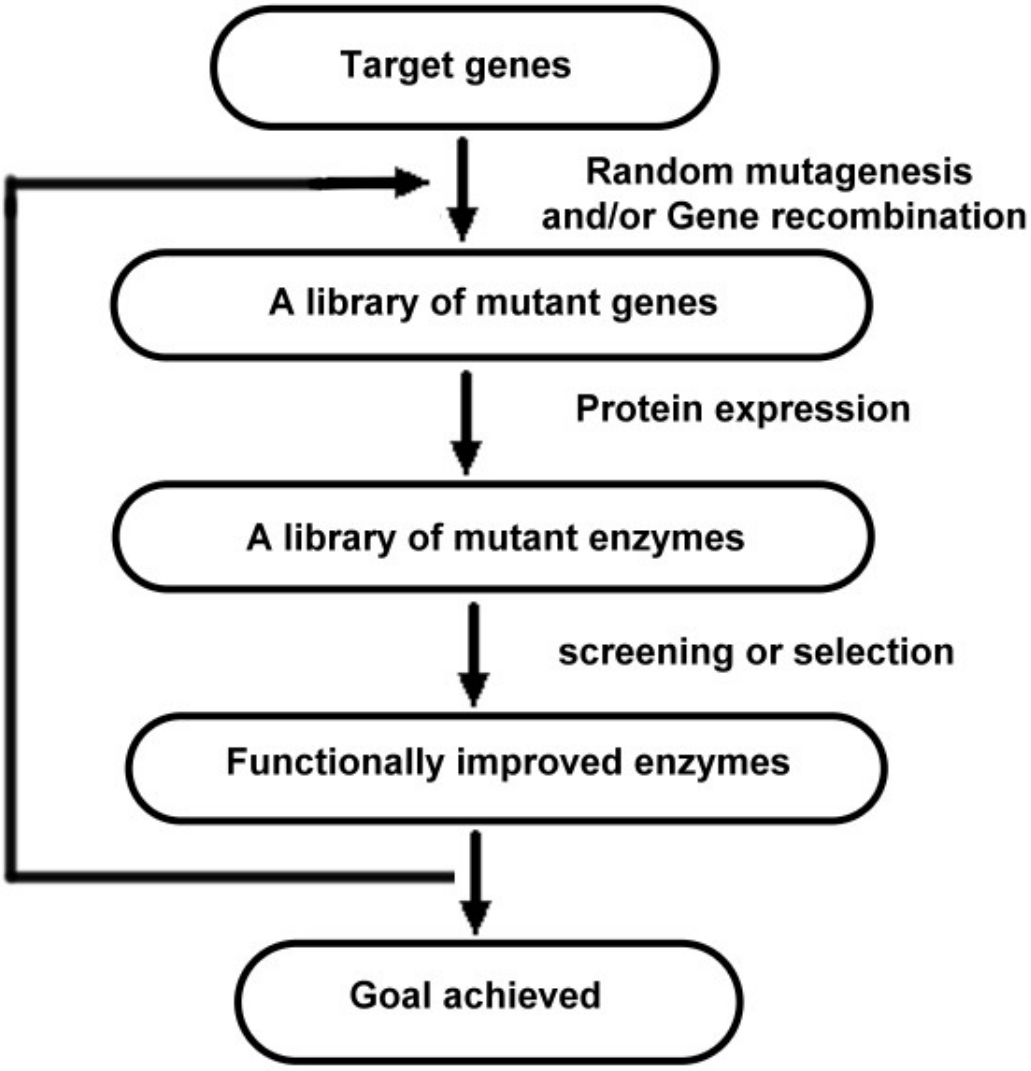

Figure 1.1 General scheme of directed evolution (*6*).

The cassette insertion method involves designing a pair of DNA oligonucleotide segments with degenerate codons at the target position. These DNA segments are then ligated into the targeted gene. The mutagenic oligonucleotide PCR amplification utilizes primer pairs with degenerate codons at the target position. QuickChange site-directed mutagenesis is performed using *Pfu* Turbo DNA polymerase. The parental methylated DNA strands are then digested by *DpnI*. No ligation step is necessary, since the nicks in the replicated DNA are repaired after transformation into *E. coli* cells. The method of splicing overlap extension (SOE) of DNA fragments requires execution of a separate PCR by amplifying multiple DNA fragments that overlap at the randomized codons in the target sequences. Each primer pair is synthesized with a mismatched random nucleotide sequence in the middle, flanked on both sides by nucleotides that specifically anneal to the target regions. These oligonucleotide fragments are then annealed by primerless PCR, the original full-length gene with randomized variants is formed. The regular PCR using upstream and downstream primers is then done to amplify this randomized library. The primers for mutagenic oligonucleotide PCR amplification, splicing overlap extension (SOE) of DNA fragments and the DNA segments for cassette insertion contain the degenerate codon NNN or NNS (NNC and NNG) at designated positions. The NNS codon is to eliminate two stop codons, TGA and TAA.

Error-prone PCR utilizes error-prone DNA polymerase in the reaction; *Taq* polymerase is the commonly used enzyme due to its higher error rate. The reaction conditions need to contain higher concentrations of $MgCl_2$ than the normal PCR reaction. $MnCl_2$ can also be added to stabilize non-complementary pairs and decrease

the fidelity of *Taq* polymerase (*10*). Mutation frequencies can be adjusted by varying the concentration of $MnCl_2$ and the template gene, or adjusting the number of PCR cycles (*11*).

DNA shuffling is a method for *in vitro* homologous recombination of pools of selected mutant genes. The selected genes are randomly fragmented by DNase I, and fragments of the desired size are purified from an agarose gel. These oligonucleotide fragments are reassembled into full length sequences by primerless PCR using cycles of denaturation, annealing, and extension by a DNA polymerase (**Figure 1.2**). Following this reassembly reaction, the full length gene is amplified by PCR with upstream and downstream primers (*12*). In addition, the recombination of a set of naturally occurring homologous genes is called "family shuffling", which is also a very powerful approach for *in vitro* protein evolution. The recombination of genes exploits the same parental gene or similar parental genes with higher than 80% identity. However, Joern and coworkers have successfully recombined parental genes with only 63% DNA sequence identity. Through these experiments they were able to create a much more diverse library (*13*).

E. coli mutator strains employ the mutator plasmids which encode genes with genetic deficiencies in DNA proofreading and editing machinery. The most commonly occurring deficiencies involve mutations in the *mutD*, *mutS*, and *mutT* genes. Specifically, *mutD* mutations can hinder the 3'-5' exonuclease activity of DNA polymerase III. Therefore the repair of incorrect bases is prevented (*14*). This method can generate large and diverse plasmid libraries, and high-frequency mutagenesis

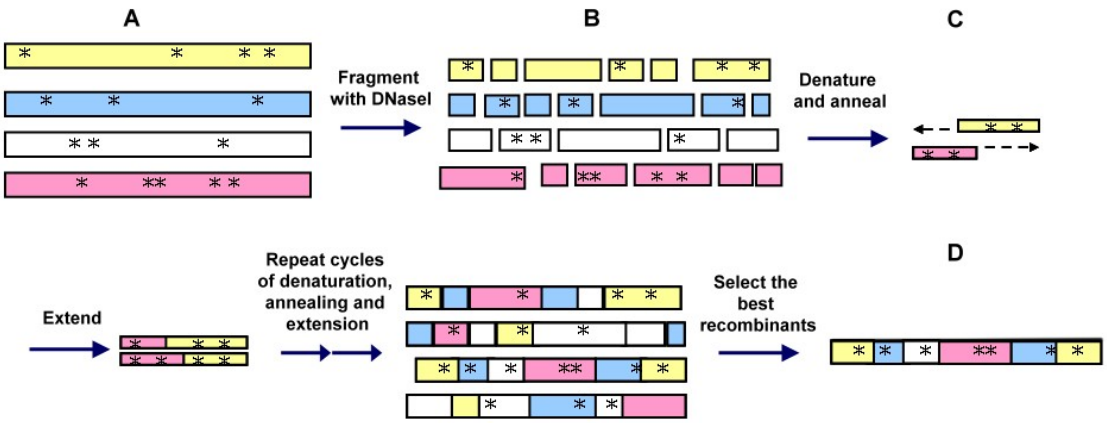

Figure 1.2 Scheme of DNA shuffling method. (*12*) (A) A pool of homologous gene with different mutations is fragmented by DNase I. (B) Certain sizes of gene fragments are collected. (C) Reassembly of random fragments into full-length gene results in frequent template switching and recombination. (D) A recombinant gene can be selected from the library based on the improved function. The selected recombinants can provide the starting point for another round of mutation and recombination.

may be required for faster evolutionary improvement. However, the mutation rate can be difficult to control. Thus, PCR-directed random mutagenesis must be continuously tested to monitor the relative number of mutations being introduced (*15*).

The mutant libraries are created and cloned into an expression vector and transformed into microorganisms for protein expression. Functionally improved mutant proteins can be identified through carefully designed screening or selection methods. Some examples of the strategies for library screening or selection include: low throughput microtiter-well assays, high throughput screening methods and genetic selections. The low throughput microtiter-well assays are suitable for the screening of a few thousand clones. This method normally relies on a quantitative chromogenic assay and in-well chemical lysis of cell cultures to release overexpressed protein into solution. The quantitative chromogenic assay can be directly assayed by following the formation of chromophoric products or indirectly assayed with coupling systems that release a chromophore that absorbs light in the visible range. Take the example of the colorimetric dehydrogenase screen based on NAD(P)H generation. The second enzyme in the pentose phosphate pathway, 6-phosphogluconate dehydrogenase (6PGDH) catalyzes the NADP-dependent transformation of 6-phosphogluconate to ribulose-5-phosphate, producing NADPH and CO_2 in the process. The activity of 6PGDH (or other dehydrogenases) is commonly measured by following the production of NADPH at 340 nm, an unsuitable approach for the screening in cell lysates. Because cell lysates have a moderate absorbance at 340 nm, the background absorbance of 96-well plates tends to be high in the UV-range, and reproducibility of measurements is low. The colorimetric

alternative uses nitroblue tetrazolium (NBT), in the presence of phenazine methosulfate (PMS), it reacts with the NAD(P)H produced by dehydrogenases to produce an insoluble blue-purple formazan that is detectable at 580 nm (*16*) (**Scheme 1.1**).

Scheme 1.1 Colorimetric assay for 6PGDH activity.

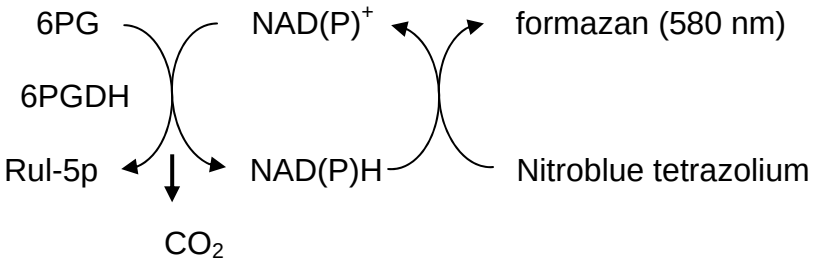

High-throughput screening methods have been widely used and developed. The phage display method is a commonly used technique for the study of protein-protein, protein-peptide, protein-DNA, and protein-small molecule interactions. It utilizes bacteriophages to connect proteins with the genetic information that encodes them. The connection between genotype and phenotype enables large libraries of proteins to be screened and amplified (*17*). Individual phages are selected through interaction of the displayed protein with ligands, and the specific phage is amplified by infection of bacteria (**Figure 1.3 (A)**). Similar biological display approaches such as bacterial display, and yeast display have many advantages over the others. However, the library size for these *in vivo* display systems is limited by the transformation efficiency of each organism. For example, the library size for phage and bacterial display is limited to ~ 10^9 different members. The library size for yeast display is even smaller. In contrast, mRNA display is an *in vitro* display system, allowing a library size as large as 10^{15} different members. The large library size improves the diversity of the sequences and

increases the probability to select very rare sequences. In addition, *in vitro* display methods remove unwanted selection pressure such as poor protein expression and rapid protein degradation, which may reduce the diversity of the selected variants (*18*). The mRNA display technique uses translated peptides or proteins associated with their mRNA progenitor via a puromycin linkage, and the mRNA- protein fusion is bound to an immobilized target in a selection step. The mRNA-protein fusions that bind well to the target are then reverse transcribed to cDNA and their sequence amplified via a PCR. The nucleotide sequence with high affinity for the target molecule is then identified (**Figure 1.3 (B)**).

The display techniques described in the previous paragraph are generally used for screening ligands with high affinity for the proteins. One of the methods that efficiently isolates enzymatic activity from very large repertoires of protein variants, displays enzyme variants on filamentous phage. The reaction substrates and products are anchored on the calmodulin-tagged phage enzymes by a calmodulin binding peptide. Phages displaying catalytically active proteins are physically isolated by means of affinity reagents specific for the products of reactions (**Figure 1.4**) (*19*).

A couple of methodologies have been developed as *in vivo* selections, such as the protein fusion with chloramphenicol acetyltransferase (CAT) and the metabolic engineering of microorganisms. The low solubility of a protein is one of the most frequent impediments for structural and functional analysis. An approach to overcome this problem is to fuse target protein variants to a reporter protein whose activity will depend on the solubility and stability of the protein of choice. The fusion of

chloramphenicol acetyltransferase (CAT) and the target protein variants is able to select the soluble mutants by visualizing the growth of the colonies on the agarose plate with chloramphenicol as the antibiotic. This phenomenon depends on a correlation between the solubility of the protein and the ability of *E. coli* to grow on chloramphenicol (*20*). The other strategy for *in vivo* selection involves metabolic engineering of microorganisms. This technique normally depletes the sole carbon or phosphorus source required for cell growth and develops new carbon or phosphorus assimilation pathways. Sugiyama and coworkers developed the endogenous *E. coli* L-rhamnose pathway that was supplemented with L-rhamnose as a carbon source. L-rhamnose, is actively incorporated into *E. coli*, which is first isomerized to the corresponding ketose, L-rhamnulose, by L-rhamonose isomerase (RhaA). Next, the phosphorylation of -rhamnulose by rhamnulose kinase (RhaB) produces L-rhamnulose-1-phosphate, the natural substrate of RhaD. RhaD cleaves rhamnulose-1-P by a retroaldol reaction into two three-carbon carbohydrates, dihydroxyacetone phosphate (DHAP) and L-lactaldehyde, which are then metabolized through glycolysis or the TCA cycle. Since the wild-type RhaD cannot cleave L-rhamnulose, the disruption of the rhamnulose kinase gene (*rhaB*-) leads to an inability to grow on minimal media supplemented with L-rhamnose as a carbon source. The newly evolved RhaD variants selected from the *in vivo* selection are capable of accepting unphosphorylated L-rhamnulose, which gives them the ability to survive on the carbon free minimum medium (**Figure 1.5 (A)**). The *E. coli* strains lacking all of the *rhaBAD* genes were co-expressed with the RhaA gene

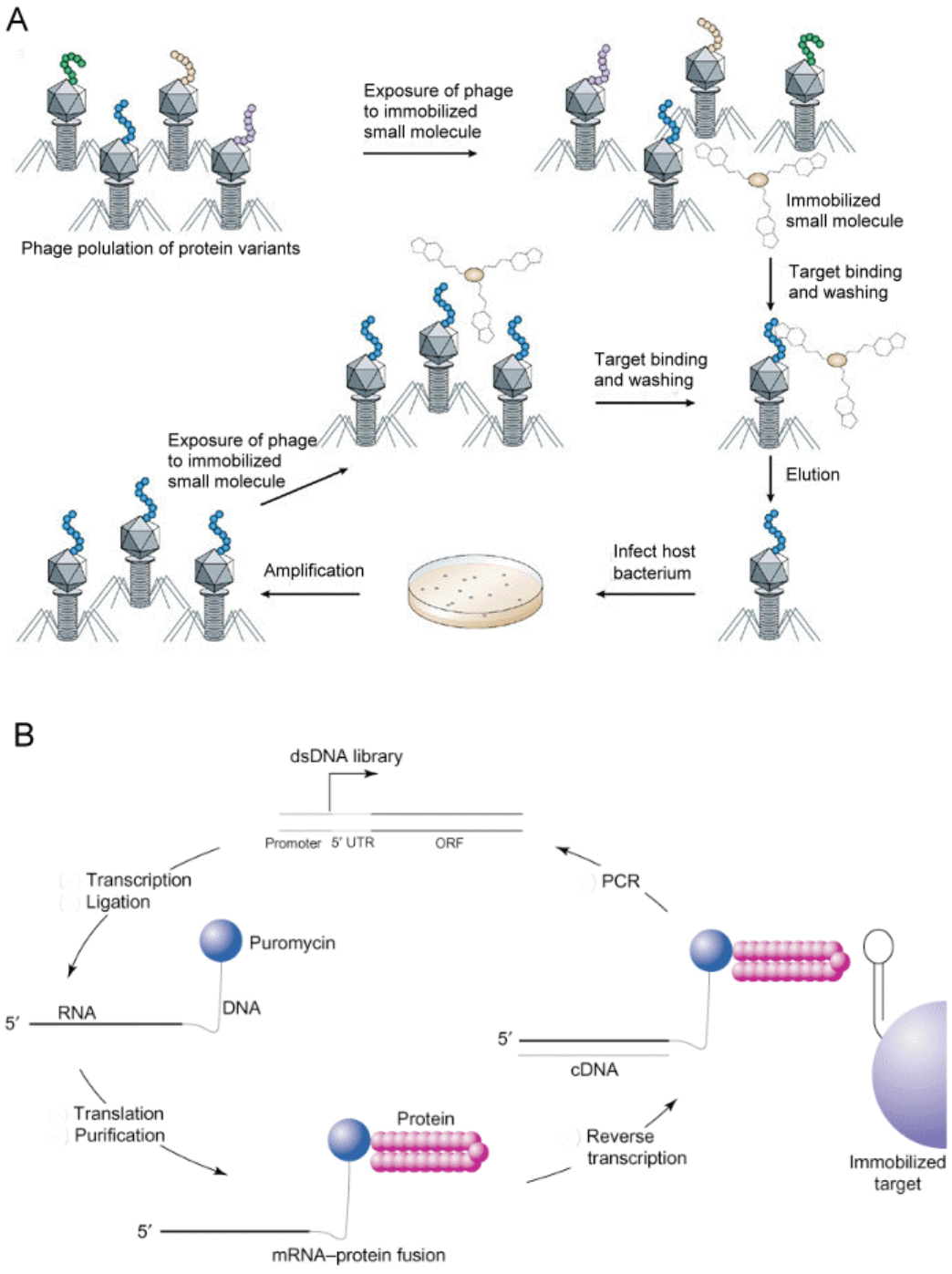

Figure 1.3 (A) Scheme of cycle of phage display method (*17*). (B) Scheme of cycle of mRNA display method (*18, 21*).

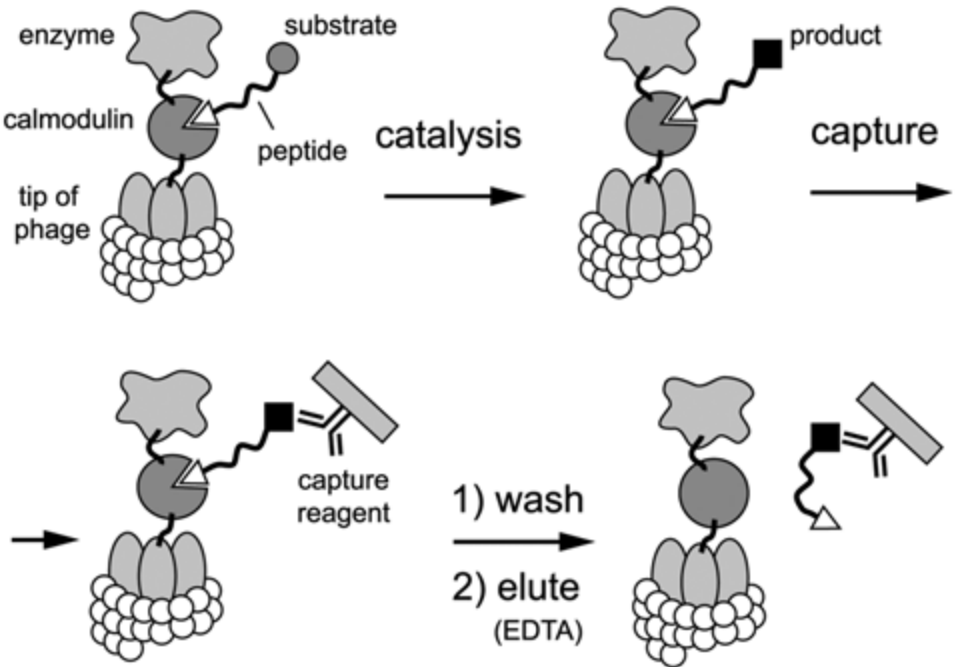

Figure 1.4 Calmodulin-tagged phage enzyme for the isolation of enzymatic activity. (*19*)

and the library of RhaD gene on a plasmid (**Figure 1.5 (B)**), the selected RhaD mutant was able to utilize $_{L}$-rhamnulose as a sole carbon source (*22*).

The Structural and Catalytic Relations within the Amidohydrolase Superfamily

Enzymes in the amidohydrolase superfamily (AHS) catalyze hydrolytic, decarboxylation, isomerization and hydration reactions within carbohydrate, nucleic acid and amino acid based substrates (*1*). Most of the structurally characterized enzymes of the AHS contain either a binuclear or mononuclear metal center embedded at the C-terminal end of a $(\beta/\alpha)_8$ barrel structural domain. The first three enzymes identified in the AHS were urease (URE), phosphotriesterase (PTE), and adenosine deaminase (ADA). Holm and Sander discovered the three-dimensional structural similarities within the active site and global protein folds in 1997. Currently, there are approximately 40 members of AHS that have been structurally characterized by X-ray crystallography. The metal centers of these enzymes are naturally populated by zinc, iron or nickel. Some members of the AHS are also active with manganese, cobalt, or cadmium (*23, 24*). There are eight structurally characterized variations of the divalent metal centers within the AHS. The most common metal center is the binuclear metal center found in phosphotriesterase (PTE), dihydroorotase (DHO), iso-apspartyl dipeptidase (IAD), urease (URE), and the three types of hydantoinases (HYD). The two divalent cations are approximately 3.6 Å apart and are ligated to the protein through electrostatic interactions with the side chains of six amino acids. The more buried metal ion, M_{α} , is coordinated to two histidine residues from strand 1 of the β– barrel and an aspartate from

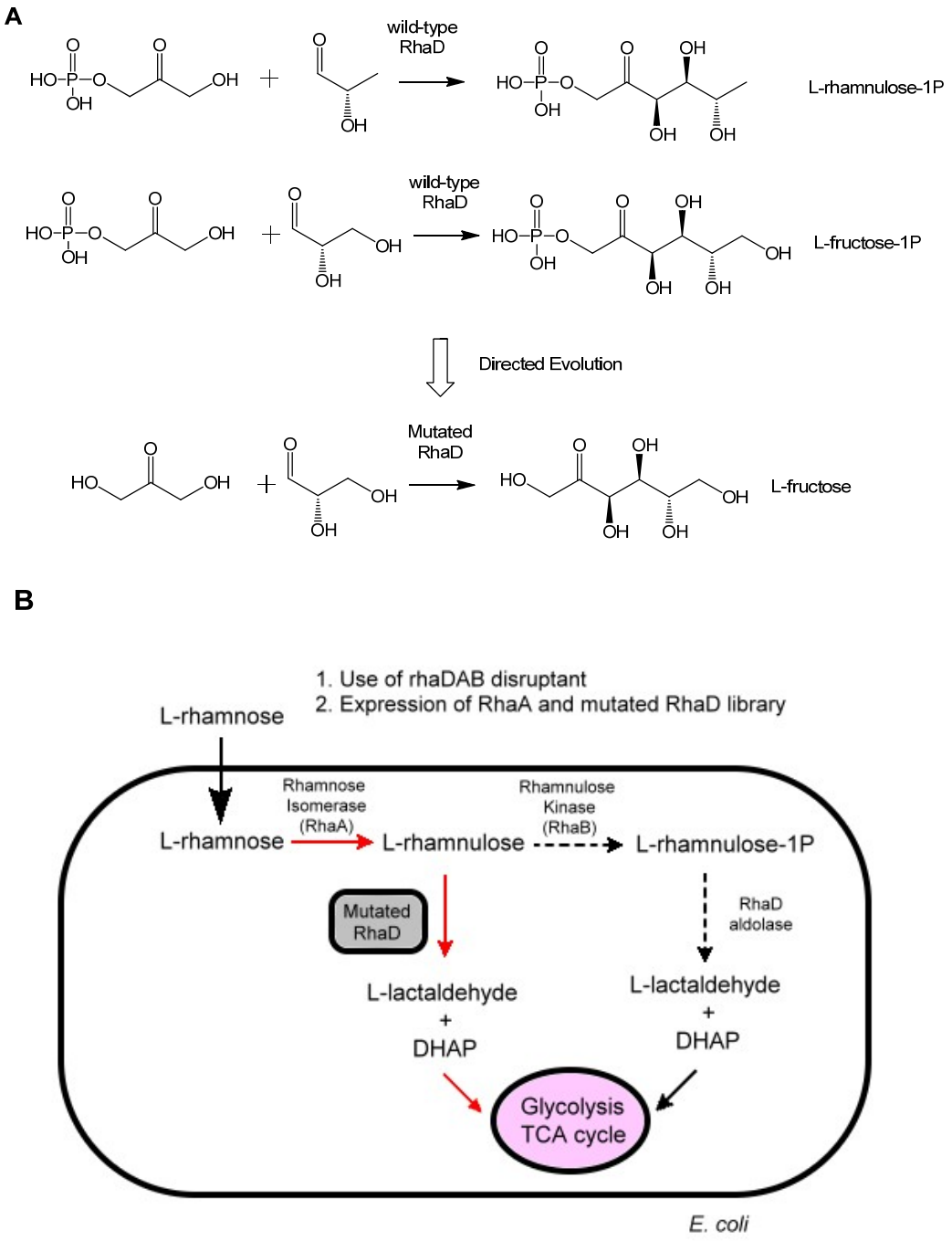

Figure 1.5 (A) Directed evolution of RhaD to alter its substrate specificity. (B) Metabolic engineering of *E. coli* rhamnose pathway for *in vivo* selection development (*22*).

strand 8; the more solvent exposed metal ion, M_β , is associated with another two histidine residues from strands 5 and 6. The two divalent cations are bridged by a hydroxide ion and a carboxylated lysine from strand 4 (**Figure 1.6**). Some other subtypes of AHS have single divalent cations at the M_α or M_β site, the glutamate residue from strands 3 or 4 replaces the carboxylated lysine from strand 4, or one cysteine residue from strand 2 serves as the metal-associated ligand.

The catalytic reactions of enzymes in the AHS are generally hydrolytic reactions with some exceptions, such as uronate isomerase (URI) and α-amino-β-carboxymuconate-ε-semialdehyde decarboxylase (ACMSD). The former catalyzes an aldose/ketose isomerization reaction between D-glucuronate and D-fructuronate and the later catalyzes a decarboxylation reaction that transforms α-amino-β-carboxymuconate-ε-semialdehyde (ACMS) to 2-aminomuconate semialdehyde (AMS) and carbon dioxide (*25, 26*). PTE catalyzes the hydrolysis of phosphorus-oxygen or phosphorus-sulfur bonds within an organophosphate or organophosphonate compounds. The rest of the structurally characterized enzymes catalyze the cleavage of C-N bonds. **Scheme 1.2** displays the chemical reactions catalyzed by enzymes in the AHS.

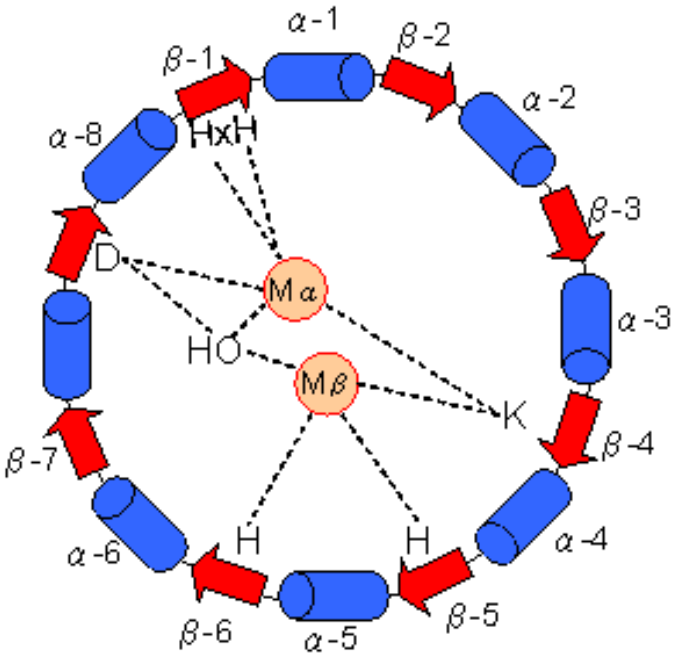

Figure 1.6 Schematic view of the most common metal center, binuclear metal centers of enzymes, in the amidohydrolase superfamily. The member with this active site representation is exemplified by PTE.

Scheme 1.2 The chemical reactions catalyzed by the enzymes in amidohydrolase superfamily.

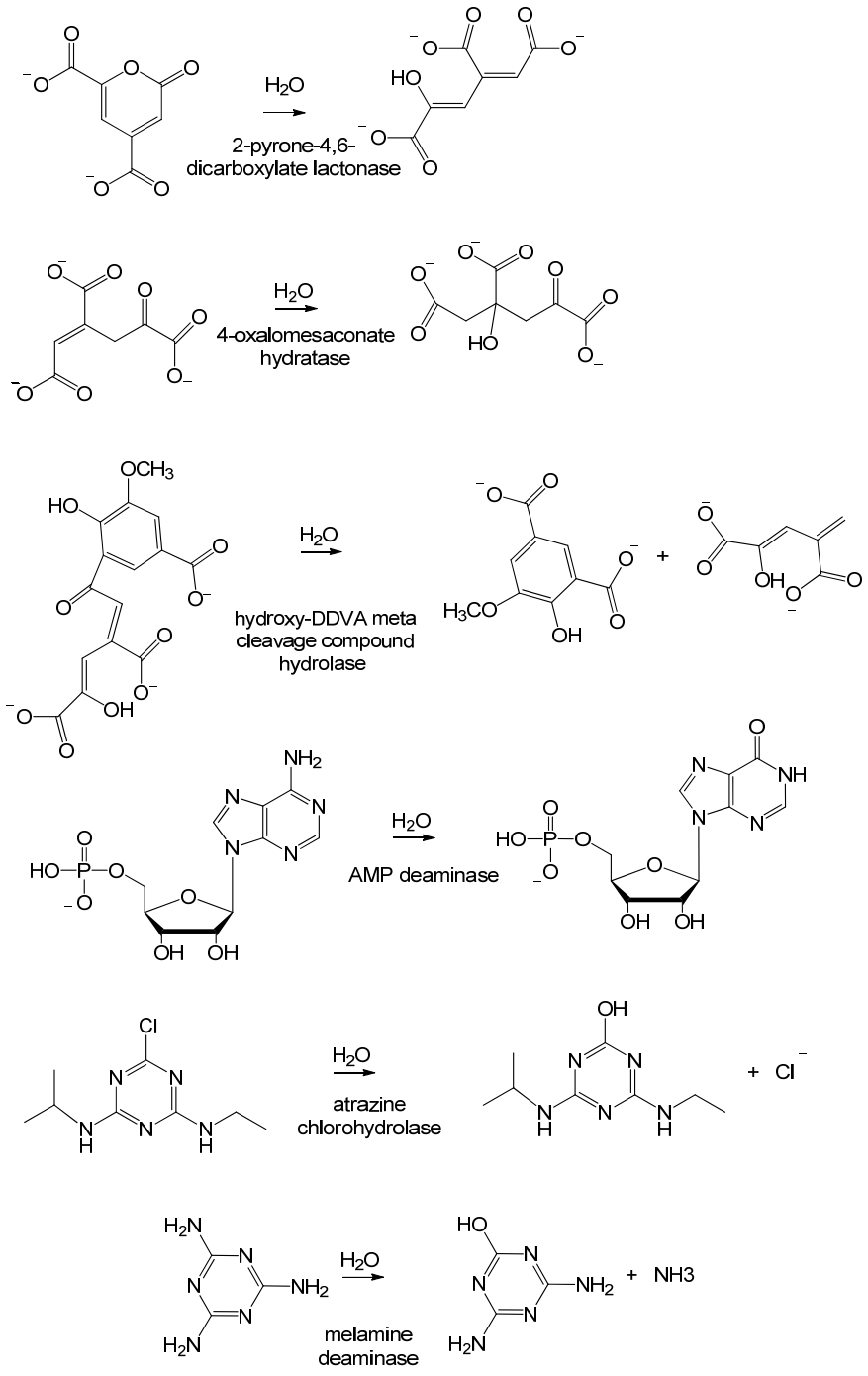

Scheme 1.2 Continued

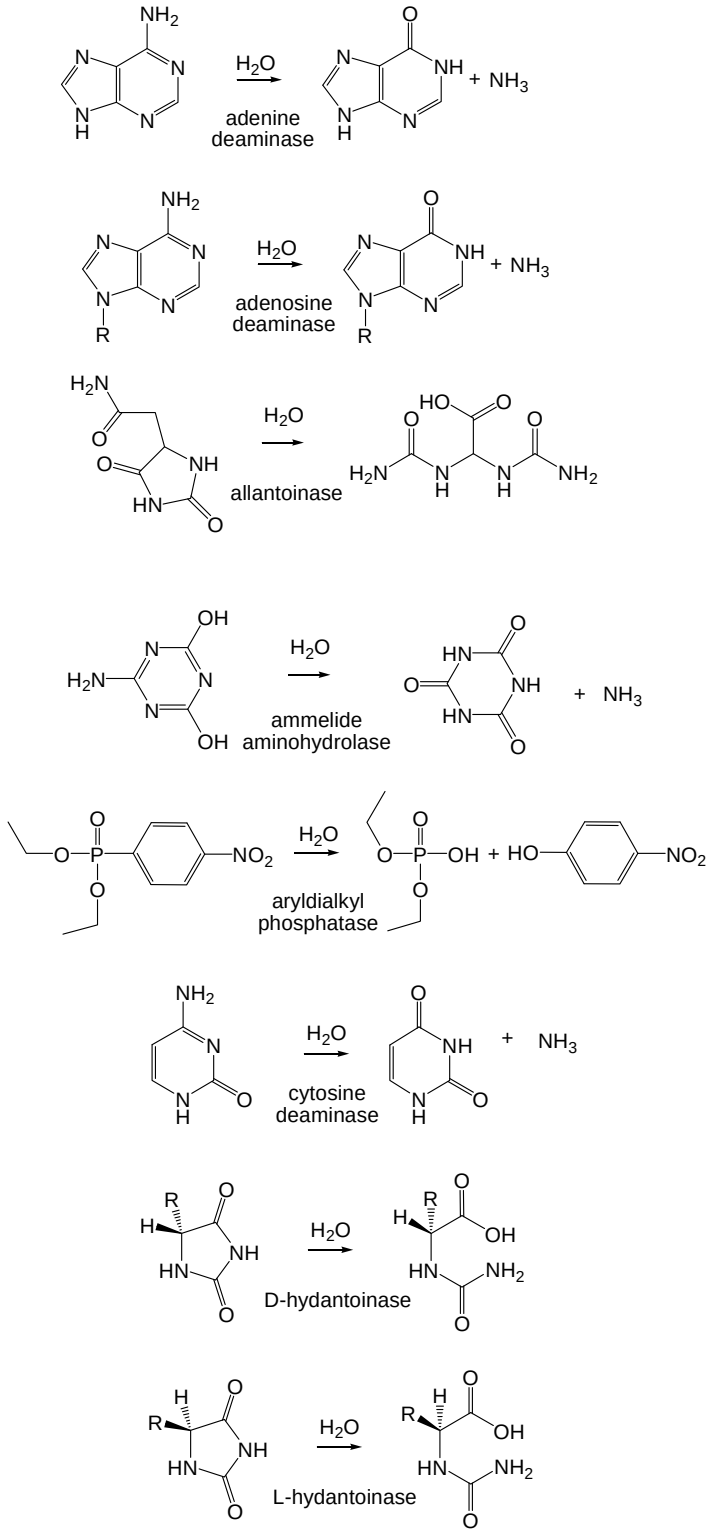

Scheme 1.2 Continued

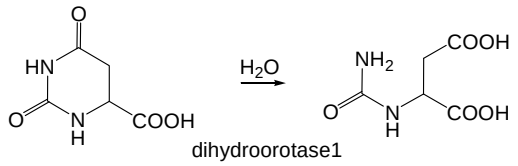

dihydroorotase1

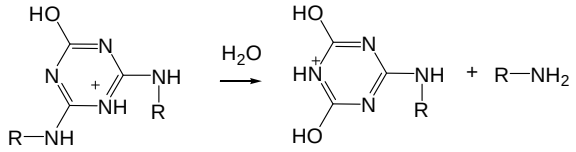

hydroxydechloroatrazine
ethylaminohydrolase

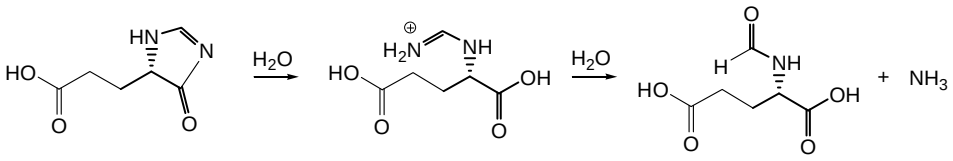

imidazolone propionate
amidohydrolase

N-formimino-l-glutamate
deiminase

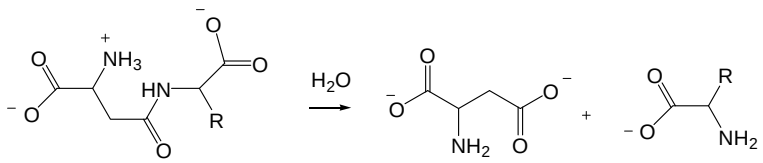

isoaspartyl dipeptidase

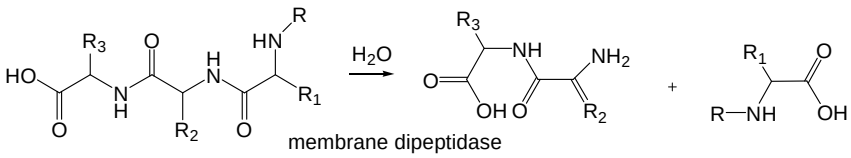

membrane dipeptidase

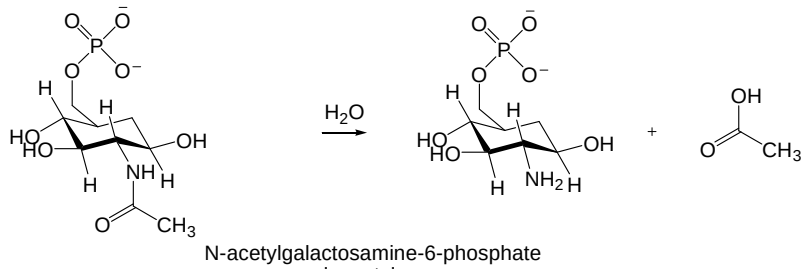

N-acetylgalactosamine-6-phosphate
deacetylase

Scheme 1.2 Continued

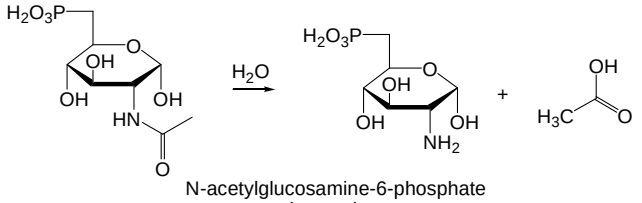

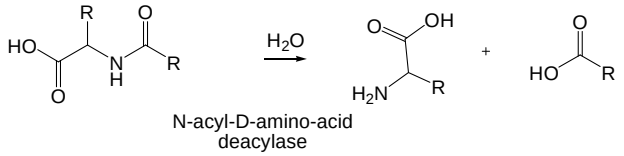

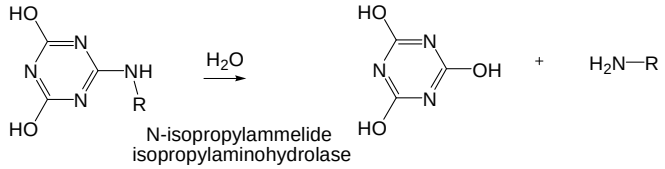

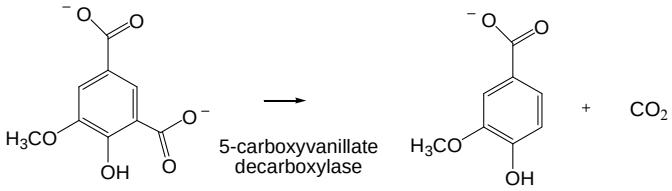

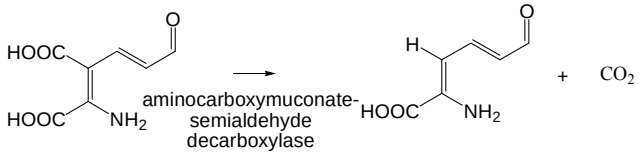

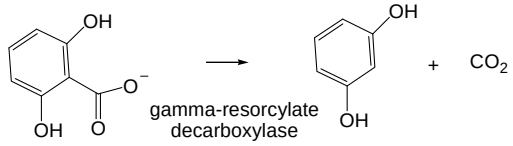

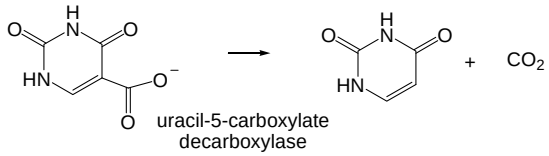

Scheme 1.2 Continued

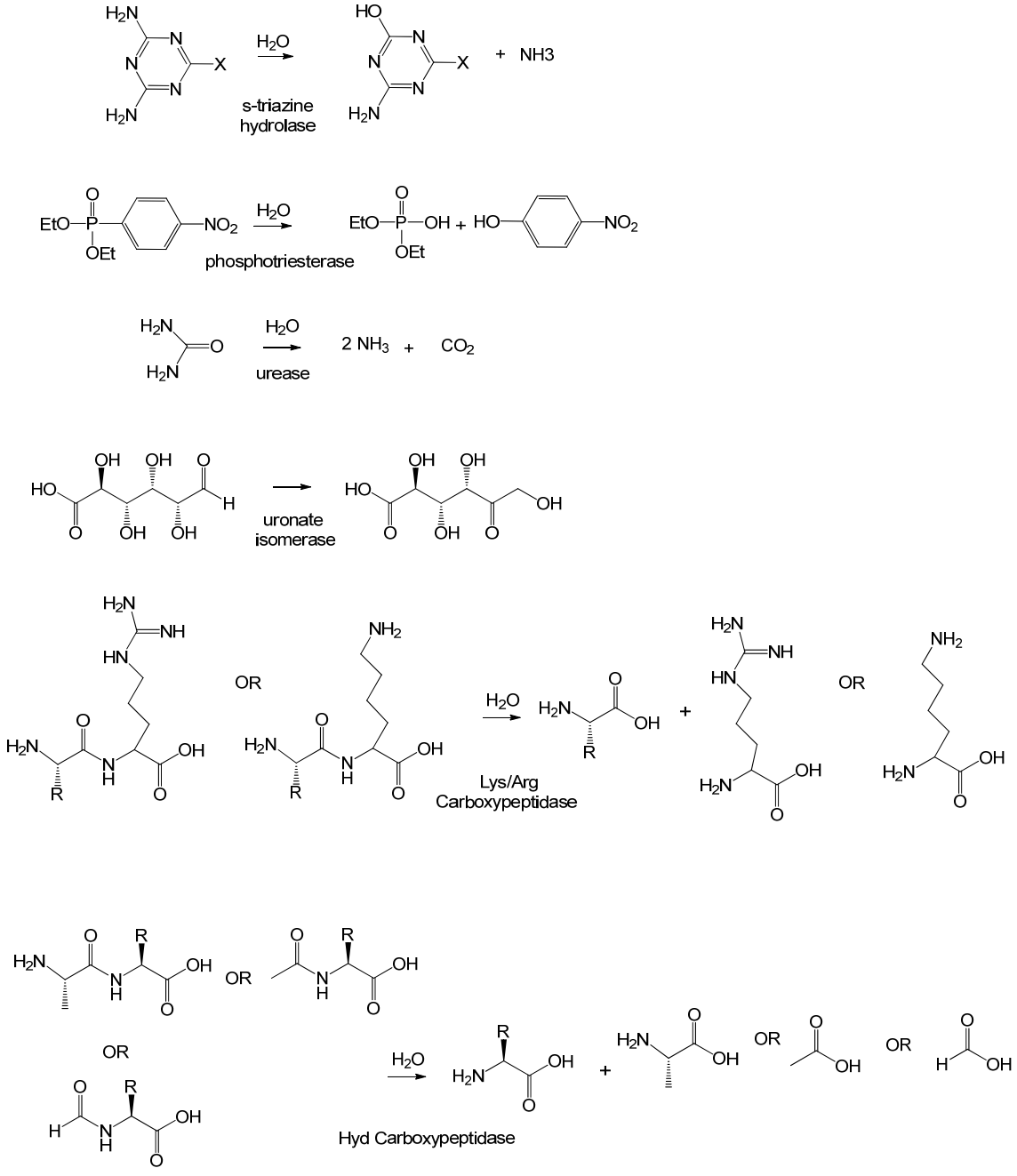

Directed Evolution of the Enzymes in the Amidohydrolase Superfamily

Most of the reported directed enzyme evolution studies in the amidohydrolase superfamily have been focused on phosphotriesterase. Wilfred Chen and coworkers have engineered PTE for the enhancement of the hydrolysis activity towards organophosphate pesticides such as paraoxon, parathion, methyl parathion and chlorpyrifos (**Scheme 1.3**) (*27, 28*). They created the randomized library of PTE by DNA shuffling and saturation mutagenesis, and subcloned it into INPNC surface display vector, pINCOP. The library was transformed into *E. coli* XL1-Blue cells and PTE variants were displayed on the surface of the cells using the truncated ice nucleation protein. The beneficial PTE variants were isolated by solid-phase top agar plate assay based on the formation of yellow products (*p*-nitrophenol) and clear haloes (the product of chlorpyifos). The best improvement they have achieved was that the variant, B3561, exhibited a 725-fold increase in the k_{cat}/K_m value for the chlorpyrifos hydrolysis. This mutant involves 8 amino acid substitutions and 7 of them are distal mutations from the active site (*27, 28*).

Scheme 1.3 The structures of paraoxon, parathion, methyl parathion and chlorpyrifos.

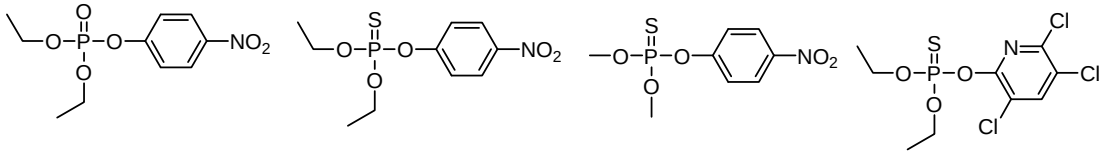

Paraoxon Parathion Methyl parathion Chlorpyrifos

James Wild and colleagues have modified the amino acid residues within the substrate binding pocket of PTE for the hydrolysis of paraoxon, *p*-nitrophenyl-*o*-pinacolyl-methylphosphonate (NPPMP), diisopropyl fluorophosphonate (DFP) and

dementon-S (**Scheme 1.4**) (*29, 30*). These experiments served as the model for the P-O bond, P-F bond and P-S bond cleavage of the organophosphate compounds. Saturation mutagenesis was performed and the H254R/H257L mutant was identified with a 6 fold enhancement in the k_{cat}/K_m value toward dementon-S (*29*). In addition, the H257L and the H254R/H257L mutants were shown to have an 11 and 18 fold increase in the k_{cat}/K_m values toward NPPMP (an analogue of nerve agent soman) respectively. In contrast, the H254R, the H257L and the H254R/H257L mutants showed a substantial decrease in the catalytic ability towards the hydrolysis of DFP (*30*).

Scheme 1.4 The structures of paraoxon, *p*-Nitrophenyl-*o*-pinacolyl-methylphosphonate (NPPMP), diisopropyl fluorophosphonate (DFP) and dementon-S.

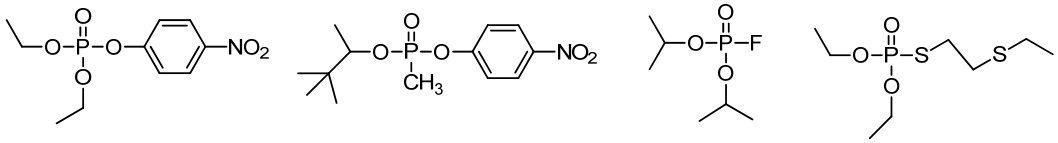

Paraoxon | *p*-Nitrophenyl-o-pinacolyl methyl phosphonate (NPPMP) | Diisopropyl phosphorofluoridate (DFP) | Demeton-S

David Ollis and coworkers have also modified the phosphotriesterase from *Agrobacterium radiobacter* P230 (OpdA), which has a 90% sequence identity to PTE (*31, 32*). They discovered the engineered OpdA variants with the enhanced protein expression levels and increased catalytic activity for the hydrolysis of organophosphate compounds, such as coumaphos-o-analogue, methyl-paraoxon, methyl-parathion and demeton-S (**Scheme 1.5**). They created OpdA and PTE libraries by error-prone PCR and DNA shuffling, and cloned the library into *E. coli* cells. They isolated the beneficial mutants for the hydrolysis of paraoxon and the increased protein expression levels by

growing the library on the paraoxon plates and selecting the largest colonies. They also grew the cells with the constructed library on indicator plates. The isolation of interesting mutants is done by visualizing the colonies with significant fluorescence. They have identified some distal mutations that improve protein expression and stability. In addition, PTE variants isolated from the indicator plates, exhibited slightly better activity for the hydrolysis of coumaphos-o-analogue, methyl-paraoxon, methyl-parathion and demeton-S than the wild-type PTE but not the wild-type OpdA. These two selection methodologies have selected the OpdA and the PTE variants with some mutations that are remote from the active site, these changes might affect the dynamics and stability of the protein in a way that improves the substrate binding or subsequent catalytic turnover (*31, 32*).

Scheme 1.5 The structures of coumaphos-o-analogue, methyl-paraoxon, methyl-parathion and dementon-S.

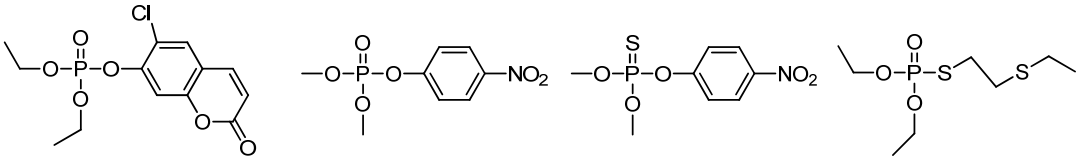

Dan Tawfik and collaborators have worked on directed evolution of PTE for increasing the stability of the metal-free enzyme and the hydrolysis activity towards paraoxon (*33, 34*). The randomized library was created by DNA shuffling and the PTE library was screened for improvements in 2-naphthyl acetate (**Scheme 1.6**) hydrolysis. *E. coli* DH5α cells was transformed with the PTE library and plated on zinc containing

LB plate. After growing colonies overnight, a layer of soft agar supplemented with 2-naphthyl acetate and Fast Red was added. The colonies that turned red first were selected for further screening for the hydrolysis of paraoxon and 2-naphthyl acetate. Through this method, they have isolated a variant called S5, which contains 3 point mutations, K185R, D208G, and R319S and 4 additional silent mutations. This protein has a 20 fold increase in functional expression (*33*). Additionally, they employed *in vitro* compartmentalization (IVC) based on linking genotype and phenotype to select the beneficial mutants for thy hydrolysis of paraoxon. The PTE mutant library was constructed and selected for the catalysis of paraoxon by compartmentalization using water-in-oil emulsions. The PTE library was linked to streptavidin-coated beads carrying antibodies through a common epitope tag, the average was less than one gene per bead. The beads were compartmentalized in a water-in-oil emulsion, and it was less than one bead per compartment. The translated protein became attached to the gene that encodes it via the bead in each compartment. After the emulsion was broken, the microbeads carrying the display library were isolated. (**Figure 1.7 (A)**) The microbead-display library was compartmentalized and the substrate, paraoxon, attached to caged-biotin was added. The product was produced only in compartments containing beads displaying active enzyme. The emulsion was then irradiated to uncage the biotin. In the compartments with the active PTE variants, the product became attached to the gene via the bead. In contrast, the compartments with the genes encode the non-active PTE variants contain the intact substrate attached to the gene. The emulsion was broken and the beads were incubated with the anti-product antibody. The product-coated beads were

purified by flow cytometry (**Figure 1.7 (B)**). Through this method, the best variant they have discovered was the I106T/F132L PTE mutant with two mutations within the active site, the k_{cat} and the k_{cat}/K_m values are 63 and 1.8 times higher than the wild-type for the hydrolysis of paraoxon. The k_{cat} value of this mutant is 1.4×10^5 s^{-1} (*34*).

Scheme 1.6 The structure of 2-naphthyl acetate.

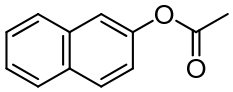

Hydantoinase is another enzyme in the amidohydrolase superfamily that has been engineered to invert the enantioselectivity (*35*). The selectivity of all known hydantoinases for D-5-(methylthioethyl)hydantoin (D-MTEH) over the L-enantiomer leads to the accumulation of intermediates and reduced the productivity for the L-amino acid (**Scheme 1.7**). Error prone PCR was performed to create a randomized library of hydantoinases from *Arthrobacter sp.* DSM 9711. The library was screened by D-MTEH and L-MTEH in the presence of cresol red solution and measured the absorbance at 580 nm. With the combination of the saturation mutagenesis, they discovered three mutations containing variant of D-selective hydantoinase that converts into an L-selective enzyme and increased total activity for 5 fold. A mutant with single amino acid substitution was found as a highly D-selective hydantoinase.

Scheme 1.7 The structure of the L- the D-enantiomers of methylthioethyl hydantoin.

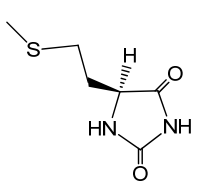

L-methylthioethyl hydantoin

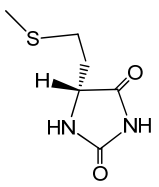

D-methylthioethyl hydantoin

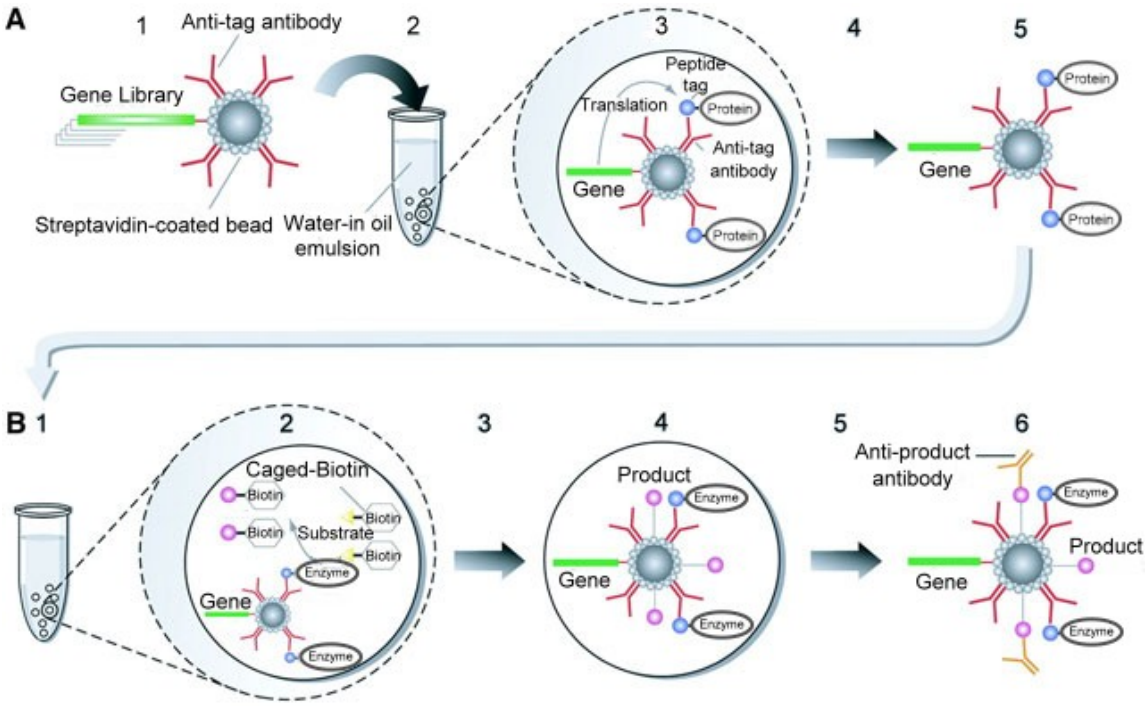

Figure 1.7 Creation of microbead-display PTE libraries and selection for catalysis by compartmentalization (*34*).

Three Dimensional Structure of Phosphotriesterase

The X-ray crystal structure demonstrates that PTE contains a binuclear metal center embedded within a $(\beta/\alpha)_8$ barrel structure. The binuclear metal center is located at the C-terminal end of β-barrel (**Figure 1.8**). PTE is a homodimeric protein with a molecular weight of 36 kDa/monomer (*36*). Native PTE contains two Zn^{2+} ions in the metal center, but they can be reconstituted with Cd^{2+}, Co^{2+}, Ni^{2+}, and Mn^{2+} without losing catalytic activity (*37*). The two metals are bridged by a carboxylated lysine (Lys-169) and a hydroxide ion. The more solvent-shielded metal (M_α) is coordinated to His-55, His-57, and Asp-301, and the more solvent-exposed metal (M_β) is coordinated to His-201 and His-230 (**Figure 1.9**). Previous investigation based on the interaction between the phosphorus center of substrates and inhibitors defined the three binding pockets within the active site of PTE: a large pocket, a small pocket and the leaving group pocket (*38*). The small pocket is defined by the side chains of Gly-60, Ile-106, Leu-303, and Ser-308; the large pocket is formed by His-254, His-257, Leu-271, and Met-317; the leaving group pocket is surrounded by four residues: Trp-131, Phe-132, Phe-306, and Tyr-309. The substrate binding site of PTE is graphically shown in **Figure 1.10**.

The Reaction Mechanism of Phosphotriesterase

The catalytic mechanism for the hydrolysis of organophosphate triesters by PTE has been studied. The kinetic parameters and pH rate profiles of Zn/Zn PTE, Cd/Cd PTE, and a mixed-metal Zn/Cd hybrid PTE were obtained with various substrates to

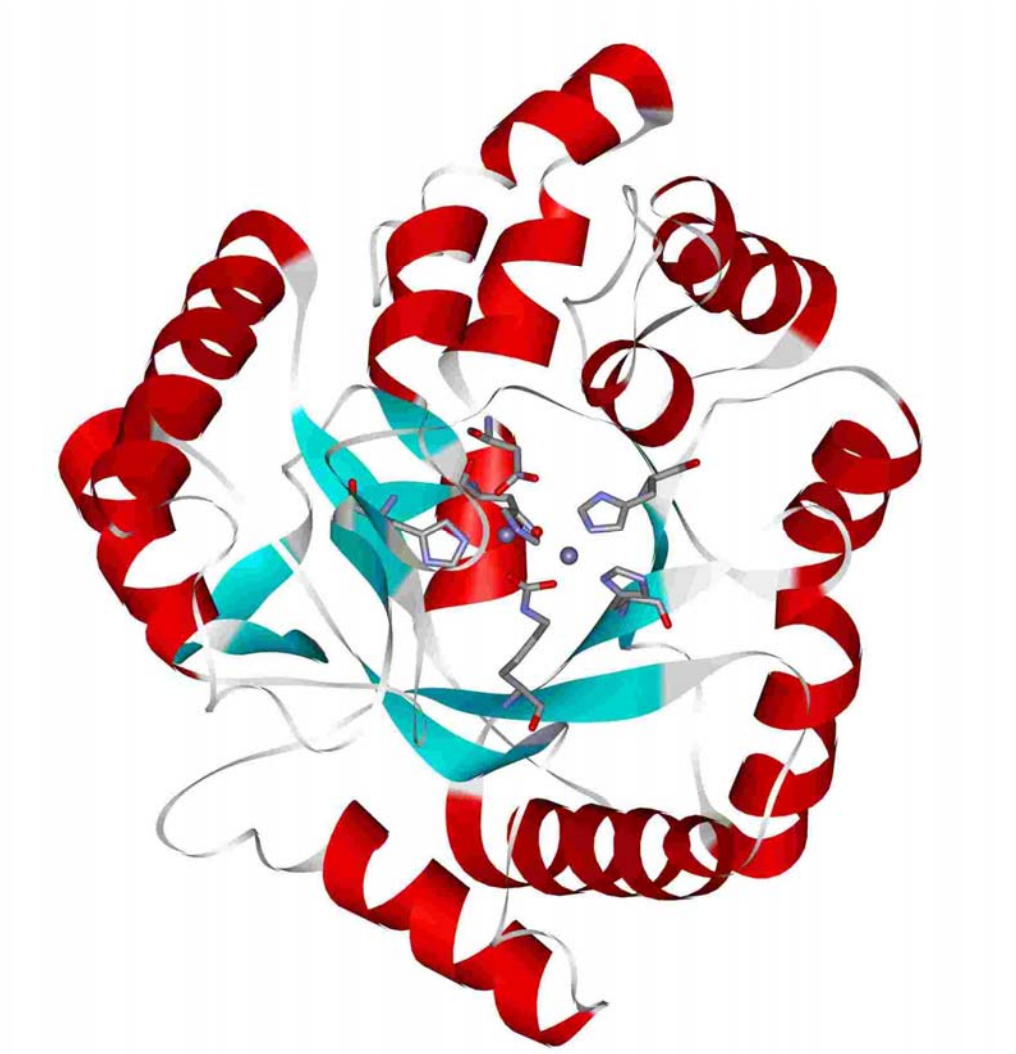

Figure 1.8 The X-ray crystal structure of phosphotriesterase displaying a $(\beta/\alpha)_8$ TIM barrel. (PDB: 1HZY)

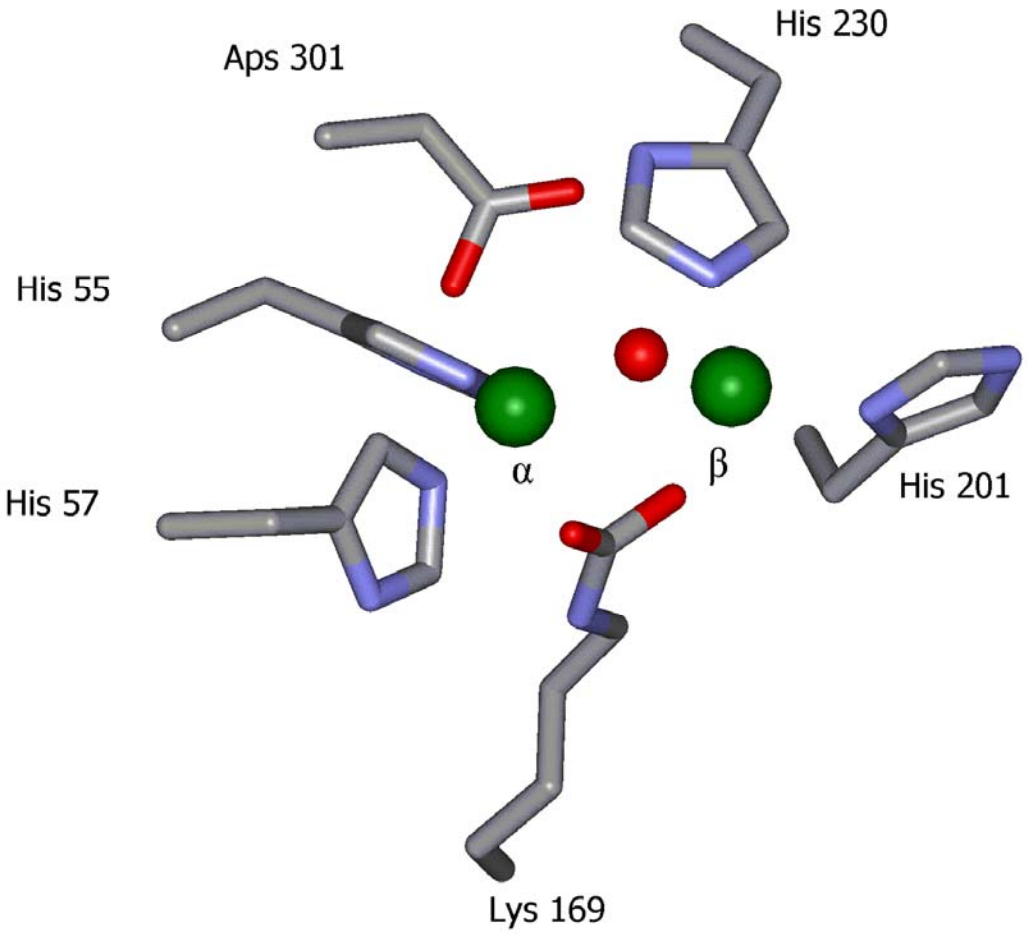

Figure 1.9 The zinc binuclear metal center of phosphotriesterase is shown with the bridged carboxylated lysine, hydroxide ion and the associated amino acid residues. (PDB: 1HZY)

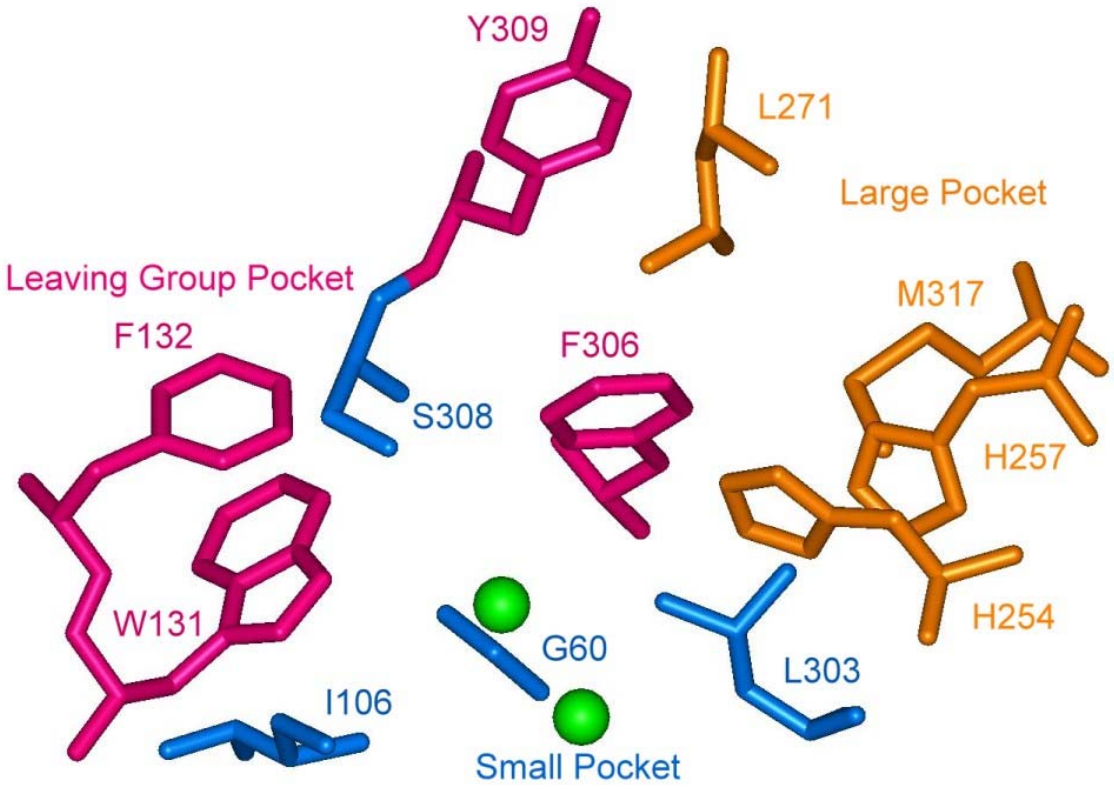

Figure 1.10 Graphic representation of the substrate binding pockets within the active site of PTE. The small pocket consists mainly of Gly-60, Ile-106, Leu-303, and Ser-308. The large pocket primarily contains His-254, His-257, Leu-271, and Met-317. The leaving group pocket is surrounded by Trp-131, Phe-132, Phe-306, and Tyr-309 (*37*).

determine the role of the α- and β- metals in binding and catalysis. The pH-rate profiles of the hybrid enzyme indicates that the α- metal determines the pK_a value for the bridging hydroxide ion (*39*). This suggests that the hydrolytic nucleophile is activated as a hydroxide via the ionization of a water molecule coordinated to the α- metal ion. In addition, EPR spectroscopy of the complex of Mn/Mn-PTE and substrate analogues supports the weakening of the interaction of the bridging hydroxide with the β–metal ion (*40*). Mutational studies at Asp-301 indicate the reactivity of the bridging hydroxide ion is enhanced by proton transfer to Asp-301 (*39, 41*). A nucleophilic attack of the activated hydroxide ion at the phosphorus center occurs with the expulsion of the leaving group. The slightly modified reaction mechanism, originally proposed by Aubert et al., for the hydrolysis of paraoxon by PTE from *P. diminuta* is presented in **Figure 1.11**. The organophosphate substrate binds to the binuclear active site with a water molecule displaced from the β-metal ion. The interaction of the substrate with the β–metal ion weakens the coordination of the bridging hydroxide ion to the β–metal ion. It also assists in the nucleophilic attack of the hydroxide on the phosphorus center of the substrate via an S_N2-like mechanism. The stereochemistry at the phosphorus center of the substrate is inverted by this attack. The P-O bond of the leaving group phenol is broken, and the single proton from the nuceophilic hydroxide is transferred to Asp-301. The diethylphosphate is bridged between the two divalent cations within the active site. The diethyl phosphate then disassociates from the active site, following the regeneration of the binuclear metal center for another round of catalysis.

Two other proposed mechanism for the hydrolysis of phosphotriesters by bacterial PTE were proposed by Jiali Gao's and David Ollis's laboratories (*41, 42*). Wong and Gao have proposed that the protonated diethyl phosphate coordinates to the β–metal ion and follows by an elongation of the metal-metal distance from 3.6 to 5.3Å. At the same time, the reaction proceeds from an enzyme-substrate complex to an enzyme-transition state complex and an enzyme-product complex (**Figure 1.12 (A)**) (*41*). Additionally, Jackson and coworkers from David Ollis's laboratory have postulated that the other reaction mechanism of the hydrolysis of phosphotriesters by a bacterial PTE from *Agrobacterium radiobacter*, OpdA. They suggested that the bridging hydroxide acts as a base, instead of acting as a nucleophile, in the abstraction of proton from a water molecule. The water molecule terminally bound to the α-metal ion becomes a hydroxide nucleophile to attack the electrophilic phosphorus atom of the substrate. After departure of the leaving group, the phosphodiester bridges two metal ions (**Figure 1.12 (B)**) (*42*).

Substrate Specificity of Phosphotriesterase

PTE has a significant activity for the hydrolysis of paraoxon and possess very broad substrate specificity for organophosphates, organophosphonates, organophosphinates, thiophosphates and phosphorothiolates. PTE exhibits very different catalytic ability with varied pK_as of the leaving group. It has been shown that the rate limiting step is dependent on the bond cleavage of the leaving groups with high pK_a values (*43*). In addition, the previous kinetic studies of the catalytic ability of

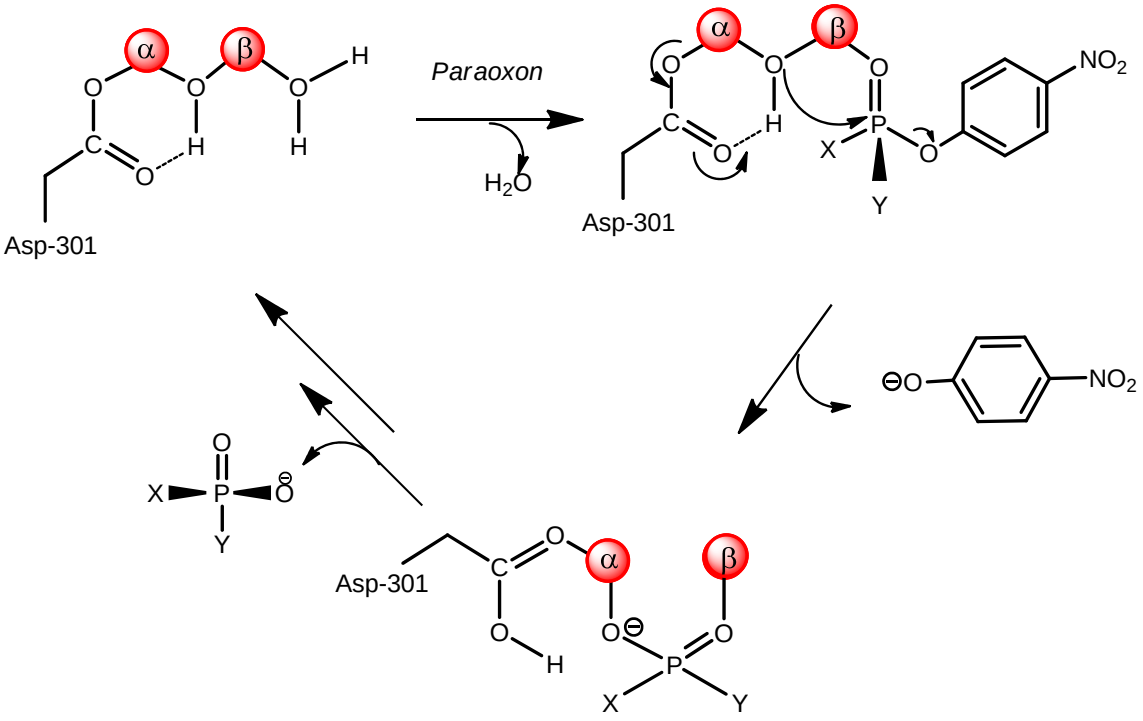

Figure 1.11 The proposed mechanism of the hydrolysis of paraoxon by PTE. The pink balls (●) represent zinc metal.

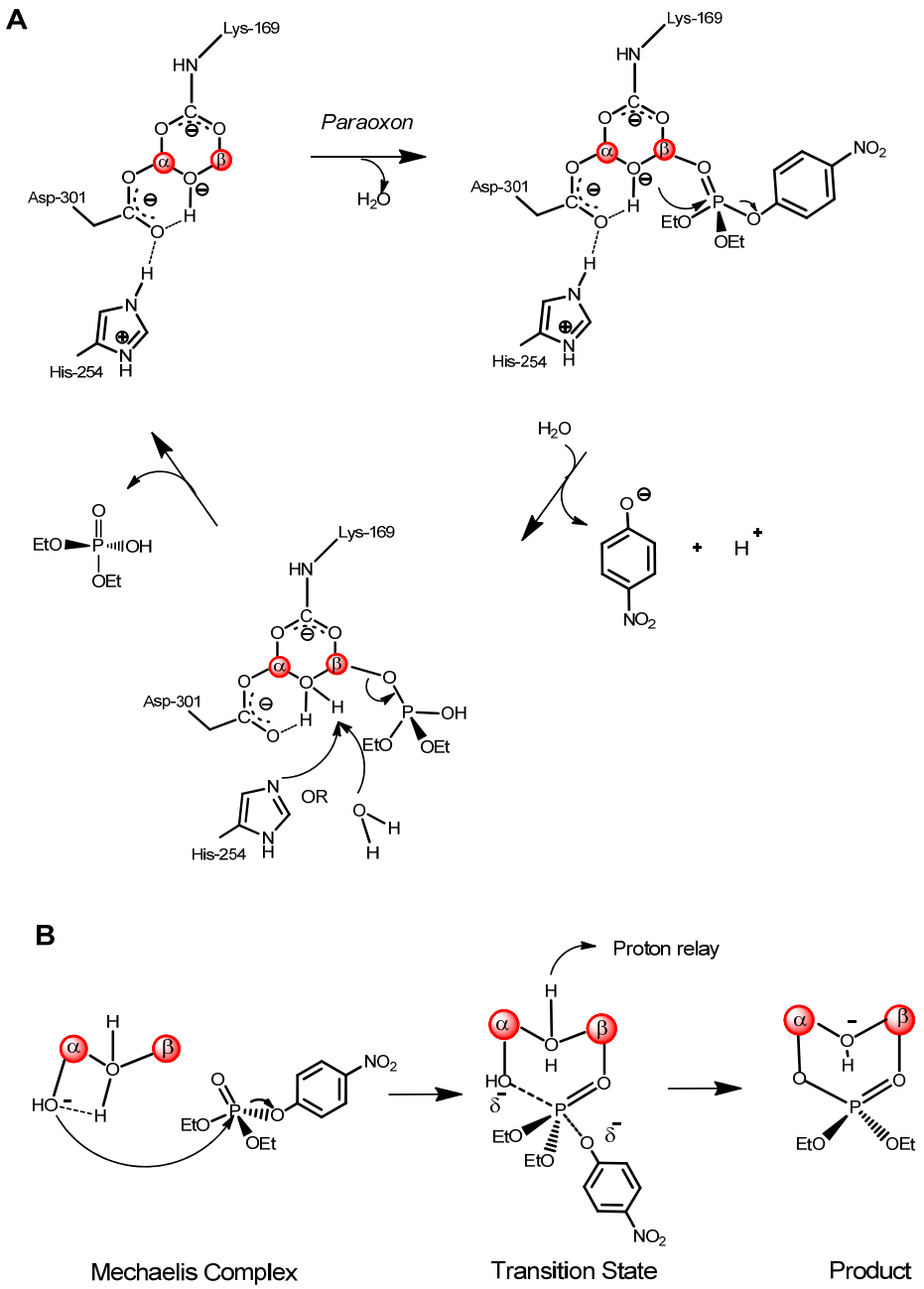

Figure 1.12 (A) Wong and Gao's proposed reaction mechanism of the hydrolysis of paraoxon by PTE from *P. diminuta* (*41*). (B) Jackson and Ollis's proposed mechanism of the hydrolysis of phosphotriesters by OpdA from *Agrobacterium radiobacte* (*42*). The pink balls (●) represent zinc metal.

the wild-type PTE towards a series of enantiomeric organophosphate triesters (**Scheme 1.8**) were shown that the S_p– enantiomers are more preferable than the R_p– enantiomers. In the case of methyl phenyl *p*-nitrophenyl phosphate (X and Y are phenyl and methyl groups), the hydrolysis of the S_p– enantiomer is 90 fold faster than the R_p– enantiomer by the wild-type PTE (*44*).

Scheme 1.8 The model of organophosphate triesters.

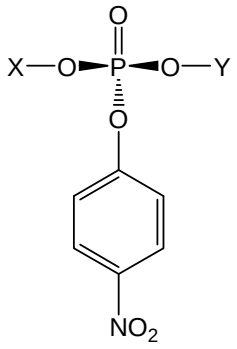

The stereoselective properties of the wild-type PTE toward chiral sarin and soman analogues have also been studied. The structures of the organophosphonate compounds sarin, soman and their analogues are shown in **Scheme 1.9**. Previous investigations have shown that the wild-type PTE is more efficient at hydrolyzing the R_p– enantiomer of the sarin analogue than the S_p– enantiomer by a factor of 20. The hydrolysis of the soman analogue by the wild-type PTE have been shown that R_pR_c-enantiomer is the most preferable isomer, with the order of the preference being R_pR_c, R_pS_c, S_pR_c, S_pS_c. A small numbers of mutations within the substrate binding pocket of PTE are able to enhance and reverse the stereoselectivity exhibited by wild-type PTE (*45*).

Scheme 1.9 The structures of sarin, soman and their analogues.

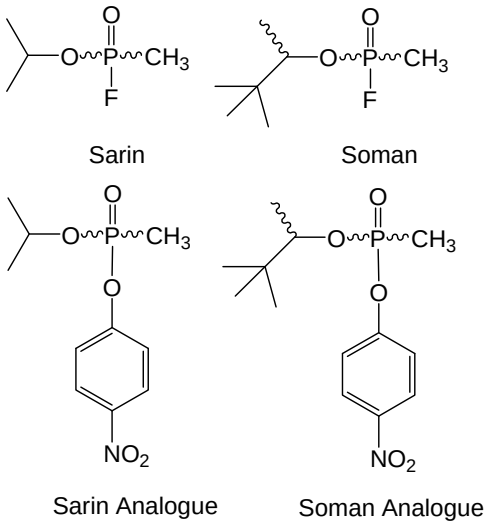

History of Organophosphate Compounds

Organophosphorus compounds (OP) are currently used as insecticides and chemical warfare agents. Organophosphates have been used as pesticides for more than 50 years and are still being used as insecticides, acaricides, and nematocides for protecting agricultural crops. One of the earliest OP insecticides synthesized was parathion (**Scheme 1.10**), which is still commonly used worldwide. Prior to World War II, the German Ministry of Defense started shifting from insecticides to chemical warfare agents. First, they synthesized diisopropyl phosphorofluoridate (DFP) and then developed more toxic OP compounds of the G series (tabun, sarin, and soman). Tabun (GA) was the first compound synthesized by the German scientist Schrader in a search for an efficient pesticide. He then developed the second nerve agent, sarin (GB), in 1938. The other G series nerve agent, soman (GD), was synthesized by Richard Kuhn,

in 1944 during World War II. Cyclosarin (GF) was developed by Schrader in 1949. A few years later, the most toxic of the reported nerve agents, VX, was synthesized by Ranajit Ghosh, who worked at the CW facility in Porton Down, England in 1952. The British government traded the VX technology with the USA for continuing with sarin as the UK chemical weapon in 1958. The US Army then went into production of large amounts of VX in 1961 at Newport Chemical Depot. The VX stockpile there has been completely destroyed since August 2008. One of the most well-known uses of the nerve agents was the 1995 terrorist attack in Japan. One of the Japanese religious groups released sarin into the Tokyo subway system.

Scheme 1.10 The chemical structures of common organophosphate insecticides and nerve agents.

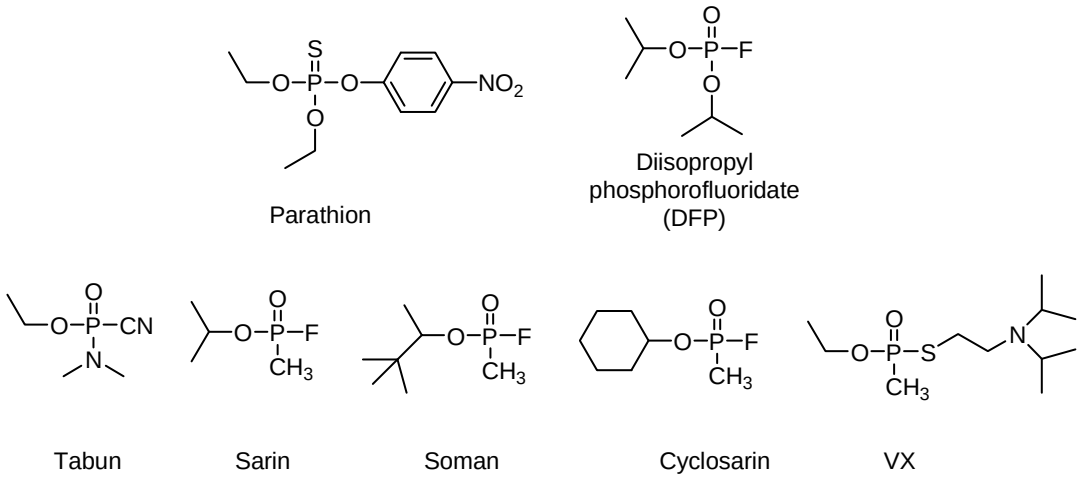

Toxicity of Organophosphate Compounds and Inactivation of Acetylcholinesterase

The toxicity of the organophosphorus compounds is due to the inactivation of acetylcholinesterase (AChE), the enzyme that catalyzes the hydrolysis of acetylcholine

to choline and acetic acid at neural synapses. The hydrolysis of acetylcholine (ACh) is initiated by the nucleophilic attack of Ser-200 on the carbonyl center to form an acetylated AChE and release the first product, choline. The free AChE is then regenerated by the hydrolysis of the acetylated AChE complex and the second product, acetic acid, is released (**Figure 1.13 (A)**). The inhibition of AChE by organophosphates results from the phosphorylation of the active site residue Ser-200 of AChE that forms a phosphorylated enzyme intermediate. In this case, the hydrolysis ability of ACh is very slow. Thus, the accumulation of ACh at the synapse causes the paralysis of the cholinergic synaptic transmission (*46*). The phosphorylated AChE can be reactivated by an oxime nucleophile such as 2-PAM. However, if the oxime nucleophile is not used, the phosphorylated AChE can undergo a base-assisted dealkylation reaction, called "aging", which result in irreversible enzyme inhibition (*47*).

The toxicity of organophosphate nerve agents is dependent on the stereochemistry of the phosphorus chiral center. Tabun, sarin, cyclosarin, and VX have two stereoisomers due to a single chiral center at the phosphorus atom, while soman has four stereoisomers due to an additional chiral center within the pinacolyl substituent. The inhibitory studies of acethylcholinesterase (AChE) determined that the S_p-stereoisomer of sarin is approximately ~10^4 times more toxic than the R_p-stereoisomer. It has been shown that the S_p-stereoisomer of soman is ~10^5 times more toxic than the R_p-stereoisomer. Similarly, the S_p-stereoisomer of VX is 100-fold more toxic than the R_p-stereoisomer. VX is the most toxic compound among all organophosphate nerve agents.

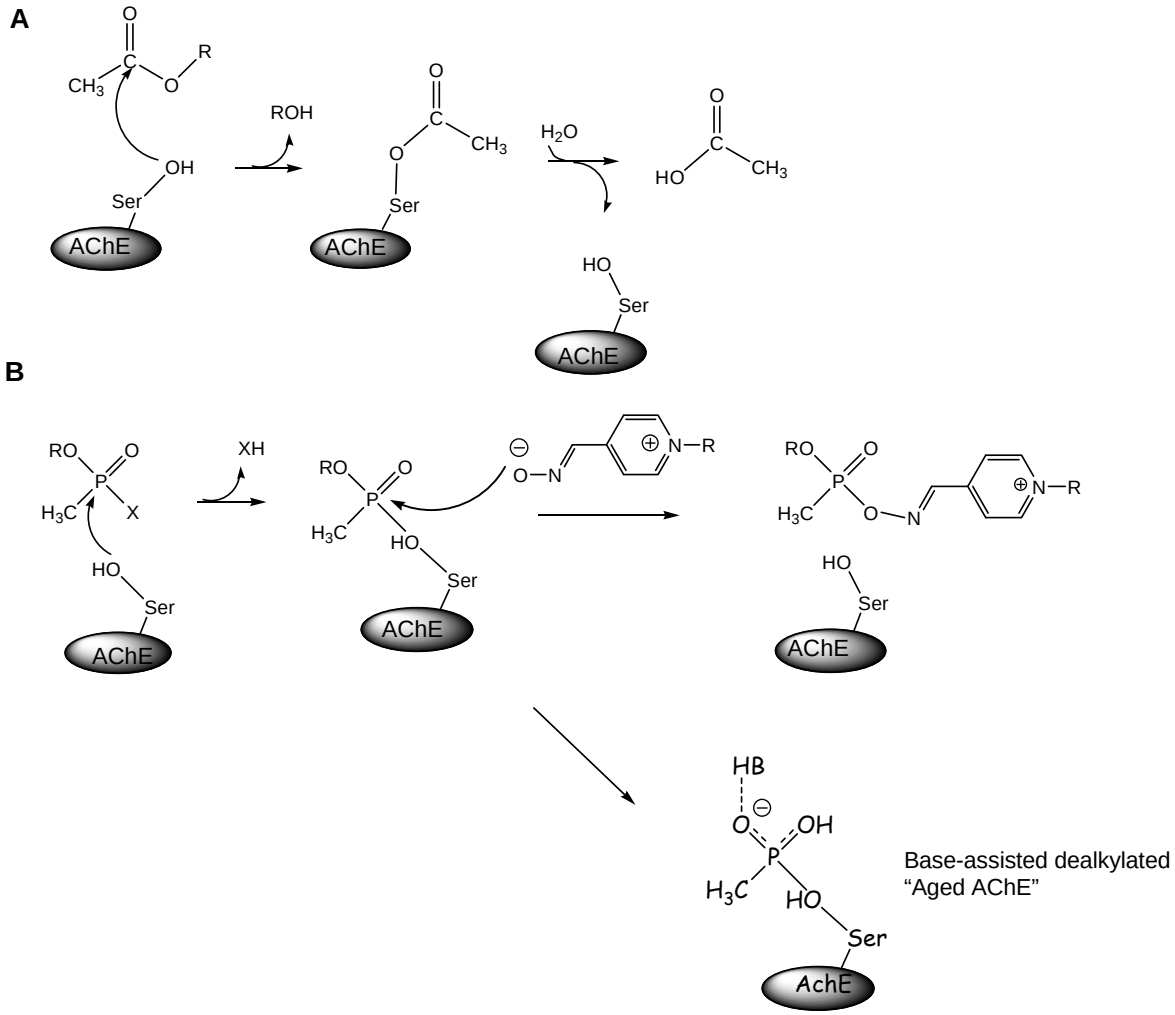

Figure 1.13 (A) The hydrolysis of acetylcholine (ACh) by acetylcholinesterase(AChE). (B) The reactivation of phosphorylated acetylcholinesterase by oxime nucleophile and the formation of an "aged" AChE without reactivation.

Table 1.1 displays the toxicity of individual stereoisomer of sarin, soman and VX in terms of LD_{50} values for mice and the inhibition rate constants for AChE (*48*).

Other Organophosphate Hydrolyzing Enzymes

There are other enzymes with the ability to detoxify organophosphate compounds, such as human paraoxonase 1 (PON1), squid DFPase and organophosphorus acid anhydrolase (OPAA). The comparison of the catalytic ability of these organophosphate hydrolyzing enzymes and PTE for the hydrolysis of organophosphate insecticides and chemical warfare agents are shown in **Table 1.2**.

DFPase was isolated from the optical ganglion of *Loligo vulgaris*. The X-ray crystal structure of DFPase shows two calcium ions are present, one is essential for structural integrity and the other is crucial for catalysis. The overall structure of DFPase is a six bladed pseudosymmetrical β-propeller with a central water filled tunnel (*49*). It was shown to be able to hydrolyze tabun, sarin, soman, cyclosarin and diisopropyl flurophosphates. The activity for the hydrolysis of diisopropyl fluorophosphates (DFP) is high, with a k_{cat} of 526 s^{-1} and a k_{cat}/K_m of 1.3 x 10^6 M^{-1} s^{-1}, but the activities for GA, GB and GD are 3 to 4 times lower (*50, 51*).

Human serum paraoxonase (HuPON1) is a calcium-dependent enzyme. The amino acid sequence alignments and the X-ray crystal structures of HuPON1 and DFPase have shown that these two protein share similar structures in which six blade-like regions of β– pleated sheets are arranged radially around a central core. HuPON1

Table 1.1 Inhibition rate constants of the nerve agent stereoisomers on AChE (*48*).

Nerve Agent Stereoisomer	LD_{50} (Mouse) μg/Kg	Inhibition Rate Constant ($M^{-1}min^{-1}$)
R_p-Sarin		$< 3 \times 10^3$
S_p-Sarin	41	1.4×10^7
R_pR_c-Soman	>5000	$<5 \times 10^3$
R_pS_c-Soman	>2000	$<5 \times 10^3$
S_pR_c-Soman	99	2.8×10^8
S_pS_c-Soman	38	1.8×10^8
R_p-VX	165	2×10^6
S_p-VX	12.6	4×10^8

Table 1.2 The kinetic parameters of organophosphate hydrolyzing enzymes toward the organophosphate insecticide and chemical warfare agents (*54-59*).

	DFPase		HuPON1		OPAA		PTE	
	k_{cat} (s^{-1})	k_{cat}/K_m (M^{-1} s^{-1})	k_{cat} (s^{-1})	k_{cat}/K_m (M^{-1} s^{-1})	k_{cat} (s^{-1})	k_{cat}/K_m (M^{-1} s^{-1})	k_{cat} (s^{-1})	k_{cat}/K_m (M^{-1} s^{-1})
Paraoxon				1.1e4			1.0e4	1.0e8
DFP	5.3e2	1.3e6		6.2e2	1.7e3		2.2e2	1.0e7
Tabun (GA)					8.5e1		7.7e1	7.6e5
Sarin (GB)	1.8e2			1.5e4	6.1e2		5.6e1	8.0e4
Soman (GD)	3.2e2	4.0e1		4.7e4	3.1e3		4.8e0	1.0e4
Cyclosarin (GF)		8.5e1			1.7e3		3.0e-2	
VX			1.8e0	7.2e2			3.0e-1	7.0e2
Dementon-S							1.0e0	3.8e2

possesses the catalytic ability to hydrolyze esters, including lactones and organophosphates compounds. Yet, the catalytic activity to hydrolyze GB, GD, and VX is low (*52*).

Organophosphorus acid anhydrolase (OPAA) from *Alteromonas* sp. JD6.5 is also capable of catalytically hydrolyzing a wide variety of organophosphoate compounds, including GB, GD and GF. However, VX is not a substrate for OPAA. The sequence and biochemical analysis of OPAA suggested it naturally functions as a prolidase, a type of dipeptidase hydrolyzing dipeptides with a proline residue in the carboxyl-terminal position (X-Pro). The stereochemical preference of OPAA is similar to PTE. OPAA has higher catalytic ability for the hydrolysis the R_p- stereoisomers of sarin and soman analogues (*53*).

CHAPTER II

PRODUCT COMPLEX WITH THE BINUCLEAR METAL CENTERS FROM THE AMIDOHYDROLASE SUPERFAMILY OF ENZYMES*

Introduction

The amidohydrolase superfamily (AHS) of enzymes catalyzes hydrolytic, decarboxylation, isomerization, and hydration reactions within carbohydrate, nucleic acid and amino acid based substrates (*23*). Most of the structurally characterized enzymes of the AHS contain either a binuclear or mononuclear metal center embedded at the C-terminal end of a $(\beta/\alpha)_8$-barrel structural domain. For those enzymes that catalyze hydrolytic reactions the metal centers have been shown to activate solvent water for nucleophilic attack. High resolution x-ray structures have been obtained for approximately 20 members of the AHS and in these enzymes the metal centers are naturally populated by zinc, iron or nickel (*23*). In addition, some members of the AHS are also active with manganese, cobalt, or cadmium (*24*). Perhaps the best characterized member of the amidohydrolase superfamily is the bacterial phosphotriesterase from *Pseudomonas diminuta* (*60*).

Phosphotriesterase (PTE) catalyzes the hydrolysis of a wide range of organophosphate esters, including agricultural pesticides and highly toxic chemical

---

*Reprinted with permission from "Structure of Diethyl Phosphate Bound to the Binuclear Metal Center of Phosphotriesterase" by Jungwook Kim, Ping-Chuan Tsai, Shi-Lu Chen, Fahmi Himo, Steven C. Almo and Frank M. Raushel, 2008. *Biochemistry*, 47, 9497-9504, Copyright 2008 by the American Chemical Society.

warfare agents (*60-62*). A natural substrate for PTE is not known, however, the purified PTE exhibits a remarkable catalytic activity towards the hydrolysis of the commercial pesticide, paraoxon. Kinetic constants for k_{cat} and k_{cat}/K_m of 10^4 s^{-1} and 10^8 M^{-1} s^{-1}, respectively, have been measured for the hydrolysis of this substrate (*63-65*). The reaction for the hydrolysis of paraoxon is presented in **Scheme 2.1**. The enzyme has been crystallized and high resolution x-ray structures of the Zn/Zn-, Cd/Cd-, Mn/Mn- and the Zn/Cd-PTE hybrid have been solved (*24*). Shown in **Figure 2.1** is the coordination scheme for the binuclear metal center of Cd/Cd-PTE. The more solvent shielded metal (M_α) is coordinated to His-55, His-57, and Asp-301, whereas the more solved-exposed metal (M_β) is coordinated to His-201, His-230 and two water molecules from solvent. The two metals are bridged to one another by a carboxylated lysine (Lys-169) and hydroxide. The bridging hydroxide is additionally hydrogen bonded to the side chain carboxylate of Asp-301.

Scheme 2.1 The reaction for the hydrolysis of paraoxon by phosphotriesterase.

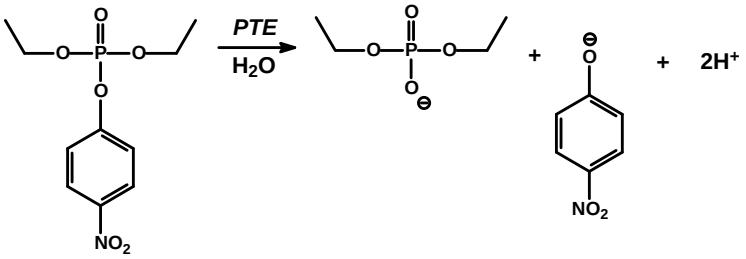

The reaction mechanism for the hydrolysis of organophosphate triesters by phosphotriesterase has received considerable experimental and computational attention (*39, 41, 42, 66*). Presented in **Scheme 2.2** is a slightly modified reaction mechanism,

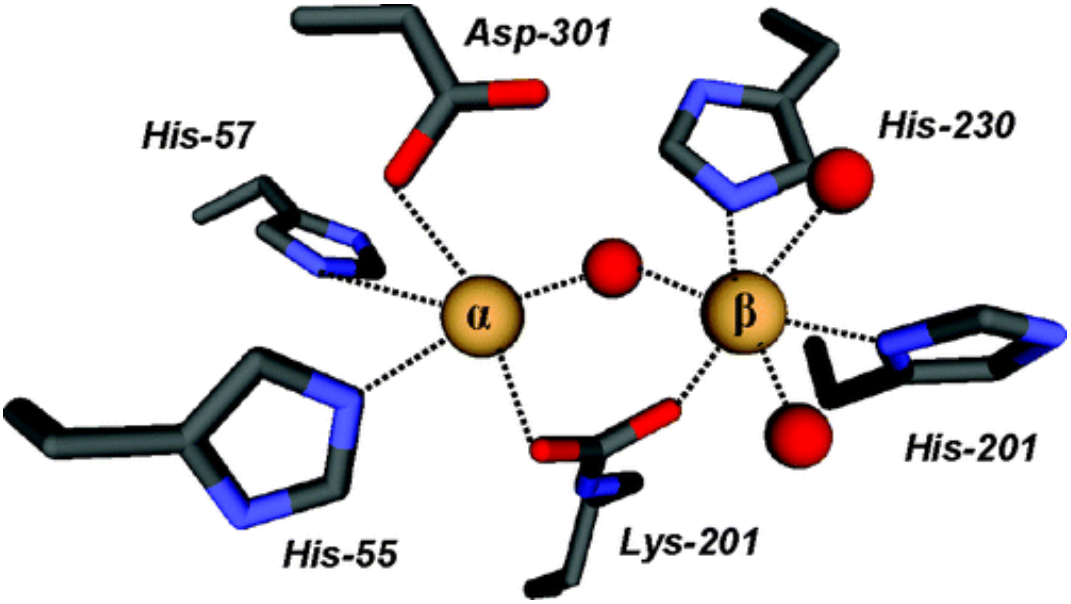

Figure 2.1 Model for the structure of the binuclear metal center within the active site of Cd/Cd-PTE (*24*). The coordinates taken from PDB code: 1JGM. The two metal ions are depicted as light brown spheres.

originally proposed by Aubert *et al*., for the hydrolysis of paraoxon by the phosphotriesterase from *P. diminuta (39)*. In this mechanism the organophosphate substrate binds to the active site with the displacement of a water molecule from the β-metal ion. The interaction of the substrate with the β-metal ion weakens the coordination of the bridging hydroxide to the β-metal ion and facilitates the nucleophilic attack of the hydroxide in an S_N2-like reaction on the phosphorus center of the substrate. The bond to the leaving group phenol is broken and the single proton from the nucleophilic hydroxide is transferred to Asp-301. The anionic diethyl phosphate is bound within the active site as a bridging ligand between the two divalent cations. The diethyl phosphate dissociates from the active site and the binuclear metal center is subsequently recharged for another round of catalysis.

Experimental evidence for the direct interaction of the substrate with the β-metal ion comes from the x-ray structure of PTE bound with a diisopropyl methyl phosphonate inhibitor (PDB code 1EZ2) and the differential effects on the kinetic constants for the hydrolysis of phosphate and thiophosphate esters with zinc and cadmium substituted variants of PTE (*39*). Support for the weakening of the interaction of the bridging hydroxide with the β-metal ion is derived from the loss of antiferromagnetic coupling between the two metal ions in Mn/Mn-PTE upon binding of substrate analogues using EPR spectroscopy (*40*). The utilization of the hydroxide that is bridging the two metal ions as the direct nucleophile is supported by the observation that in the presence of substrate analogues there are no other water molecules bound to either of the two metal ions in Zn/Zn-PTE (PDB:3CAK).

General support for the reaction mechanism of **Scheme 2.2** was also provided by recent density functional theory (DFT) calculations by Chen *et al (66)*. A model of the PTE active site was devised based on the crystal structure of the wild-type Zn/Zn-enzyme (PDB code 1HZY). The calculations showed that the bridging hydroxide is sufficiently nucleophilic to attack the phosphorus center of organophosphate triester substrates. The barrier for the nucleophilic attack was calculated to be very feasible.

Recently, two provocative modifications to the mechanism presented in **Scheme 2.2** have been proposed (*41, 42*). In a computational assessment of the PTE reaction mechanism, Wong and Gao have postulated a mononuclear coordination scheme of protonated diethyl phosphate to the β-metal ion that is coupled with a lengthening of the metal-metal distance from 3.6 Å to 5.3 Å as the reaction proceeds from an enzyme-substrate complex to an enzyme-product complex (*41*). A representation of this product complex is provided in **Scheme 2.3**. In addition, Ollis and colleagues have proposed that the bridging hydroxide acts not as a nucleophile but as a base in the abstraction of a proton from a water molecule that is apparently loosely coordinated to the α-metal ion. The chemical mechanism and product complex proposed by Ollis and colleagues are illustrated in **Scheme 2.3** (*42*). Experimental support for this proposal derives primarily from an x-ray structure of a dimethyl thiophosphate complex of the PTE from *Agrobacterium radiobacter* and catalytic properties of model complexes that are purported to mimic the active site of PTE (*67*).

In this investigation, the structure of diethylphosphate bound to the active site of PTE was probed by X-ray diffraction techniques. This structure has been used to help

Scheme 2.2 The proposed mechanism of the hydrolysis of paraoxon by bacterial phosphotriesterase. The pink balls (●) represent zinc metal.

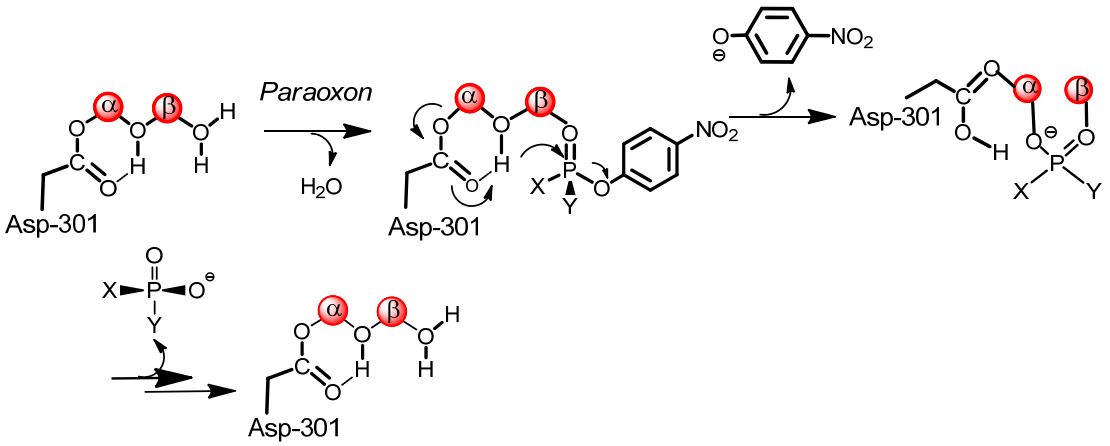

Scheme 2.3 Wong and Gao's and Ollis's proposed reaction mechanisms of the hydrolysis of organophosphotriesters by phosphotriesterase (*41, 42*). The pink balls (●) represent zinc metal.

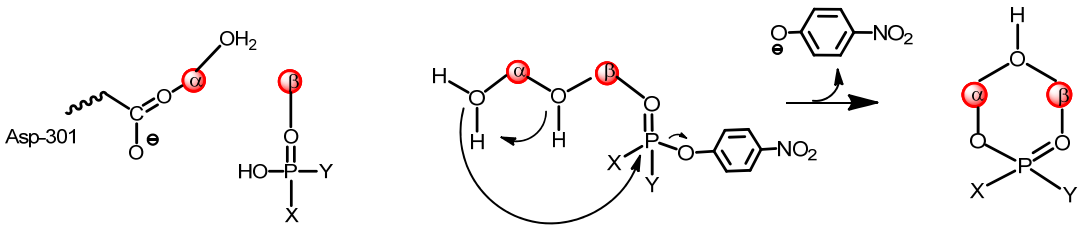

Gao product complex

Ollis mechanism and product complex

differentiate among the three mechanistic possibilities for the hydrolysis of organophosphate esters by PTE. In addition, we have performed DFT calculations to assess the energetic feasibility of the base mechanism proposed by Ollis and co-workers.

Materials and Methods

Purification of Wild-Type and G60A Mutant. The genes encoding the wild-type PTE (*opd*) and the G60A mutant were ligated between the *Nde*I and *Eco*RI sites of a pET20b (+) plasmid. The wild-type and mutant plasmids were transformed into *E. coli* strain BL-21 cells (DE3) (*64*). The transformed BL-21cells were inoculated in Luria-Bertani (LB) broth overnight at 37 ^{o}C. The overnight cultures were then incubated in Terrific Broth (TB) containing 100 μg/mL ampicillin and 1.0 mM $CoCl_2$ at 30˚C. IPTG was added when the OD_{600} reached 0.4, followed by incubation for 36-42 hours at 30 ˚C to reach the stationary phase. The cell paste was harvested by centrifugation at 4 °C. The wild-type PTE and G60A mutant were purified as previously described (*39*). SDS-polyacrylamide gel electrophoresis demonstrated that the wild-type PTE and the G60A mutant migrated with proteins having a molecular weight of ~36 kDa. The purity was estimated to be greater than 95%.

Measurement of Kinetic Constants. The kinetic parameters were obtained by fitting the data to equation 1, where *v* is the initial velocity, k_{cat} is the turnover number, [A] is the substrate concentration, E_t is the enzyme concentration, and K_a is the Michaelis constant. The inhibition constants, K_{ii} and K_{is}, for the noncompetitive inhibition of cacodylate in the presence of the substrate paraoxon, were determined by fitting the data to equation 2, where [I] is the concentration of inhibitor and the other constants have been defined previously. The concentration of paraoxon was varied from 0.05 mM to 2.5 mM. Six different cacodylate concentrations were used in these assays,

ranging from 0 mM to 250 mM. The rate was measured by following the change in absorbance at 400 nm.

$$\nu/E_t = k_{cat}\,[A] / (K_m + [A]) \quad (2.1)$$

$$\nu/E_t = k_{cat}\,[A]/(K_m\,(1 + ([I]/\,K_{is})) + [A](\,1 + ([I]/\,K_{ii}))) \quad (2.2)$$

Synthesis of Diethyl Phosphate. Diethyl phosphate was synthesized by Dr. Yingchun Li of Texas A&M University. Diethyl phosphorochloridate was reacted with phenol in ethyl ether in the presence of triethylamine to yield diethyl phenyl phosphate after purification using silica gel chromatography. Hydrogenation of the resulting organophosphate in methanol using Pd/C as a catalyst provided diethyl hydrogen phosphate quantitatively after separation of the catalyst by filtration and removal of the solvent by evaporation under reduced pressure(*68*). The identity and the purity (>98%) of the diethyl phosphate were confirmed by ^{1}H and ^{31}P NMR spectroscopy.

X-ray Structure Determination and Refinement. The G60A mutant was crystallized by hanging drop vapor diffusion at 21 ^{o}C by mixing 1 L of the protein with 1 L of reservoir solution (0.2 M magnesium acetate, 0.1 M sodium cacodylate (pH 6.5), 20% polyethylene glycol (PEG) 8000) and equilibrating over 1.0 mL of reservoir solution. X-ray data were collected on a MAR CCD 165 mm detector at the NSLS X3A beam line, using x-ray wavelength at 0.97904 Å and processed with HKL2000 (*69*). The G60A crystal exhibited diffraction consistent with the space group P_1 (a = 55.29 Å, b = 68.30 Å and c = 90.03 Å). There were four G60A molecules two homodimers of in the asymmetric unit.

The wild-type Co/Co-PTE was co-crystallized with 17 mM diethyl phosphate (DEP) in 0.1 M Bis-Tris (pH 6.5) and 20% PEG monomethyl ether 5000. X-ray data were collected on an R-Axis IV^{++} image plate detector using CuKα radiation from a Rigaku RU-H3R X-ray generator and processed using HKL2000 (*69*). The co-crystals of wild-type PTE with DEP exhibit diffraction consistent with space group P_1 (a = 43.29 Å, b = 45.34 Å and c = 78.91 Å). Two protein molecules are observed in the asymmetric unit.

The structures of G60A and wild-type PTE with bound DEP were determined by molecular replacement using program MOLREP using 1P6B and 2OB3 as initial search models, respectively (*70*). Solvent water molecules were built using Arp/ wArp (*71*). All subsequent model building and refinement was carried out with Coot (*72*) and REFMAC5 (*73*). The final models were refined to 1.95 and 1.83 Å with R_{work}/R_{free} of 0.167/0.224 and 0.140/0.196, respectively (**Table 2.1**). The crystallization, structure determination and refinement of the wild-type PTE and the G60A mutant were performed by Dr. Jungwook Kim from Albert Einstein College of Medicine.

Computational Details. All theoretical calculations were performed using the hybrid density functional theory (DFT) functional B3LYP (*74-76*). Geometry optimization were carried out with 6-31G(d,p) basis set for all elements except the Zn, for which the effective core potential LANL2DZ basis set was used. Based on these geometries, more accurate energies were obtained by performing single point calculations with the larger basis set 6-311+G(2d,2p) for all elements. Solvation effects were calculated at the same theory level as the optimizations by performing single point

Table 2.1 Data collection and refinement statistics

Data collection	**G60A-cacodylate**	**wild-type PTE-DEP**
Resolution, Å	31.64-1.95	20.49-1.83
Observed reflections	270,828	137,406
Unique reflections	91,515	47,158
Completeness	96.3(80.7)[1]	93.2(81.8)[1]
I/sigma	15.8 (3.4)[1]	13.2 (3.0)[1]
Rmerge[2]	0.076(0.286)[1]	0.061(0.319)[1]
Refinement	**G60A-cacodylate**	**wild-type PTE-DEP**
Protein nonhydrogen atoms	10,161	5,116
Water molecules	1,026	863
R_{cryst}[3]	0.164	0.141
R_{free}[3]	0.226	0.192
Average B-factor, (Å^2)		
Main chain	19.9	13.1
Side chains	22.4	15.0
Waters	28.2	14.0
RMSD from ideal geometry		
Bond length, Å	0.015	0.014
Bond angles, (°)	1.4	1.4

[1]Values in parentheses correspond to highest resolution shell 2.02 to 1.95 Å for G60A, 1.90 to 1.83 Å for wild-type PTE with DEP.

[2]$R_{merge} = \Sigma\Sigma j|Ij(hkl) - \langle I(hkl)\rangle|/\Sigma\Sigma j|\langle I(hkl)\rangle|$, where Ij is the intensity measurement for reflection j and <I> is the mean intensity over j reflections.

[3]$R_{cryst}/(R_{free}) = \Sigma||F_{obs}(hkl)| - |F_{calc}(hkl)||/\Sigma|F_{obs}(hkl)|$, where F_{obs} and F_{calc} are observed and calculated structure factors, respectively. No σ-cutoff was applied. 5% of the reflections were excluded from the refinement and used to calculate R_{free}.

calculations on the optimized structures using the CPCM method (*77-80*). The dielectric constant (ε) was chosen to be 4. Frequency calculations were performed at the same theory level as the optimizations to obtain zero-point energies (ZPE) and to confirm the nature of the stationary points. All calculations were performed using the Gaussian03 (*81*). This computational study was performed by Dr. Shi-Lu Chen and Dr. Fahmi Himo from Royal Institute of Technology at Sweden.

Results

Inhibition by Cacodylate. The kinetic constants of k_{cat}, k_{cat}/K_m, and K_m for the hydrolysis of paraoxon by Co/Co-G60A are 2900 s^{-1}, 1.34 x 10^7 M^{-1} s^{-1}, and 210 μM, respectively. The inhibition of Co/Co-G60A was measured using cacodylate as an inhibitor of paraoxon hydrolysis. The double reciprocal plots (data not shown) intersect to the left of the vertical axis and thus cacodylate is a noncompetitive inhibitor versus paraoxon. The kinetic inhibition constants, K_{is} and K_{ii}, determined from fits of the data to equation 2, are 260 ± 100 mM and 110 ± 10 mM, respectively.

Structure of G60A with Cacodylate. The crystals of G60A contain two homodimers in the asymmetric unit. As expected, two metal atoms were found in the active site for each monomer; however, an additional strong feature in the electron density was observed close to the binuclear metal center in all subunits during the refinement. The tetrahedral electron density appeared to interact directly with both zinc atoms and was consistent with cacodylate. The average B-factors for main chain protein atoms and cacodylate are 20.52 and 20.70 $Å^2$, respectively. Cacodylate is bound to both

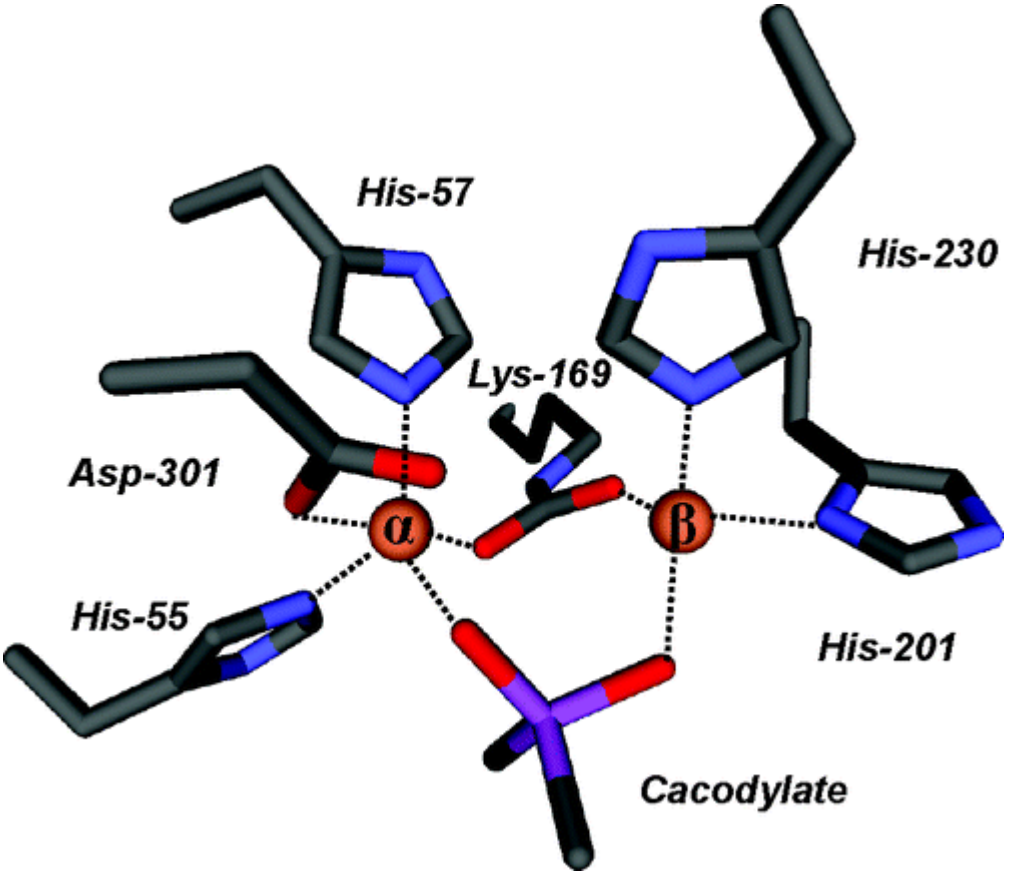

Figure 2.2 Model for the active site of Co/Co-PTE hybrid (mutant G60A) obtained from crystals grown in the presence of cacodylate.

metal ions with an average distance of 1.98 ± 0.03 and 2.07 ± 0.06 Å to the α- and β-metal, respectively. The α-metal ion is coordinated to His-55, His-57, and Asp-301 whereas the β-metal ion is coordinated to His-201 and His-230. An image of these interactions is presented in **Figure 2.2**. The cacodylate ligand has replaced the bridging hydroxide that has been observed in a number of PTE structures (*24*). No water molecules are observed to interact with either metal ion in any of the four molecules in the asymmetric unit of the G60A structure. In addition to zinc, cacodylate is within hydrogen bonding distance of Trp-131, the carboxylated Lys-169, His-201, and Asp-301.

Structure of Wild-Ttype PTE with Diethyl Phosphate. Diethyl phosphate (DEP) is the hydrolysis product of paraoxon, the best known substrate for PTE. Various concentrations of DEP, as high as 100 mM, were tested for co-crystallization with wild-type PTE before an optimized condition was determined. In the co-crystals, electron density for DEP was unambiguously located around the binuclear metal site in one subunit. However, the lack of electron density corresponding to one of the two ethyl groups within the ligand was observed in the second subunit. The electron density was modeled as mono ethyl phosphate during the refinement for this subunit. The phosphoryl oxygen atom, which is not coordinated to either metal, is relatively solvent exposed and the ethyl group occupies a more buried hydrophobic pocket. Subsequent NMR experiments showed that the initial concentration of mono ethyl phosphate in the sample of diethyl phosphate was negligible (<1%), and the enzymatic hydrolysis of DEP by PTE was beyond the detection limit even after incubation of PTE with DEP for 5

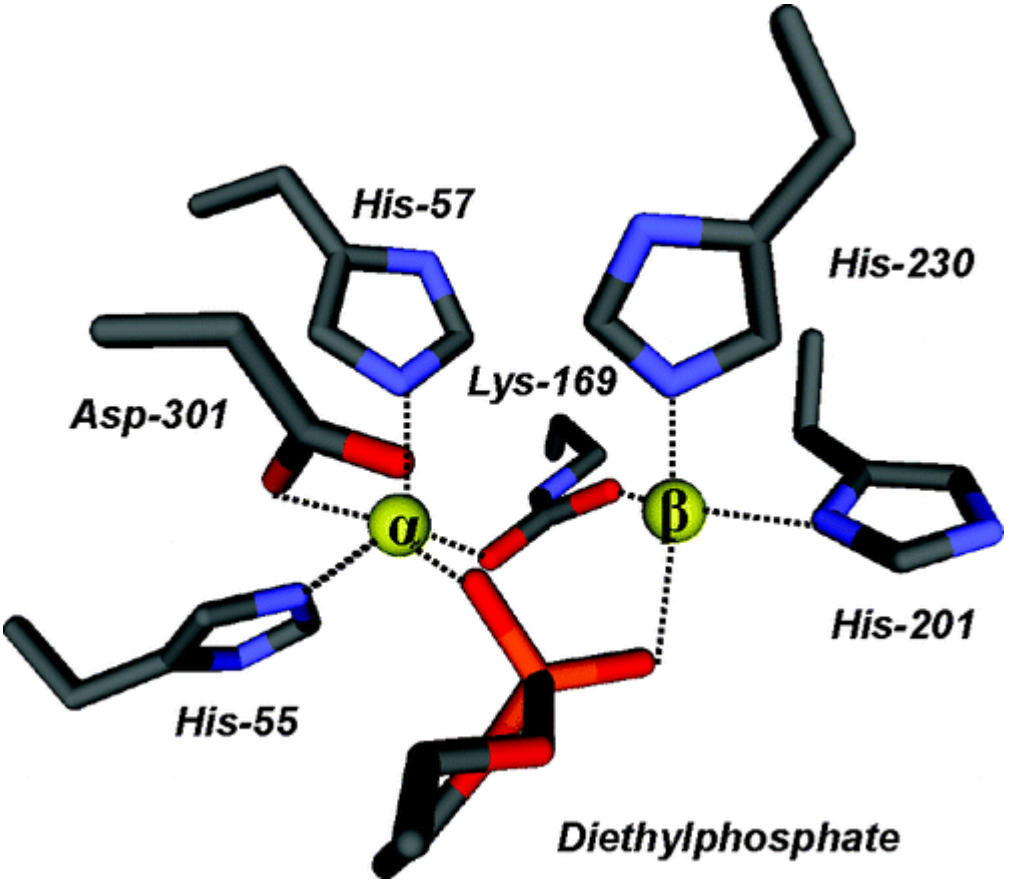

Figure 2.3 Model for the active site of wild-type Co/Co-PTE from crystals grown in the presence of diethylphosphate.

days (data not shown). These observations suggest that the ethyl group of the second DEP is not observed due to disorder.

With the exception of the missing ethyl group, both ligands of DEP bind in a very similar manner within the binuclear metal center. Therefore, the following discussion will refer only to the first subunit that contains the fully modeled DEP. One of ethyl groups orients toward a hydrophobic patch, composed of Gly-60, Ile-106, Trp-131, and Leu-303. The other ethyl group is more solvent exposed and forms hydrogen bonds through the phosphate ester oxygen with two water molecules. One of the phosphoryl oxygen atoms of DEP is 1.97 Å away from α-metal ion while the other oxygen is 2.17 Å away the β-metal. The orientation of diethyl phosphate within the active site of PTE is presented in **Figure 2.3**. These distances are similar to the orientation of cacodylate in the G60A PTE structure. Moreover, there is no bridging water observed in the binuclear metal site, as a result of the complete displacement by DEP. The DEP ligand is within hydrogen bonding distance from *N*ε1 of Trp-131, carboxy oxygen atoms of the carboxylated Lys-169, and carboxy oxygen atoms of Asp-301. $N_{\delta 1}$ of His-201 is slightly further away from DEP (3.39 Å) in the structure of the wild-type enzyme than from cacodylate (3.19 Å) in the G60A structure.

DFT Calculations. To examine the feasibility of the base mechanism proposed by Ollis and co-workers (*42*), we have performed DFT calculations using the same model of the Zn/Zn-enzyme active site as in the previous calculations (*66*). The model is based on the high resolution crystal structure of wild-type Zn/Zn-PTE from *P. diminuta* (PDB code: 1HZY) and consists of the two zinc ions and their first shell

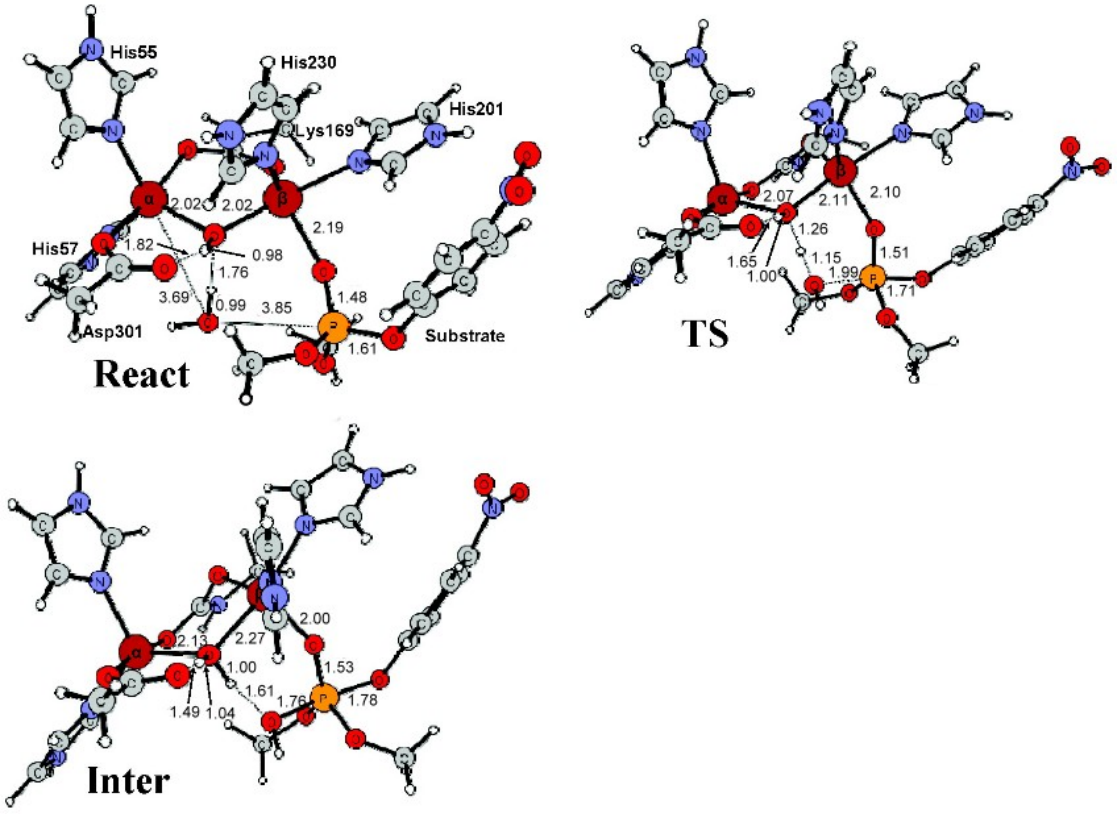

Figure 2.4 Optimized geometries of the Zn/Zn−PTE active site model with dimethyl 4-nitrophenyl phosphate and a water molecule bound (React), the transition state for the water attack on the phosphorus (TS), and the resulting pentacoordinate intermediate (Inter). Distances are in angstroms.

ligands, including the bridging hydroxide, the four histidines (His-55, His-57, His-201, His-230), the Asp-301, and the carboxylated Lys-169. Hydrogen atoms were added manually and the ligands were truncated so that in principle only side chains were kept in the model. The histidines were thus represented by imidazoles, the aspartate by an acetate, and the carboxylated lysine by a carboxylated methylamine (see **Figure 2.4**). Dimethyl-4- nitrophenyl phosphate was chosen as a model substrate, as in the previous study (*66*). The water molecule, postulated to be the nucleophile in the base mechanism, was added to the model. The model consists thus of 85 atoms and has a total charge of +1.

In the reactant species (**Figure 2.4**, **React**), the phosphoryl oxygen of the substrate binds to the more solvent-exposed β-Zn site and the leaving group is located at the position opposite to the bridging hydroxide. According to the base proposal, the nucleophilic water molecule is bound to the α-Zn. In the calculations, we first placed the water molecule there, but we could not locate a stable conformation with the water bound to the α-Zn. Instead, it dissociates from the Zn during the optimization and forms a hydrogen bond to the bridging hydroxide (see **Figure 2.4**, **React**). From these calculations it can thus be concluded that a hexacoordinate α-Zn is quite unlikely.

We have furthermore optimized the transition state for the nucleophilic attack with the bridging hydroxide acting as a base. The optimized structure is displayed in **Figure 2.4** with important distances indicated. The critical distance between the water oxygen to the phosphorus center (O_W-P) is 1.99 Å. Simultaneously with the O_W-P bond formation, one proton of water molecule is transferred to the bridging oxygen, indicating

that the bridging hydroxide serves as the general base to activate the attacking water. This attack results in the penta-coordinate intermediate shown in **Figure 2.4**. The barrier and reaction energy for this step are calculated to be +17.3 and +13.3 kcal/mol, respectively. The barrier for the base mechanism is thus significantly higher than the previously calculated barrier where the bridging hydroxide is the nucleophile (11.7 kcal/mol, 10). These findings provide thus additional evidence that the bridging hydroxide acts as a nucleophile and not as a general base in the Zn/Zn-PTE reaction.

Discussion

Enzyme-Product Complexes with PTE. The X-ray crystal structures of the diethyl phosphate product complex and an inhibitor complex with cacodylate has been determined with the phosphotriesterase from *P. diminuta*. The structures of these two complexes were elucidated in an attempt to provide experimental support for recent variations in the reaction mechanism that have been postulated for this enzyme (*41, 42*). With the diethyl phosphate product, the ligand is found bridging the two divalent cations as illustrated in **Figure 2.3**. The two metal ions are separated by a distance of 4.0 Å, where one of the negatively charged phosphate oxygens of the product is 2.1 Å from the α-metal ion while the other oxygen is 1.9 Å from the β-metal ion. There are no water molecules associated with either metal within a distance of 5.4 Å. The distances are summarized in **Figure 2.5**. The symmetrical bridging observed in this complex differs from the prediction of this structure based upon the calculations of Wong and Gao (*41*).

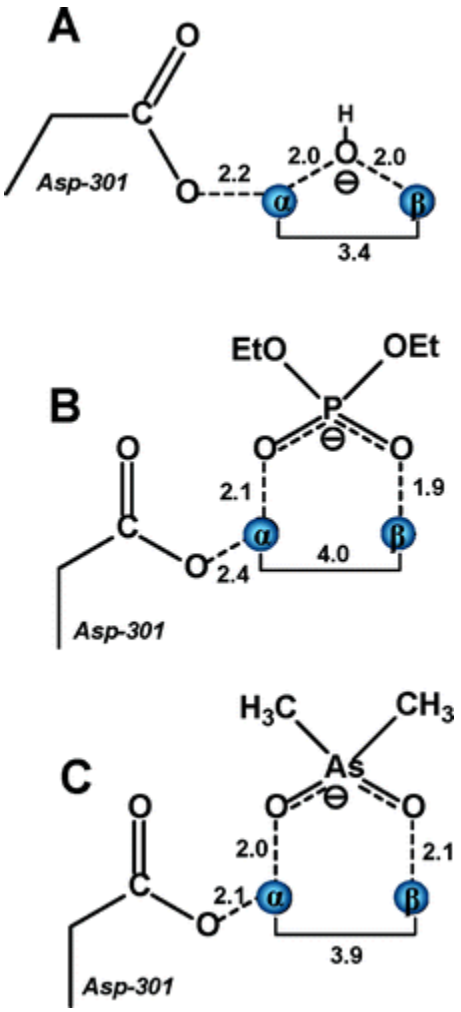

Figure 2.5 Schematic representations of the binuclear metal centers of the binuclear metal centers from the Co/Co−PTE hybrid in the presence and absence of diethyl phosphate and cacodylate. (A) Zn/Zn−PTE hybrid in the absence of added ligands (PDB entry 1HZY). (B) Co/Co−PTE hybrid in the presence of added diethyl phosphate (PDB entry 3CAK). (C) Co/Co−G60A PTE hybrid in the presence of cacodylate (PDB entry 2O4Q).

They have postulated that the diethyl phosphate product would be bound asymmetrically to the binuclear metal center with exclusive coordination to the β-metal ion and a metal-metal separation of 5.3 Å. It is unclear from the structure determined here whether or not the carboxylate side chain of Asp-301 is protonated or not. However, the distance of the nearest carboxylate oxygen of Asp-301 is found 2.4 Å from the α-metal ion in the diethyl phosphate complex compared with a distance of 2.5 Å in the unliganded complex (*39*). In any event, the structure of diethyl phosphate bound to PTE determined here is consistent with the complex proposed by Aubert *et al*. (*39*). There is no indication that the two divalent cations can be separated by a distance that approaches that of 5.3 Å predicted by Wong and Gao. The experimentally determined complex resembles that of a highly symmetric bridge with nearly equal distances between each metal ion and the nearest phosphate oxygen.

A nearly identical structure is observed in the complex with the cacodylate anion (**Figure 2.3**). The G60A mutant has kinetic constants nearly identical to those of the wild-type enzyme for the hydrolysis of paraoxon but is more stereoselective for the hydrolysis of substrates with larger substituents attached to the phosphorus core (*44, 82-84*). Cacodylate is an analogue of the diethyl phosphate product since it bears a single negative charge within a tetrahedral architecture. The coordination geometry of this ligand to the binuclear metal center is nearly symmetric with oxygen-metal distances of 2.0 and 2.1 Å to the α- and β-metal ions respectively. There are no water molecules coordinated to either metal within a distance of 3.0 Å.

The coordination geometry of the diethyl phosphate and cacodylate bound to the binuclear metal center of PTE is not consistent with the mechanism for phosphotriester hydrolysis proposed by Jackson *et al (42).* For the phosphotriesterase isolated from *A. radiobacter* it has been postulated that the bridging hydroxide acts not as a nucleophile but as a general base in the abstraction of a proton from a water molecule coordinated to the α-metal ion. The primary experimental support for this conjecture stems from the determination of the structures of diethyl thiophosphate and dimethyl thiophosphate bound to the active site of the PTE from *A. radiobacter (42, 67)*. These structures reveal a bridging complex for either thiophosphate product plus the coordination of an additional bridging hydroxide. These complexes are consistent with the mechanism illustrated depicted in **Scheme 2.3**. However, to the best of our knowledge, there have been no crystal structures of PTE, or any other member of the amidohydrolase superfamily, where the α-metal ion is 6-coordinate with an additional water molecule that could function as the primary nucleophile. Thus, experimental support for an additional water molecule that is activated by the bridging hydroxide is lacking. The identities of the metal ions bound to the PTE from *A. radiobacter* are also different from the PTE from *P. diminuta*. The structure of this enzyme was determined with Fe in the α-position and Zn in the β-position. Hexacoordinate zinc complexes are extremely rare and thus it seems quite unlikely that the PTE from *P. diminuta* could function in the manner as proposed by Ollis and coworkers. The DFT calculations presented here give further support to this conclusion. It was not possible to optimize a structure in which an additional water molecule is bound to the R-Zn atom and the barrier for the base

mechanism is calculated to be significantly higher than that for the nucleophile mechanism.

Product Complexes in the Amidohydrolase Superfamily. X-ray crystal structures have been determined for other members of the amidohydrolase superfamily (*23*). It seems reasonable to assume that for those enzymes in this superfamily that contain a binuclear metal center that many aspects of the chemical reaction mechanisms would be quite similar to one another. Structures of these enzymes, determined in the presence of their respective hydrolysis products, should illuminate whether or not the diethyl phosphate structure, determined for PTE, provides a common mechanistic or structural theme for the rest of the amidohydrolase superfamily.

Isoaspartyl dipeptidase (IAD) catalyzes the hydrolysis of amide bonds formed with the side chain carboxylate of aspartic acid (*85*). A 2.1 Å resolution structure of this enzyme has been determined in the presence of aspartate, the reaction product (*86*) . A representation of the structure is illustrated in **Figure 2.6** showing the bound aspartate. The carboxylate side chain is found bridging the two zinc atoms within the active site in a somewhat asymmetric arrangement. The two metal ions are separated by a distance of 3.8 Å. The carboxylate oxygen nearest the α-metal is separated by a distance of 2.8 Å while the other oxygen is 2.3 Å away from the β-metal ion. There are no other water molecules within 4.1Å of either metal ion. A similar complex is also observed in the structure of acetate bound within the active site of D-aminoacylase (**Figure 2.6**). This enzyme catalyzes the hydrolysis of the amide bond of N-acetyl-Damino acid derivatives (*87, 88*). This particular enzyme requires a divalent cation bound to the β-site but is less

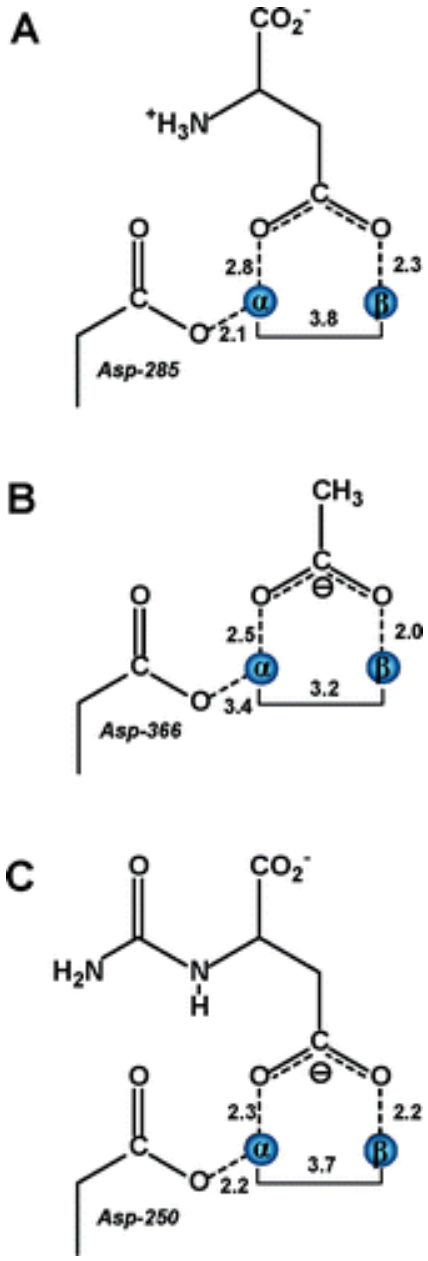

Figure 2.6 Schematic representations of the binuclear metal centers for isoaspartyl dipeptidase, d-aminoacylase, and dihydroorotase in the presence of bound reaction products. (A) Isoaspartyl dipeptidase in the presence of aspartic acid (PDB entry 1ONX). (B) d-Aminoacylase in the presence of acetate (PDB entry 1M7J). (C) Dihydroorotase in the presence of carbamoyl aspartate (PDB entry 1J79).

particular about the requirement for the occupancy of α metal ion at the α-site. In any event, the coordination of acetate to the active site shows that the two metal ions are 3.2 Å from one another. One of the oxygens of the bound acetate is 2.5 Å from the α-metal whereas the other oxygen is 2.0 Å from the β-metal. There are no other water molecules that are bound to either metal ion.

Dihydroorotase catalyzes the reversible interconversion of carbamoyl aspartate and dihydroorotate in the biosynthetic pathway for the assembly of pyrimidine nucleotidess. When the structure of this enzyme was determined in the presence of added dihydroorotate it was found, quite remarkably, that in one subunit of the dimer dihydroorotate was bound, while in the adjacent subunit carbamoyl aspartate was bound. Thus the structure of this enzyme-substrate/product complex provided a nearly unprecedented view of the reaction immediately before and after the chemical reaction had been catalyzed. In the complex with the bound carbamoyl aspartate the two zinc atoms are separated by a distance of 3.7 Å. One of the carboxylate oxygens is 2.3 Å away from the α-metal ion while the other oxygen is 2.2 Å away from the β-metal ion (*89*). Thus, the bridging complex is symmetric and there are no other visible water molecules that could function as the nucleophile in the complex with dihydroorotate.

Conclusion

The structure of PTE from *P. diminuta* has been determined in the presence of the hydrolysis product diethyl phosphate and a product analogue, cacodylate. In either structure the complex is formed as a bridging ligand between the two divalent cations is

a symmetric orientation where the average oxygen-metal distance is 2.0 Å. The average metal-metal separation in this complex is 3.9 Å, compared with 3.4 Å in the unliganded complex. In either structure there is no evidence for the additional binding of hydroxide to either of the two divalent cations. These results provide strong experimental support for the coordination geometry of the reaction product, originally postulated by Aubert *et al*. and illustrated in **Scheme 2.2**. The enzyme-product complex, predicted by Wong and Gao to be asymmetrically associated with only the β-metal ion coupled with a metal-metal separation of 5.3 Å, is not supported by these results (*41*). The structures presented in this paper are also at variance with the proposed mechanism postulated by Ollis and coworkers (*42, 67*). In the complex with diethyl phosphate there is no evidence for the binding of an additional hydroxide as a bridging ligand between the two divalent cations. These results support the computational assessment of the reaction mechanism of PTE which have concluded that the bridging hydroxide is sufficiently nucleophilic to attack the phosphorus center of organophosphate triester substrates (*66, 90*). The formation of product complexes with the simultaneous complexation of hydroxide and product in the active site of PTE from *A. radiobacter* are likely the result of iron occupying the α-metal ion site of that enzyme.

CHAPTER III

STEREOSELECTIVE DETOXIFICATION OF ORGANOPHOSPHATE NERVE AGENT ANALOGUES BY BACTERIAL PHOSPHOTRIESTERASE

Introduction

Organophosphorus compounds have been utilized for more than 50 years as insecticides for the protection of agricultural crops (*91*). Similar compounds have been developed as chemical warfare agents (*48*). The structures for some of these compounds are presented in **Scheme 3.1** including tabun (GA), sarin (GB), soman (GD), cyclosarin (GF), VX and rVX. GA contains a cyanide leaving group, while the three other G-agents (GB, GD, and GF) have a fluorine leaving group and the two versions of VX contain a thiolate leaving group. The primary toxicity of organophosphorus compounds is due to the inhibition of acetylcholinesterase (AChE). AChE is an enzyme that catalyzes the hydrolysis of acetylcholine at neural synapses through the phosphorylation of an active site serine residue (*92*). GA, GB, GF, VX, and rVX contain a chiral phosphorus center and thus each of these nerve agents has two stereoisomers, while soman has four stereoisomers due to an additional chiral center within the pinacolyl substituent. The enantiomers are different in toxicity. The S_p-stereoisomer of sarin reacts with AChE approximately ~10^4 times faster than the R_p- stereoisomer and the S_p-stereoisomers of soman react ~10^5 times faster than the R_p-isomers. Similarly, the S_p-stereoisomer of VX is 100-fold more toxic than is the R_p- stereoisomer (*48*).

Scheme 3.1 The chemical structures of the organophosphate nerve agents, tabun (GA), sarin (GB), soman (GD), cyclosarin (GF), VX and rVX.

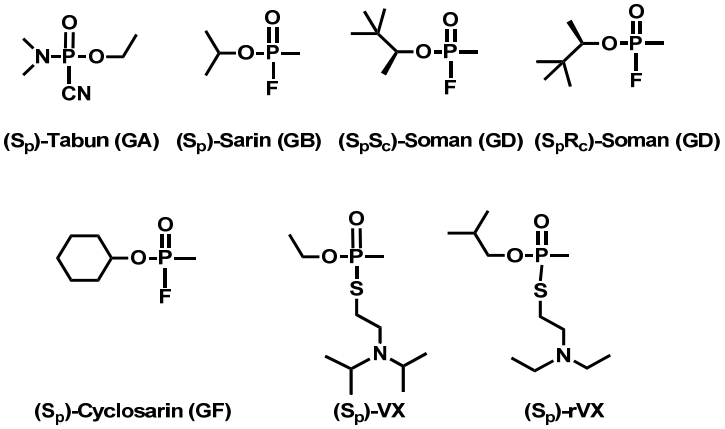

The detoxification of the organophosphorus nerve agents has been accomplished through the utilization of organophosphate degrading enzymes such as the human paraoxonase 1 (PON1), squid DFPase, organophosphorus acid anhydrolase (OPAA), and phosphotriesterase (PTE). Human paraoxonase is capable of hydrolyzing GB, GD, and VX but the overall catalytic activity is relatively low (*52*). DFPase, isolated from *Loligo vulgaris*, is able to hydrolyze GA, GB, GD, GF, and DFP. The values of k_{cat} and k_{cat}/K_m for the hydrolysis of DFP are 526 s^{-1} and 1.3 x 10^6 M^{-1} s^{-1}, respectively, but the catalytic activities towards the hydrolysis of GB and GD are significantly lower (*50, 51*). Organophosphorus acid anhydrolase (OPAA) from *Alteromonas* sp. JD6.5 is a member of a family of enzyme that is capable of hydrolyzing a wide variety of organophosphorus compounds, including GB, GD and GF but not VX (*53*). Phosphotriesterase was first isolated from soil microbes *(93)*. The best substrate for PTE is the agricultural pesticide paraoxon and the value for k_{cat}/K_m approaches the diffusion controlled limit of ~ 10^8 M^{-1}

s^{-1} (*64*). The enzymatic reaction for the hydrolysis of paraoxon to *p*-nitrophenol and diethyl phosphate is shown in **Scheme 3.2.** The substrate specificity of PTE is quite broad and it is capable of hydrolyzing GA, GB, GD, GF, and VX (*58*). PTE is reported to be one of the few enzymes capable of hydrolyzing the P-S bond in the nerve agents VX and rVX (*94*).

Scheme 3.2 The chemical reaction for the hydrolysis of paraoxon catalyzed by the PTE.

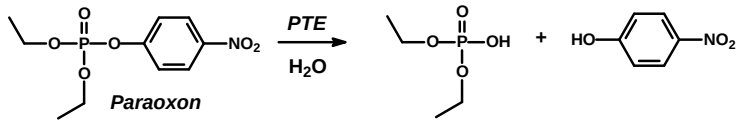

PTE is a homodimeric protein that contains a binuclear metal center embedded within an $(\beta/\alpha)_8$ barrel structure and is a member of the amidohydrolase superfamily (*24*). The native enzyme contains two Zn^{2+} ions that can be substituted with Cd^{2+}, Co^{2+}, Ni^{2+}, and Mn^{2+} without loss of catalytic activity (*64*). The two metals are bridged by a carboxylated lysine (Lys-169) and a hydroxide ion. The more solvent-shielded metal (M_α) is coordinated to His-55, His-57, and Asp-301. The more solvent-exposed metal (M_β) is coordinated to His-201 and His-230. Previous investigations have identified three binding subsites within the active site of PTE. These include a small, a large and a leaving-group pocket (*37*). The small pocket is defined by the side chains of Gly-60, Ile-106, Leu-303, and Ser-308. The large pocket is formed by His-254, His-257, Leu-271, and Met-317. The leaving group pocket is surrounded by four residues: Trp-131, Phe-132, Phe-306, and Tyr-309. The substrate binding site of PTE is graphically shown in **Figure 3.1**.

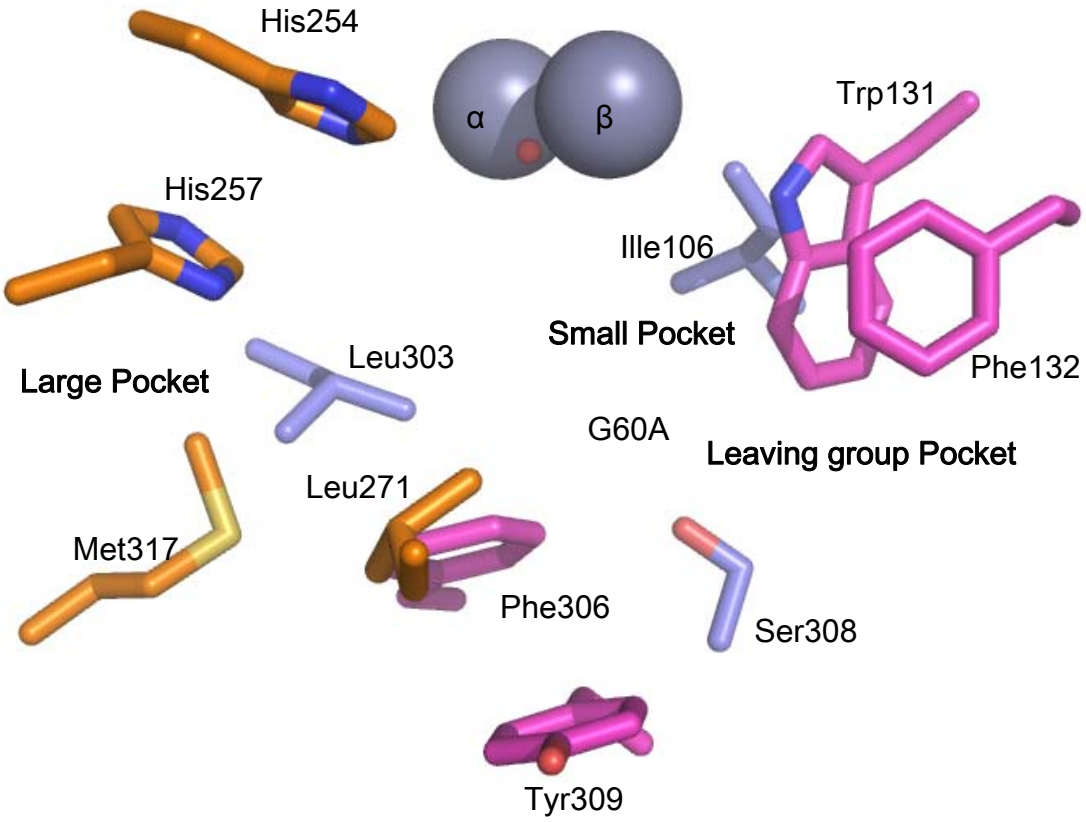

Figure 3.1 Graphic representation of the binding pockets within the active site of PTE. The small pocket consists mainly of Gly-60, Ile-106, Leu-303, and Ser-308. The large pocket primarily contains His-254, His-257, Leu-271, and Met-317. The leaving group pocket is surrounded by Trp-131, Phe-132, Phe-306, and Tyr-309 (*37*).

The wild-type PTE is stereoselective for the hydrolysis of chiral organophosphates (*44, 95, 96*). The degree of stereoselectivity depends on the specific substituents attached to the central phosphorus core. For example, the wild-type PTE hydrolyzes the S_p-enantiomer of methyl phenyl 4-acetylphenylphosphate approximately two orders of magnitude faster than the R_p-enantiomer (*96*). In addition, the active site has been shown to be susceptible for manipulation of the stereoselectivity through the mutation of residues that contact the substrates prior to catalytic turnover. The G60A mutant hydrolyzes the S_p-enantiomer of methyl phenyl 4-acetylphenylphosphate about 5 orders of magnitude faster than the R_p-enantiomer and thus the stereoselectivity can be significantly enhanced (*96*). Unfortunately, the inherent stereoselectivity of the wild-type PTE does not match that of AChE. It preferentially hydrolyzes the less toxic enantiomer of chiral organophosphates (*45*). However, it has been demonstrated that the stereoselectivity of the wild-type PTE can be inverted through multiple mutations to the small and large pockets in the active site. For example, the I106G/F132G/H257Y mutant catalyzes the hydrolysis of the R_p-enantiomer of methyl phenyl 4-acetylphenylphosphate about 3 orders of magnitude faster than the S_p-enantiomer (*96*). This represents a change in stereoselectivity of 8 orders of magnitude relative to the G60A mutant with only four amino acid changes.

In this chapter, we describe the synthesis of chiral analogues of GB, GD, GF, VX, and rVX with a 4-acetylphenol leaving group (**Scheme 3.3**). We have utilized these compounds to identify mutants of PTE that are enhanced in their ability to hydrolyze the

more toxic S_p- enantiomers. In the following chapter we describe the crystal structures and molecular dynamics calculations of a subset of the more optimized mutants in an attempt to correlate the changes in active site structure with changes in the catalytic properties of the various mutant enzymes.

Scheme 3.3 The chemical structures of organophosphonate nerve agent analogues.

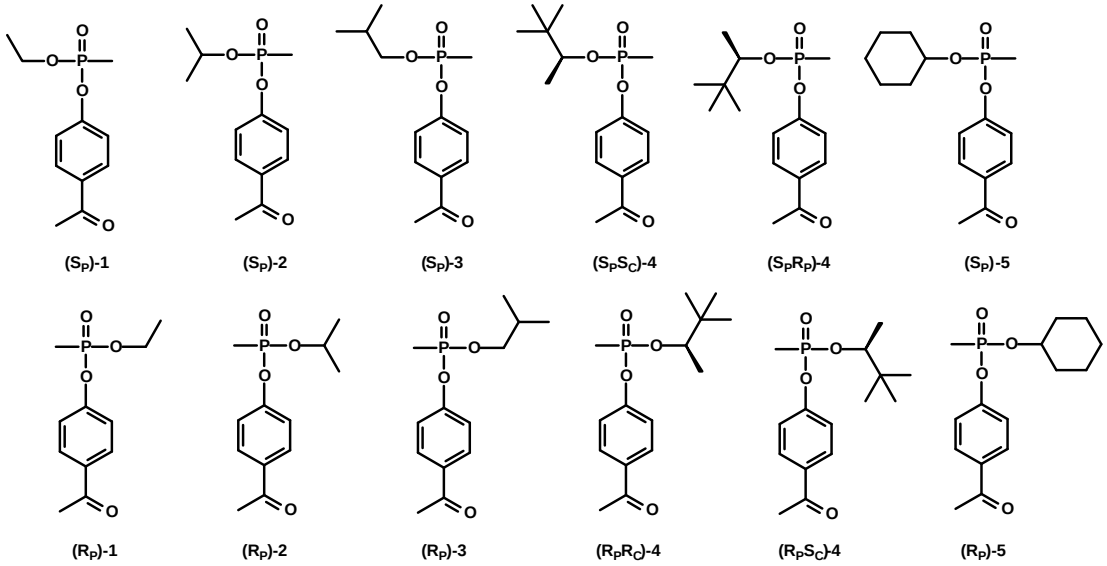

Materials and Methods

Materials. Racemic mixtures and the isolated S_p- and R_p- enantiomers of the organophosphonate compounds shown in **Scheme 3.3** were synthesized by Dr. Yingchun Li. *Escherichia coli* (DE3) and XL1-blue cells were purchased from Stratagene. The expression plasmid pET20b (+) was obtained from Invitrogen. The bacterial phosphotriesterase and the site-directed mutants (G60A, I106G, F132G, S308G, I106G/H257Y, I106G/F132G/H257Y, I106A/F132A/H257Y, I106A/H257Y/S308A, and H254G/H257W/L303T) were purified to homogeneity as

previously described (*44, 95, 97*). The H254Q/H257F mutant was discovered by creating a H254X/H257X library based on the wild-type PTE sequence as the template (*59*). The H257Y/L303T mutant was found using a H254X/H257X library based with the L303T mutant as the parental template (*98*). The H254Q/H257F mutant was isolated as a more active variant by screening the VX analogue, dementon-S. The H257Y/L303T mutant was isolated as an improved variant from screening the S_p- enantiomers of GB and GD analogues.

Expression, Growth, and Preparation of Wild-Type and Mutant Enzymes. The gene for the expression of PTE (opd) was cloned between the *Nde*I and *EcoR*I sites of a pET20b (+) plasmid. The plasmids for the expression of the wild-type and mutant enzymes were transformed into the *E. coli* strain BL-21 cells (DE3) (*64*). The transformed BL-21cells were inoculated in Luria-Bertani (LB) broth overnight at 37 °C. The overnight cultures were then incubated in Terrific Broth (TB) containing 100 μg/mL ampicillin and 1.0 mM $CoCl_2$ at 30 °C. The expression of PTE was induced by the addition of 1.0 mM IPTG when the OD_{600} reached 0.4. The cells were harvested at 4 °C by centrifugation at 6,000 rpm after allowing the culture to reach stationary phase after 36-42 hours at 30 °C. All subsequent steps were carried out at 4 °C (or on ice). When the wild-type and mutants of PTE were purified, the cells were suspended with 10 mM HEPES buffer, pH 8.5, and lysed with a 5-s pulsed sonication for 24 min at 0 °C at medium power setting using a Heat System-Ultrasonics, Inc. (Farmington, NY) model W830 ultrasonic processor. The lysed cell suspensions were combined and centrifuged at 13,000 rpm for 15 min. The supernatant was decanted, and then a solution of

protamine sulfate (2% w/v) was added dropwise over a 20-min period while stirring until the protamine sulfate concentration reached 0.4%. The mixture was allowed to stir for an additional 20 min before centrifugation at 13,000 rpm. The supernatant solution was then subjected to ammonium sulfate fractionation by the addition of solid ammonium sulfate to 60% saturation (371 mg/mL of protein solution) while stirring for 45 min. The pellet was collected by centrifugation at 13,000 rpm for 30 min and the protein was recovered by resuspending the pellet in buffer. The protein was loaded onto a gel filtration column containing Ultrogel AcA 54 (IBF, Columbia, MD) and eluted at a flow rate of 1.0 mL/min. The fractions were pooled based on enzymatic activity and absorbance at 280 nm. The pooled fractions were then loaded to a column containing DEAE-Sephadex A-25 previously equilibrated with 10 mM HEPES buffer, pH 8.5. SDS-polyacrylamide gel electrophoresis demonstrated that all of the mutant enzymes were the same size as the wild-type PTE and that the purity of all proteins was greater than 95%.

Spectrophotometric Enzyme Assays. The kinetic constants for each substrate were determined by monitoring the formation of *para*-acetylphenol at 294 nm ($\varepsilon = 7710$ $M^{-1}cm^{-1}$) at 30 °C using a SpectraMax plate reader (Molecular Devices Inc., Sunnyvale CA). The assay mixtures contained 50 mM CHES buffer pH 9.0, 100 μM $CoCl_2$, and various concentrations of substrates. The reactions were initiated by the addition of enzyme. Due to the limited solubility of compounds **4** and **5**, 10% methanol (v/v) was added to the assay mixtures for these compounds.

Data Analysis. The kinetic constants (k_{cat} and k_{cat}/K_m) were obtained from a fit of the data to equation 1, where *v* is the initial velocity, k_{cat} is the turnover number, [A] is the substrate concentration, E_t is the enzyme concentration, and K_m is the Michaelis constant.

$$v / E_t = k_{cat} [A] / (K_m + [A]) \quad (3.1)$$

Results

Selection of Mutants. The residues in the binding pocket were selected as targets for the mutations. The smallest residue in the small pocket of PTE, Gly-60, was mutated to alanine in order to explore the effect of the size reduction of the small pocket. To investigate the enlargement of the small pocket or the leaving group pocket, the residues, Ile-106 and Ser-308, in the small pocket, and Phe-132 in the leaving group pocket, were mutated to glycine as single site mutants of PTE. Other mutants contain alternations of both the small and the large pockets. The size of the small pocket was enlarged and the size of the large pocket was decreased, or the configuration of the large pocket was adjusted. All of the mutants were expressed in *E. coli* and purified for measurement of catalytic activity. The kinetic parameters of the wild-type and the mutants of PTE towards the compounds that appear in **Scheme 3.3** are shown in **Tables 3.1** and **3.2**. The stereoselectivity of the wild-type and each mutant towards the chiral enantiomers are shown in **Table 3.3**.

The Catalytic Activity and the Stereoselectivity of the Wild-Type PTE. The k_{cat} and k_{cat}/K_m values for the wild-type PTE towards compounds **2**, **3**, **4** and **5** illustrate the

Table 3.1 Maximum velocity (s^{-1}) for the wild-type and mutants of PTE.

	WT	G60A	I106G	F132G	S308G	H254Q/ H257F	H257Y/ L303T	I106G/ H257Y	I106G/ F132G/ H257Y	I106A/ F132A/ H257Y	I106A/ H257Y/ S308A	H254G/ H257W/ L303T
R_p/S_p-**1**	3.9e2	1.6e2	1.8e2	1.8e2	ND[a]	3.8e1	1.7e2	4.8e2	1.5e2	7.9e2	2.3e3	2.7e2
R_p-**1**	1.5e2	1.3e2	6.8e1	6.8e1	1.1e2	1.7e2	7.3e0	8.9e1	3.4e1	ND	2.0e2	1.4e1
S_p-**1**	6.7e2	1.1e2	3.0e2	3.0e2	2.9e2	3.2e1	4.1e2	6.8e2	3.5e2	9.0e2	1.4e3	1.9e2
R_p/S_p-**2**	9.7e1	1.1e2	3.9e1	2.9e1	1.8e2	1.2e1	3.2e2	5.9e1	5.3e1	1.6e2	6.5e2	1.2e2
R_p-**2**	1.0e2	1.2e2	4.0e1	3.9e1	2.5e2	4.8e1	1.8e1	4.7e1	ND	4.5e1	1.3e2	ND
S_p-**2**	4.0e1	7.4e0	2.8e1	1.6e1	1.5e1	7.2e0	3.7e2	1.0e2	4.8e1	5.1e2	3.4e2	9.2e1
R_p/S_p-**3**	5.4e1	4.7e1	4.9e1	3.5e1	1.2e2	1.1e1	1.3e2	4.7e2	ND	6.3e2	6.7e2	4.7e1
R_p-**3**	9.3e1	3.7e1	3.1e1	2.8e1	1.1e2	7.0e1	5.1e1	8.4e0	ND	ND	2.2e1	2.0e1
S_p-**3**	2.2e1	ND	4.8e1	2.5e1	1.2e1	6.3e0	1.0e2	2.1e2	2.3e2	2.3e2	5.3e2	5.0e1
R_pR_c/R_pS_c $/S_pR_c/S_pS_c$-**4**	2.1e0	4.1e0	1.2e0	ND	1.1e0	1.3e0	2.4e0	2.4e-1	2.9e-2	4.3e-1	1.1e0	1.8e1
R_pR_c/S_pR_c-**4**	2.5e0	3.9e0	ND	ND	2.5 e0	8.2e-1	3.0e0	4.8e-1	4.2e-2	5.0e-1	7.8e-1	1.1e1
R_pS_c/S_pS_c-**4**	6.1e-1	1.3e0	9.0e-2	1.3e-1	4.2e-1	4.2e-1	8.0e-1	1.6e-2	4.1e-2	1.1e-1	1.4e-1	4.6e0
R_pR_c-**4**	3.4e0	8.5e0	3.3e0	1.2e1	2.2 e0	5.5e-1	4.1e-1	7.6e-2	4.9e-2	5.0e-2	1.7e-1	2.0e0
R_pS_c-**4**	4.5e-1	1.5e0	1.5e-1	1.5e-1	6.2e-1	1.7e-1	ND	6.5e-2	5.5e-3	ND	4.2e-2	2.1e-1
S_pR_c-**4**	7.7e-1	9.5e2	5.0e-2	3.2e-1	5.0e-1	6.3e-1	6.3e0	3.7e-2	1.6e-1	7.4e-1	1.0e0	1.2e1
S_pS_c-**4**	1.6e-2	ND	ND	1.2e-1	1.2e-1	3.3e-1	2.1e0	2.2e-2	5.3e-2	2.4e-1	3.5e-1	2.9e0
R_p/S_p-**5**	2.8e1	1.9e1	1.1e1	5.4e0	8.4e1	3.8e1	4.5e0	7.8e0	1.6e1	2.4e0	ND	1.3e1
R_p-**5**	ND	9.3e1	ND	1.4e1	1.5e2	3.8e1	5.9e0	ND	ND	ND	4.2e0	8.1e-1
S_p-**5**	ND	ND	5.1e0	3.3e-1	1.4e-1	ND	5.1e0	1.8e1	1.3e1	4.7e0	4.5e0	1.9e1

[a] ND represents the enzymes were not saturated under 3mM of the substrates.

Table 3.2 k_{cat}/K_m ($M^{-1}s^{-1}$) for the wild-type and mutants of PTE.

	WT	G60A	I106G	F132G	S308G	H254Q/ H257F	H257Y/ L303T	I106G/ H257Y	I106G/ F132G/ H257Y	I106A/ F132A/ H257Y	I106A/ H257Y/ S308A	H254G/ H257W/ L303T
R_p/S_p-**1**	7.2e5	2.7e5	9.4e4	2.2e5	9.8e4	1.9e6	7.6e4	1.8e5	8.3e4	1.6e5	2.6e5	7.8e4
R_p-**1**	4.9e5	5.2e5	6.2e4	3.5e4	7.5e4	1.5e6	2.4e3	3.3e4	6.3e3	6.9e3	6.0e4	1.5e3
S_p-**1**	1.2e6	1.3e5	7.7e4	3.3e5	1.5e5	7.1e6	1.6e5	3.8e5	1.1e5	3.5e5	7.2e5	2.2e5
R_p/S_p-**2**	2.4e5	2.5e5	3.3e4	2.7e4	5.4e4	8.4e5	3.9e4	1.2e4	4.9e3	3.0e4	3.1e4	4.0e4
R_p-**2**	5.8e5	5.2e5	5.8e4	5.9e4	1.1e5	8.2e5	2.5e3	8.9e3	1.5e3	2.3e3	1.9e4	1.8e3
S_p-**2**	2.7e4	6.2e3	3.3e3	5.5e3	3.1e3	1.2e6	1.1e5	3.0e4	6.8e3	5.0e4	6.7e4	5.9e4
R_p/S_p-**3**	2.7e5	5.2e5	5.4e4	8.3e4	1.1e5	5.2e5	5.3e4	6.0e4	3.6e4	5.9e4	1.7e5	9.9e4
R_p-**3**	8.5e5	7.6e5	6.2e4	1.2e5	1.8e5	3.1e5	1.3e4	2.3e3	4.5e2	4.9e2	9.5e3	1.5e3
S_p-**3**	3.4e4	9.9e1	4.4e4	3.6e4	9.5e3	1.6e6	7.3e4	1.5e5	9.1e4	1.3e5	3.9e5	1.8e5
R_pR_c/R_pS_c $/S_pR_c/S_pS_c$-**4**	3.8e2	8.2e2	7.1e1	1.6e2	5.0e2	2.8e2	7.3e2	2.6e1	7.6e0	6.2e1	1.2e2	1.9e3
R_pR_c/S_pR_c-**4**	5.4e2	1.6e3	1.5e2	1.7e2	7.4e2	5.5e2	9.3e2	3.1e1	8.8e0	1.3e2	1.7e2	3.3e3
R_pS_c/S_pS_c-**4**	1.2e2	2.6e2	2.8e1	2.3e1	2.1e2	6.3e1	3.1e2	3.9e0	2.8e0	1.7e1	2.3e1	7.7e2
R_pR_c-**4**	1.3e3	3.0e3	3.8e2	3.3e2	2.3e3	1.9e2	5.8e1	1.7e1	8.4e0	2.3e1	5.9e1	2.2e2
R_pS_c-**4**	2.0e2	5.9e2	5.0e1	4.5e1	4.9e2	5.5e1	1.6e1	2.3e0	1.1e0	1.2e0	4.5e0	1.3e2
S_pR_c-**4**	1.1e2	1.7e1	1.4e1	8.4e1	1.1e2	1.6e3	1.8e3	8.0e0	1.3e1	1.5e2	2.4e2	8.1e3
S_pS_c-**4**	3.2e0	1.1e0	1.0e1	5.2e0	6.7e0	6.2e1	2.5e2	2.1e0	4.5e0	2.2e1	3.0e1	1.7e3
R_p/S_p-**5**	7.4e3	9.6e3	3.6e3	1.9e3	1.4e4	3.2e3	2.9e3	1.1e3	1.5e3	4.4e2	4.0e2	1.5e4
R_p-**5**	1.6e4	2.1e4	4.9e3	2.9e3	2.8e4	5.2e3	1.9e3	3.8e2	5.2e1	7.5e1	8.4e2	2.5e2
S_p-**5**	2.1e1	9.4e-1	8.4e2	8.1e1	1.0e2	3.3e2	5.8e3	2.6e3	4.6e3	1.0e3	5.7e2	2.8e4

Table 3.3 k_{cat}/K_m ratios [$((k_{cat}/K_m)_R/(k_{cat}/K_m)_S$) for the hydrolysis of chiral substrates by the wild-type and mutants of PTE.

	1	**2**	**3**	R_pR_c:R_pS_c:S_pR_c:S_pS_c -**4**	**5**
Wild-type	1/2	22	25	398:63:35:1	755
G60A	4	84	7650	3630:702:20:1	23000
I106G	1	18	1	38:5:1.5:1	6
F132G	1/9	11	3	64:8.5:16:1	35
S308G	1/2	34	19	339:73:17:1	277
H254Q/H257F	1/5	1/2	1/5	3:1:29:1	16
H257Y/L303T	1/64	1/44	1/6	4:1:115:16	1/3
I106G/H257Y	1/12	1/3	1/64	8:1:3:1	1/7
I106G/F132G/H257Y	1/18	1/5	1/205	7:1:11:4	1/89
I106A/F132A/H257Y	1/51	1/22	1/265	19:1:125:19	1/14
I106A/H257Y/S308A	1/12	1/4	1/41	13:1:54:7	2
H254G/ H257W/ L303T	1/142	1/33	1/121	2:1:65:14	1/111

preference of the wild-type enzyme for the R_p- enantiomers of the chiral organophosphonates, although a slight preference is shown for the S_p- enantiomer of compound **1**. The bigger the size of the substituent of the substrate, the greater the preference for the R_p- enantiomer. For example, compound **2** has an O-isopropyl group as the substituent, the $(k_{cat}/K_m)_R/(k_{cat}/K_m)_S$ ratio is 22, while the R_p- enantiomer of compound **4** contains an O-pinacolyl group as the substituent, the $(k_{cat}/K_m)_R/(k_{cat}/K_m)_S$ ratio increases to 63. The largest $(k_{cat}/K_m)_R/(k_{cat}/K_m)_S$ ratio, 755, is seen with compound **5** which contains an O-cyclohexyl group. The wild-type enzyme displays the highest activity relative to other selected mutants to hydrolyze the R_p- enantiomers of compounds **2** and **3** with k_{cat}/K_m values of 5.8×10^5 $M^{-1}s^{-1}$ and 8.5×10^5 $M^{-1}s^{-1}$, respectively. The catalytic ability of the wild-type enzyme towards the S_p- enantiomer of compound **1** is remarkable with a k_{cat}/K_m value of 1.2×10^6 $M^{-1}s^{-1}$. However, the activity of the wild-type enzyme towards the S_p- enantiomers of compounds **2**, **3**, **4**, and **5** is lower. The k_{cat}/K_m values are approximately 10^4 $M^{-1}s^{-1}$ for the S_p-enantiomers of compounds **2** and **3**, and 10^1 $M^{-1}s^{-1}$ for the S_p- enantiomer of compound **5** and the S_pR_c-enantiomer of compound **4**. The catalytic efficiency for the S_pS_c- enantiomer of compound **4** is even lower with a k_{cat}/K_m value 3.2 $M^{-1}s^{-1}$. The mutants containing the modification of the substrate binding pocket that reverses the stereoselectivity and enhances the hydrolytic activity were purified and studied for the detoxification of the more toxic S_p- stereoisomers of organophosphonates.

Enhancement of Stereoselectivity. The small pocket residue, Gly 60, was mutated to alanine to decrease the size of the substrate binding pocket of PTE. The k_{cat}

and k_{cat}/K_m values of the G60A mutant were decreased for all of the S_p- enantiomers as shown in **Scheme 3.3**. The catalytic efficiency of the G60A mutant towards the S_p- enantiomers of the organophosphonate compounds was decreased up to 340-fold relative to the wild-type enzyme. In contrast, the catalytic activity of the G60A mutant is increased towards the R_p- enantiomers of compounds **4** and **5** compared with the wild-type enzyme. The G60A mutant has the highest k_{cat}/K_m values for all of the PTE mutants towards the R_p- enantiomers of compound **4**, 3.0×10^3 $M^{-1}s^{-1}$ and 5.9×10^2 $M^{-1}s^{-1}$ for R_pR_c- 4 and R_pS_c- 4, respectively. While the k_{cat}/K_m values of the wild-type are 1.3×10^3 $M^{-1}s^{-1}$ and 2.0×10^2 $M^{-1}s^{-1}$ for R_pR_c- 4 and R_pS_c- 4, respectively. For all of the compounds shown in **Scheme 3.3**, the larger the substituents, the greater degree of discrimination between the R_p- and the S_p- enantiomers for the wild-type and the G60A are greater. The $(k_{cat}/K_m)_R/(k_{cat}/K_m)_S$ ratios of the G60A mutant are increased relative to the wild-type. The most drastic case is seen with compound **5** in which the R_p-enantiomer is preferred by a factor of 23,000 compared to a factor of 755 for the wild-type. The catalytic preference of the G60A mutant for the hydrolysis of compounds **1**-**5** is significantly enhanced due to the additional methyl group of the alanine which reduces the size of the small pocket of the active site. Hence, the G60A is observed to have more pronounced stereoselectivity for the selected organophosphonates than the wild-type PTE.

Relaxation of Stereoselectivity. A mutation to a smaller residue within the small pocket or the leaving group pocket of the substrate binding site of PTE will increase the size of the small or the leaving group pocket. The stereoselectivity for the compounds in

Scheme 3.3 are predicted to be relaxed. For example, the I106G mutant increases the size of the small pocket and diminishes the stereoselectivity for compounds **1**, **3**, **4** and **5** relative to the wild-type with $(k_{cat}/K_m)_R/(k_{cat}/K_m)_S$ ratios less than 10. The F132G mutant increases the size of the leaving group pocket and the stereoselectivity for compounds **2**, **3**, **4** and **5** compared to the wild-type enzyme are reduced. The $(k_{cat}/K_m)_R/(k_{cat}/K_m)_S$ ratios of the I106G mutant are less than 35.

The H257Y/L303T (YT) mutant increases the size of the small pocket and reduces the size of the large pocket. The stereoselectivity of this mutant is inverted for each racemic mixture. Interestingly, the H257Y/L303T (YT) exhibited more relaxed enantioselectivities for the compounds with larger substituents. The $(k_{cat}/K_m)_R/(k_{cat}/K_m)_S$ ratio is 1/3 for compound **5**, which contains the substituent, O-cyclohexyl. However, the enantioselectivity is less relaxed for the compounds with smaller substituents. For example, the ratio is 1/64 for compound **1**, which contains an O-ethyl substituent. The I106A/H257Y/S308A mutant also increases the size of the small pocket and reduces the size of the large pocket. This mutant displays a reversal in stereoselectivity for compounds **1**, **2**, **3**, and **4**. However, the I106A/H257Y/S308A mutant shows the most relaxed stereoselectivity for the compound with the biggest substituent, compound **5.** The ratio of $(k_{cat}/K_m)_R/(k_{cat}/K_m)_S$ is only 2, whereas the ratio for the wild-type is 755.

Modification of the large pocket was done by mutating His-254 and His-257 to glutamine and phenylalanine, respectively. For the hydrolysis of compounds **1**, **2** and **3** by the H254Q/H257F (QF) mutant, the turnover number for the R_p- enantiomers is higher than for the S_p- enantiomers, but the K_m value of the S_p- enantiomers of

compounds **1**, **2,** and **3** are more than 10-fold smaller than the R_p- enantiomers (less than 10 μM). Thus, the H254Q/H257F (QF) displays a relaxed stereoselectivity with $(k_{cat}/K_m)_R/(k_{cat}/K_m)_S$ ratios of 1/5, 1, and 1/5 for compounds **2** and **3**. The k_{cat}/K_m values of the S_p- enantiomers of compound **1**, **2**, and **3** are remarkably high. They are 7.2×10^6 $M^{-1}s^{-1}$, 1.2×10^6 $M^{-1}s^{-1}$ and 1.6×10^6 $M^{-1}s^{-1}$, respectively.

Reversal of Stereoselectivity. The mutants that exhibit relaxed enatioselectivity towards the chiral substrates contain an expanded small pocket. However, the inherent stereoselectivity can be inverted by enlarging the size of the small pocket and shrinking the size of the large pocket simultaneously. The residues in the small pocket such as Ile-106, Phe-132, and Ser-308 are replaced with smaller residues including glycine or alanine. For the H257Y/L303T (YT) mutant, Leu-303 is changed to a relatively smaller residue, threonine. In addition, these mutants include His-257 in the large pocket that has been mutated to a relatively larger residue, tyrosine. Hence, reversed stereoselectivities are observed. For example, the wild-type PTE prefers the R_p-enantiomer of compound **3** by a factor of 25, whereas the I106A/F132A/H257Y mutant inverts the stereoselectivity of this compound and prefers the S_p- enantiomer by a factor of 265. One of the most interesting cases is observed with the H257Y/L303T mutant. This enzyme possesses a larger stereoselectivity for compound **1**, which contains an ethyl group as the substituent. The $(k_{cat}/K_m)_R/(k_{cat}/K_m)_S$ ratio is 1/64. The observed trend is the larger the substituent, the smaller the enantioselectivity. The $(k_{cat}/K_m)_R/(k_{cat}/K_m)_S$ ratios are 1/44 and 1/6 for compounds **2** and **3**, respectively

The H254G/H257W/L303T mutant contains an extended small pocket and a reduced large pocket. Leu-303 in the small pocket was mutated to a comparatively smaller threonine residue, and the two histidines in the large pocket were changed to glycine and tryptophan. The H254G/H257W/L303T (GWT) mutant displays a more distinct effect in the reversal of the stereoselectivity than the other mutants for the hydrolysis of compounds **1** and **5**, with preferences for the S_p- enantiomers by a factor 142 and 111, respectively.

The difference in the rate of hydrolysis for two stereoisomers of compound **5** is exhibited in **Figure 3.2**. **Figure 3.2 (A**) indicates that the H254G/H257W/L303T (GWT) mutant hydrolyzes one of the stereoisomers much faster than another based on two of the time courses for the hydrolysis of compound **5** at different concentrations of enzyme. The gray dots represent the hydrolysis of the faster stereoisomer and the red dots indicate the hydrolysis of the slower stereoisomer. The G60A mutant is shown to prefer the R_p- enantiomer of compounds **1**-**5** (**Table 3.3**). **Figure 3.2 (B)** indicates that the H254G/H257W/L303T (GWT) mutant hydrolyzes the S_p- enantiomer of compound **5.** The G60A mutant is added to hydrolyze the residual R_p- enantiomer. It is shown that the S_p- enantiomer of compound **5** is more preferred by the H254G/H257W/L303T (GWT) by a factor of 111.

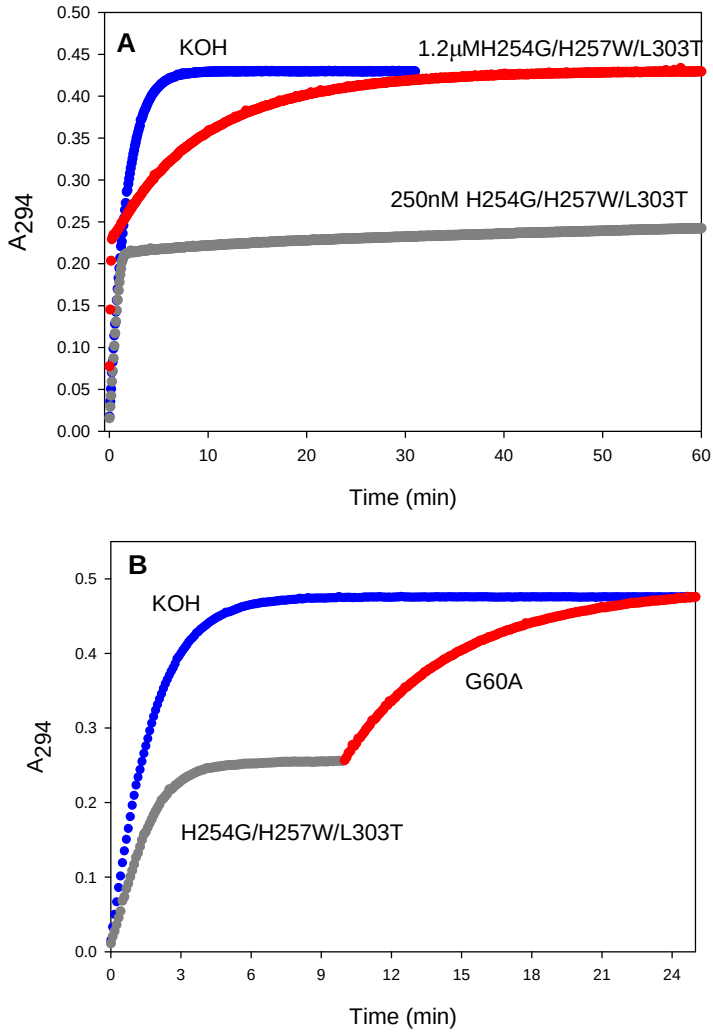

Figure 3.2 Time courses for the hydrolysis of the racemic compound **5** using the mutants of PTE. The total concentration of compound **5** was determined by the addition of KOH. (A) The hydrolysis of compound **5** by 1.2 μM (red line) and 250 nM (gray line) H254G/H257W/L303T mutant of PTE. (B)The hydrolysis of the preferred enantiomer (S_p) of compound **5** was hydrolyzed by 165nM H254G/H257W/L303T mutant of PTE. After 10 minutes, the G60A mutant of PTE was added to hydrolyze the R_p-enantiomer. **5**

Discussion

Phosphotriesterase possesses a broad substrate selectivity and is able to detoxify chemical warfare agents such as GA, GB, GD, GF, and VX. The wild-type PTE was demonstrated to prefer the less toxic R_p- enantiomers of the organophosphorus nerve agents and their analogues (*45*). The preference of the wild-type PTE for compounds **1**-**5** is increased by enlarging the size of the substituent of the organophosphonate substrates. The G60A mutant enhances the stereoselectivity by substituting a larger residue in the small pocket. It is shown to have a significant improvement in the $(k_{cat}/K_m)_R/(k_{cat}/K_m)_S$ ratios, especially the compounds with larger substituents like compound **5**. This feature is utilized to isolate S_p- stereoisomers from the racemic mixtures, due to the fact that the G60A mutant has a faster catalytic rate for the hydrolysis of the R_p- stereoisomers.

The relaxation of stereoselectivity for compounds **1**-**5** was observed by some mutants that contain a enlarged small pocket or the leaving group pocket, such as the I106G and the F132G mutants. Some mutants with an enlarged small pocket and a reduced large pocket relax the stereoselectivity with compound **5**, such as the H257Y/L303T (YT) and the I106A/H257Y/S308A mutants. The preference ratios of these two mutants with compound **5** are less than 3, while the wild-type prefers the R_p-enantiomer by a factor of 755. The H257Y/L303T (YT) mutant prefers the S_p-enantiomer and the I106A/H257Y/S308A mutant prefers the R_p- enantiomer.

Enlargement of the small pocket and the shrinking of the large pocket simultaneously can alter the stereoselectivity of PTE to prefer the more toxic S_p-

enantiomers rather than the R_p- enantiomers. The I106G/F132G/H257Y and the I106A/F132A/H257Y mutants have the highest inversion of the stereoselectivity towards compound **3**, the I106G/F132G/H257Y mutant prefers the S_p- enantiomer by a factor of 265 and the I106A/F132A/H257Y mutant prefers the S_p- enantiomer by a factor of 205, while the wild-type prefers the R_p-enantiomer with a factor of 25. The difference in stereoselectivity of these mutants relative to the wild-type PTE is changed up to 6000 fold.

In addition, the H254G/H257W/L303T (GWT) mutant contains a reduced large pocket and an enlarged small pocket, and the stereoselectivity is reversed for compounds **1**-**5**. The order of preference for compounds **1**-**5** is not based on the size of the substituent for the mutant with reversed stereoselectivity, unlike the wild-type and the G60A enzyme. For the hydrolysis of compound **5**, the H254G/H257W/L303T (GWT) mutant has the highest preference for the S_p- enantiomer, the $(k_{cat}/K_m)_R/(k_{cat}/K_m)_S$ ratio is 1/111. Conversely, the G60A mutant prefers the R_p- enantiomer of compound **5** by a factor of 23,000. This suggests that with the mutation of only four residues of PTE, the difference in stereoselectivity can be altered by a factor of 2.5×10^6. In addition to the inversion of the enantioselectivity, the H254G/H257W/L303T (GWT) mutant possesses the highest catalytic activity for the more toxic S_p- enantiomers of compounds **4** and **5**. The k_{cat}/K_m values for the hydrolysis of the S_pR_c- and S_pS_c- enantiomers of compound **4** have been enhanced by 73 and 543 fold relative to the wild-type. The most noticeable case is that the k_{cat}/K_m value for the S_p- enantiomer of compound **5** is 1340 fold higher than the wild-type.

Conclusion

The modification of the amino acid residues within the substrate binding site of PTE influences the enantiomeric selectivity significantly. Most of the toxic organophosphorus nerve agents contain a chiral center. Previous studies have shown that the wild-type PTE has less activity for the hydrolysis of the more toxic S_p-stereoisomers (*84*). The G60A mutant exhibits an enhancement of stereoselectivity and is utilized to obtain the S_p-stereoisomers of the organophosphonates by hydrolyzing the R_p- stereoisomers. The mutants containing the reversal of stereoselectivity can be utilized to acquire the R_p- steroisomers and enhance the hydrolysis reactivity against the more toxic nerve agent stereoisomers. The more toxic S_p- entantiomers of compounds **2-5** are not efficiently catalyzed by the wild-type PTE. The k_{cat}/K_m values are less than 10^5 $M^{-1}s^{-1}$ for the S_p- entantiomers of compounds **2** and **3**, and the values are even smaller (less than 120 $M^{-1}s^{-1}$) for the more toxic nerve agent analogues, the S_p-entantiomers of compounds **4** and **5**. The selected mutants that modulate the substrate binding pocket are able to increase the catalytic activity for the hydrolysis of the S_p-entantiomers of compounds **2-5**. The wild-type PTE and selected mutants with increased activity towards the S_p and R_p -enantiomers of compound **2-5** are graphically displayed in **Figure 3.3 (A)** and **(B**), respectively. The best mutants to hydrolyze the S_p-entantiomers of compounds **2** and **3** are H257Y/L303T (YT) and I106A/H257Y/S308A, respectively. The k_{cat}/K_m values for these two mutants are enhanced to more than 10^5 $M^{-1}s^{-1}$. The increase in the catalytic activity is 4-fold and 11-fold relative to the wild-type with the S_p- entantiomers of compounds **2** and **3**, respectively. The

H254G/H257W/L303T (GWT) mutant has the highest activity for the hydrolysis of the more critical organophosphorus nerve agent (soman and cyclosarin) analogues, compounds **4** and **5**. The k_{cat}/K_m values are enhanced to approximately 10^3 $M^{-1}s^{-1}$ for the S_pS_c- entantiomer of compound **4** and are around 10^4 $M^{-1}s^{-1}$ for the S_pR_c- entantiomer of compound **4** and the S_p- entantiomer of compound **5**. The enhancements are 540-fold for the S_p- entantiomers of compound **4** and 1340-fold for the S_p- entantiomer of compound **5**. These results suggest that the mutations in the active site based on the beneficial mutant as the template would be capable of reaching higher activities for these organophosphonates compounds and organophosphorus nerve agents.

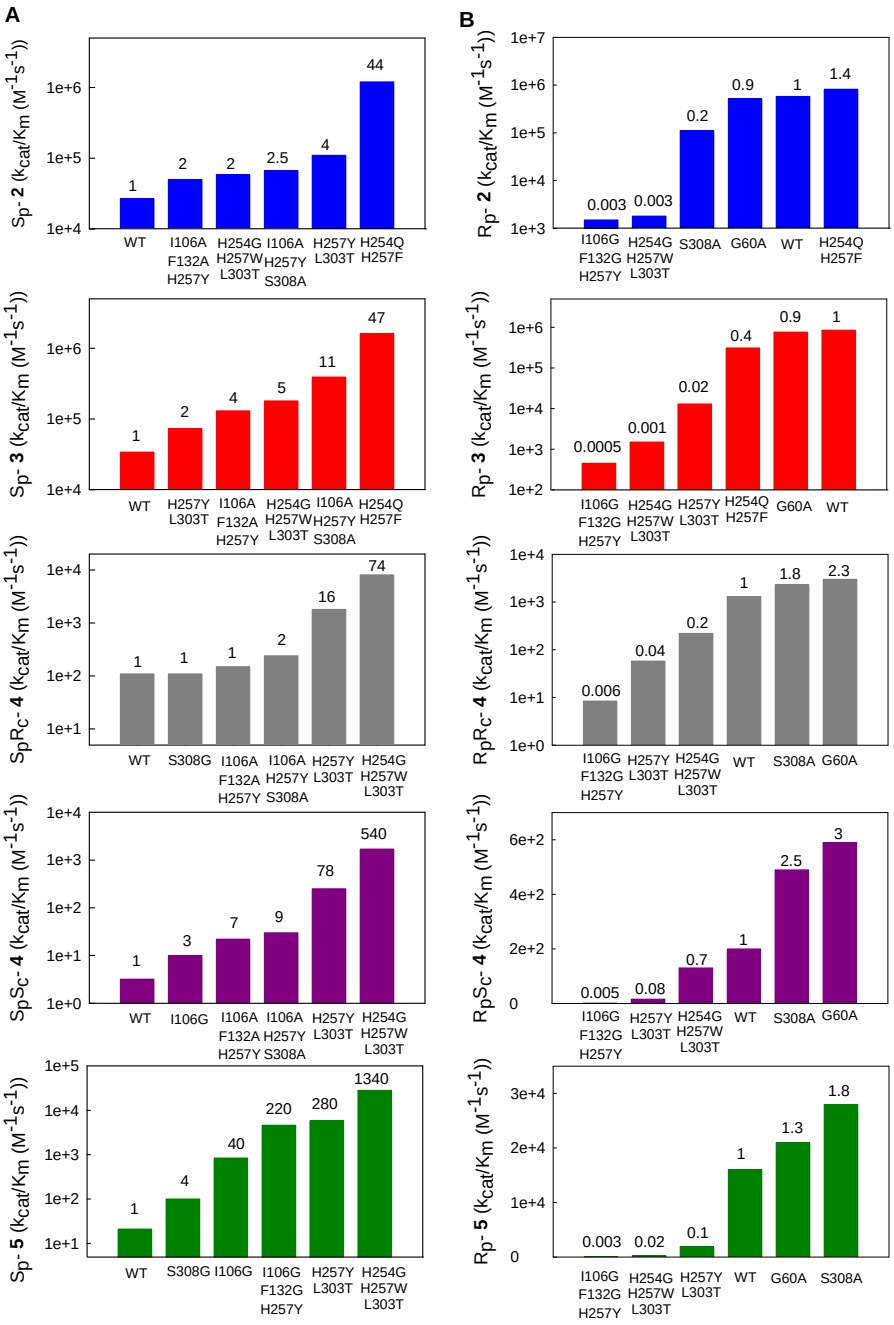

Figure 3.3 Bar graphs illustrating increased values of k_{cat}/K_m for the S_p- (A) and the R_p- (B) enantiomers of compounds **2**, **3**, **4**, and **5** catalyzed by the wild-type and mutants of PTE. The numbers represent the increase and decreasein activity relative to the wild-type enzyme.

CHAPTER IV

ENGINEERING PHOSPHOTRIESTERASE FOR THE ENHANCEMENT OF STEREOSELECTIVITY TOWARDS NERVE AGENT ANALOGUES

Introduction

Protein engineering is a powerful tool to improve the functions of enzymes, such as catalytic activity, stability under certain conditions, protein expression levels, and stereoselectivity. For example, the stereoselectivity of enzymes can be enhanced or reversed for use in synthetic organic chemistry, unnatural substrate decomposition and unnatural product production. The reactivity of the hydantoinase from *E. coli* for D-5(2-methylthioethyl) hydantoin is higher than for the L-enantiomer. Hydantoinase mutants with inverted stereoselectivity and high D-selectivity were discovered by directed evolution (*99*). Thus whole-cell catalysts for efficient production of chiral compounds can be improved by introducing stereoselective enzymes into multienzyme pathways. The wild-type hydantoionase has a ~40% ee_D and a mutant with enhanced selectivity has a 90% ee_D. A mutant that inverted the stereoselectivity was increased 5-fold for conversion of the substrate but has only ~20% ee_L. The selectivity of *E. coli* D-sialic acid aldolase was reversed to catalyze the formation of the unnatural sugar L-3-deoxy-*manno*-2-octulosonic acid (L-KDO). The best mutant exhibits a >1,000-fold preference for L-KDO relative to the D-sialic acid (*100*). An epoxide hydrolase from *Aspergillus niger* was engineered to increase stereoselectivity. The wild-type epoxide hydrolase prefers to produce the S-enantiomer of glycidyl phenyl ether 4.6-fold higher than the R-

enantiomer (E = 4.6) from 2-phenoxyoxirane. The best mutant was discovered by directed evolution and shown to have an enhanced stereoselectivity (E = 115). This could be a useful tool in asymmetric catalysis.

The bacterial phosphotriesterase (PTE) from *Psuedomonase diminuta* is an enzyme that can detoxify a wide range of organophosphate insecticides and chemical warfare agents, including tabun (GA), sarin (GB), soman (GD), cyclosarin (GF) and VX (**Scheme 4.1**) (*58*). The catalytic ability of PTE for the hydrolysis of paraoxon is close to the diffusion-control limit ($k_{cat}/K_m \sim 10^8$ M^{-1} s^{-1}) (*3*). The stereoselectivity of the wild-type PTE towards GB, GD, GF, VX and rVX analogues was presented in Chapter III. The wild-type PTE generally shows higher activity and substrate specificity for the R_p-enantiomers. However, the S_p-enantiomers of these nerve agents are more toxic than the R_p-enantiomers (*48*). PTE mutants with reversed stereoselectivity were identified and shown to have enhanced catalytic ability to hydrolyze the more toxic S_p-enantiomers.

Directed evolution and rational design of phosphotriesterase for the enhancement of hydrolysis activity towards organophosphate compounds have been studied by several laboratories. Wilfred Chen and coworkers created a randomized library of PTE by DNA shuffling and saturation mutagenesis. The library of PTE mutants was displayed on the surface of *E. coli* cells and the beneficial mutants were isolated by a solid-phase top agar assay. They discovered that some distal mutations, such as K185R and I274N, are important for improvement of the hydrolysis activity toward paraxon, parathion,

Scheme 4.1 The chemical structure of paraoxon, tabun (GA), sarin (GB), soman (GD), cyclosarin (GF), VX and rVX.

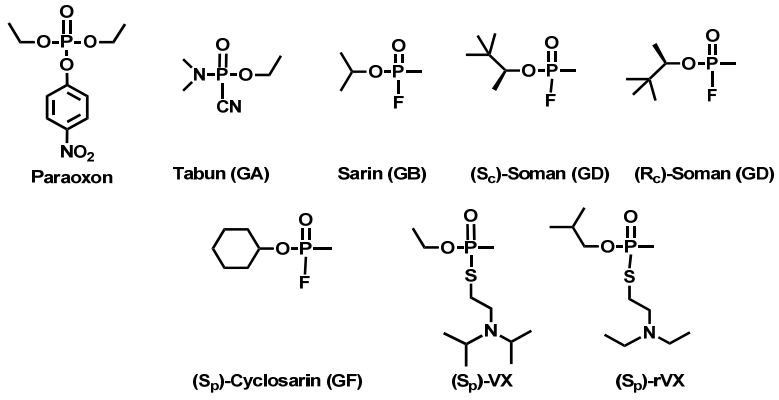

chlorpyrifos and coumaphos (*28, 101*). Dan Tawfik and colleagues also utilized DNA shuffling to construct randomized PTE libraries. The libraries were transformed and screened with 2-naphthyl acetate on LB agar plates or screened by an *in vitro* compartmentalization technique. PTE variants with enhanced stability in the metal-free state and increased hydrolysis activity toward paraoxon were discovered. The S5 mutant that contains three mutations beyond the substrate binding pocket (K185R, D208G and R319S) was shown to have a 20-fold increase in protein expression (*33*).

The organophosphate degrading enzyme OpdA from *Agrobacterium radiobacter* P230, has 90% sequence identity with PTE, and was modified by David Ollis and collaborators. OpdA and PTE libraries were created by error-prone PCR and DNA shuffling. The cells with transformed libraries were grown on paraoxon with indicator plates. The variants were selected and shown to have improved protein expression and slightly better activity towards methyl-paraoxon, methyl-parathion and demeton-S.

These mutants contain some alternations on the surface of the protein. They suggested that these mutations might contribute to protein stability (*31, 32*).

Single and double substitution libraries contain 20 and 400 protein variants, respectively. The screening of these small libraries can be conducted by growing single colonies in 96 deep-well growth blocks cultures and screened with selected substrates. A high throughput *in vivo* selection technique that incorporated a new phosphate assimilation pathway was utilized to isolate the active PTE variants when the sizes of the randomized libraries are large (> 1,000 variants). In a previous study, the *in vivo* assays that have glycerophosphodiesterase (GpdQ) from *Enterobacter aerogenes* and PTE coexpressed in *E. coli* cells indicated that cells could grow by utilizing the organophosphate and organophosphonate esters as the sole phosphorus source (*102*). In *E. coli* cells, PTE can hydrolyze a wide range of organophonate esters to methyl phosphonate esters, GpdQ can subsequently hydrolyze the methyl phosphonate esters to produce methyl phosphonate. The C-P lyase complex that belongs to the *phn* operon in *E. coli* can metabolize methyl phosphonate to inorganic phosphate and methane (*103, 104*). The proposed phosphate assimilation catabolic pathway is presented in **Scheme 4.2**.

Scheme 4.2 Proposed catabolic pathway of organophosphonate esters.

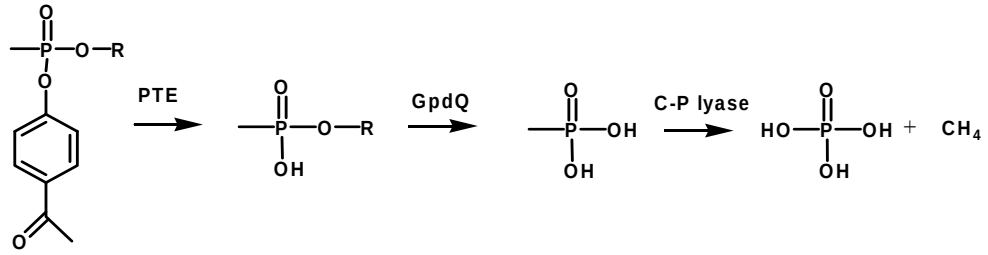

In this chapter, directed evolution and rational design of PTE were utilized based on the active mutants of the first generation of mutants as templates. More active mutants toward the hydrolysis of the toxic S_p-enantiomers of organophosphate nerve agent analogues were discovered. Kinetic parameters of the wild-type and mutants of PTE towards the chiral analogues of GB, GD, GF, VX, and rVX with a 4-acetylphenol leaving group (**Scheme 4.3**) were characterized. X-ray crystal structures of the mutants in the second generation were determined.

Scheme 4.3 Chemical structures of organophonate nerve agent analogues.

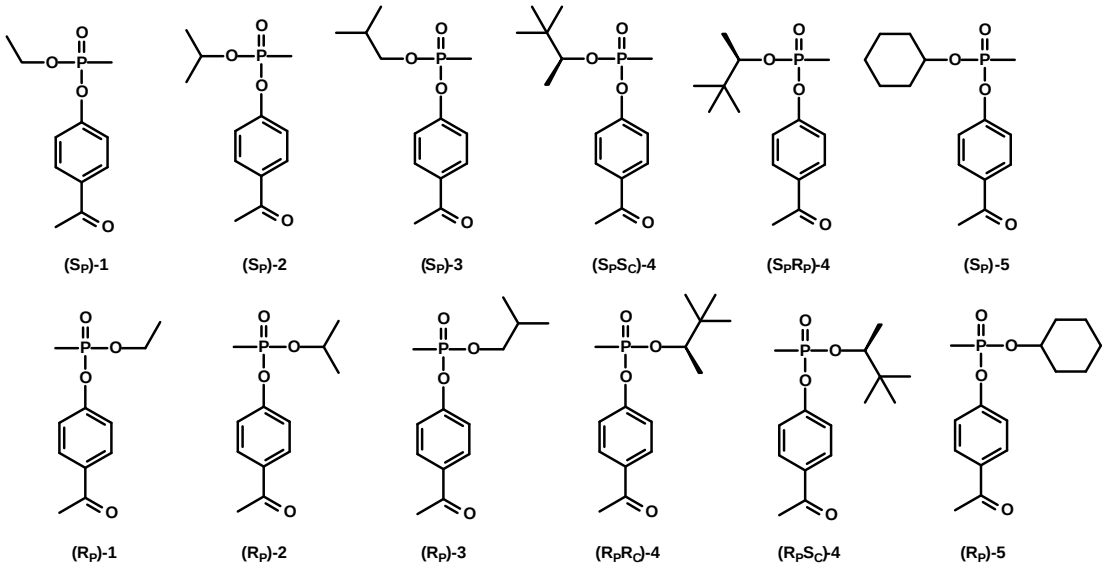

Materials and Methods

Site-Directed Mutagenesis. The A80V, K185R and I274N mutations of the wild-type PTE were created by the QuikChange site directed mutagenesis technique using *pfu* Turbo DNA polymerase from Stratagene. The oligonucleotide pairs that contained the mutated codon at a specific site were used as the primers to amplify the wild-type, the H254Q/H257F (QF), H257Y/L303T (YT) and the H254G/H257W/L303T (GWT) mutants by PCR. DpnI was used to digest the parental DNA plasmids without the mutated codon. The digested PCR products were transformed into *E. coli* XL1-blue electro-competent cells for DNA sequencing. The mutations were added to the template sequentially. Thus, the RN (K185R/I274N), the QFRN (H254Q/H257F/ K185R/I274N), the YTRN (H257Y/L303T/K185R/I274N), the GWT-d1 (H254G/H257W/L303T/ K185R/I274N) and the GWT-d2 (H254G/H257W/L303T/ K185R/I274N/A80V) mutants were created.

Construction of Single and Double Substitution PTE Libraries. The single substitution library, M317X, and the double substitution libraries, W131X/F132X, S308X/Y309X and L271X/S308X, of PTE were created using the gene for GWT-d1 (H254G/H257W/L303T/K185R/I274N) as the initial template for QuikChange mutagenesis. The primers contained the degenerate codon NNS at the targeted position to eliminate two stop codons, TGA and TAA (N = A, T, G, C; S = C, G). The M317X, W131X/F132X, F306X/Y309X and S308X/Y309X libraries were created using one pair of primers. The I106X/S308X library was made using the degenerate primers at the Ile106 site to perform the first round of QuikChange mutagenesis. Colonies from the

I106X library were collected and plasmids from this library were isolated for the second round of QuikChange mutagenesis using the primers with the degenerate codon at the Ser-308 site. The double substitution libraries, C59X/S61X and I255X/W302X, were constructed using the GWT-d2 (H254G/H257W/L303T/K185R/I274N/A80V) mutant as the template. The degenerate primers targeted for the Cys-59 and Ser-61 sites were for a single round of QuikChange mutagenesis. Two pairs of primers that contain the degenerate codon at the Ile-255 and the Trp-302 sites were utilized for QuikChange mutagenesis sequentially. PCR products were transformed into *E. coli* BL21 (DE3) cells for DNA sequencing and protein expression.

Construction of a Multisite Randomized PTE Library. A PTE library was constructed using the gene for the GWT-f1 (H254G/H257W/L303T/M317L/K185R/I274N) mutant as the template. Six residues in the substrate binding pocket were randomized, including Ile-106, Phe-132, Leu-271, Phe-306, Ser-308 and Tyr-309. The randomized residues at these six sites were selected from the results of screening 228 single site PTE mutants towards the hydrolysis of paraoxon (unpublished data). The randomized residues for the Ile-106 site are Ala, Cys, Gly, Ile, Met and Val. The randomized residues for the Phe-132 site are Ala, Cys, Phe, Gly, His, Ile, Leu, Pro, Arg, Ser, Thr, Val and Tyr. The randomized residues for the Leu-271 site are Phe, Ile, Leu, Tyr and Gln. The randomized residues for the Phe-306 are Phe, Ile, Leu and Met. The randomized residues for the Ser-308 site are Ala, Cys, Gly, Ser, Thr, Glu, Leu, Gln, Val and Asn. The randomized residues for the Tyr-309 sites are Ala, Cys, Asp, Phe, Gly, Leu, Asn, Ser, Thr, Val, Tyr and Trp.

Scheme 4.4 The creation of six site randomized library of PTE.

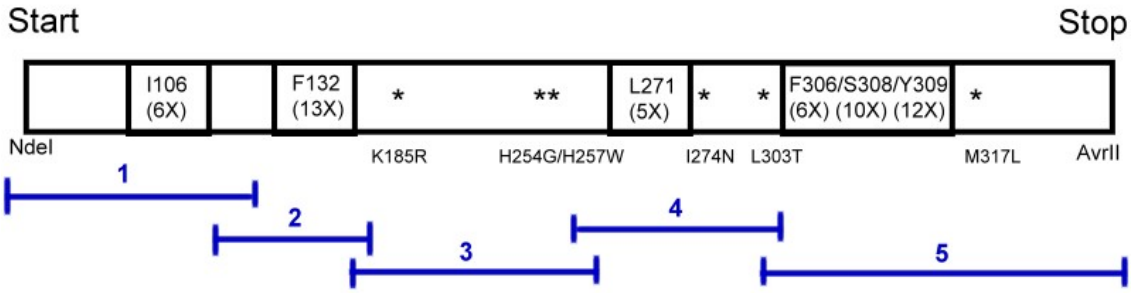

This multisite randomized PTE library was constructed by combining five segments of the gene for PTE. These five segments of the PTE gene were amplified using the primers shown in **Table 4.1**. **Scheme 4.4** shows the five segments of the PTE gene. The first segment was amplified using primers 1 and 2 from **Table 4.1**. The mixture of the genes for I106A, I106C, I106G, I106M, and I106V mutants, and the wild-type PTE was served as the initial template. The genes for I106A, I106C, I106G, I106M and I106V mutants were previously made and they were mixed with the gene for the wild-type PTE in approximately equal concentrations. The second segment was amplified using primers 3 and 4 from **Table 4.1**. The mixture of genes for I132A, I132C, I132F, I132G, I132H, I132L, I132P, I132R, I132S, I132T, I132V, and I132T mutants, and the wild-type PTE was served as the initial template. The genes for I132A, I132C, I132F, I132G, I132H,I132L, I132P, I132R, I132S, I132T, I132V and I132T mutants were previously made, and they were mixed with the gene for the wild-type PTE in approximately equal concentrations. The third segment was amplified using primers 5 and 6, and the gene for the GWT-f1 mutant was used as the template. The fourth segment was amplified using the combination of primers 7, 8 and 9 as the forward

primer, and primer 10 as the backward primer using the gene of GWT-f1 mutant as the template. The fifth segment was amplified using the combination of primers 11, 12, 13, 14, 15 and 16 as the forward primer, and primer 17 as the backward primer using the gene of GWT-f1 mutant as the template.

Primer 7 encodes three residues (F, I, L) for residue 271. Primer 8 encodes tyrosine for residue 271. Primer 9 encodes glutamine for residue 271. The forward primer for the amplification of the fourth segment was mixed with primers 7, 8 and 9 to residues (A, C, D, G, N, S, T, and Y) for residue 309. Primer 12 encodes four residues (F, I, L, and M) for residue 306, four residues (E, L, Q, and V) for residue 308, and eight residues (A, C, D, G, N, S, T, and Y) for residue 309. Primer 13 encodes four residues (F, I, L, and M) for residue 306, one residue (N) for residue 308, and eight residues (A, have equal concentration for each genotype. Primer 11 encodes four residues (F, I, L, and M) for residue 306, five residues (A, C, G, S, and T) for residue 308, and eight C, D, G, N, S, T, and Y) for residue 309. Primer 14 encodes four residues (F, I, L, and M) for residue 306, five residues (A, C, G, S, and T) for residue 308, and six residues (C, F, G, L, V, and W) for residue 309. Primer 15 encodes four residues (F, I, L, and M) for residue 306, four residues (E, L, Q, and V) for residue 308, and six residues (C, F, G, L, V, and W) for residue 309. Primer 16 encodes four residues (F, I, L, and M) for residue 306, one residue (N) for residue 308, and six residues (C, F, G, L, V, and W) for residue 309. The forward primer for the amplification of the fifth segment was mixed with primers 11, 12, 13, 14, 15 and 16 to have equal concentration for each genotype.

Table 4.1 Sequences of the primers for creating the six sites randomized library.

No.	Name	Sequences of primers
1	NdeI-pJames 5' (+)	5'-CCC GCG GGG **CAT ATG** TCC ATC GGG ACC GGT GAC CGT ATC-3'
2	130-121 pJames (-)	5'-CAG ACC GGT AGC AGC AAC GAT GTG TAC ATC -3'
3	108-118 pJames (+)	5'- CGT GAC GTT TCC CTG CTG GCT GAA GTT TCC C -3'
4	182-174 pJames(-)	5'-C GAG CTC CTG GAA CGG GGT AGC TTT ACC-3'
5	134-142 pJames (+)	5'-CCG CCG CTG AGC ATG CGT CTG CGT TCC -3'
6	270-259 pJames (-)	5'- C GGA AGC GGA TGC ATT GTC TTC CAG ACC GAT AGC -3'
7	L271(FIL)-pJames(+)	5'- C GGT CTG GAA GAC AAT GCA TCC GCT TCC GCT **HTC** CTG GGT AAT CGT TCC TGG C -3'
8	L271(Y)-pJames(+)	5'- C GGT CTG GAA GAC AAT GCA TCC GCT TCC GCT **TAC** CTG GGT AAT CGT TCC TGG C -3'
9	L271(Q)-pJames(+)	5'- C GGT CTG GAA GAC AAT GCA TCC GCT TCC GCT **CAG** CTG GGT AAT CGT TCC TGG C -3'
10	305-291 pJames (-)	5'- CC GAA AGT CCA GTC GTT GGA AAC CAA GAT CTG TTT CAT GTA ACC -3'
11	F306(4)S308(5)Y309(8) pJames(+)	5'- CC AAC GAC TGG ACT TTC GGT **HTS** TCG **DSC DVC** GTT ACC AAC ATC ATG GAC GTT TTG GAC C -3'
12	F306(4)S308(4)Y309(8)pJames(+)	5'- CC AAC GAC TGG ACT TTC GGT **HTS** TCG **SWG DVC** GTT ACC AAC ATC ATG GAC GTT TTG GAC C -3'
13	F306(4)S308(N)Y309(8)pJames(+)	5'- CC AAC GAC TGG ACT TTC GGT **HTS** TCG **AAC DVC** GTT ACC AAC ATC ATG GAC GTT TTG GAC C -3'
14	F306(4)S308(5)Y309(6)pJames(+)	5'- CC AAC GAC TGG ACT TTC GGT **HTS** TCG **DSC KKS** GTT ACC AAC ATC ATG GAC GTT TTG GAC C -3'

Table 4.1 Continued

15	F306(4)S308(4)Y309(6)pJames(+)	5’- CC AAC GAC TGG ACT TTC GGT **HTS** TCG **SWG KKS** GTT ACC AAC ATC ATG GAC GTT TTG GAC C -3’
16	F306(4)S308(N)Y309(6)pJames(+)	5’- CC AAC GAC TGG ACT TTC GGT **HTS** TCG **AAC KKS** GTT ACC AAC ATC ATG GAC GTT TTG GAC C -3’
17	AvrII –pJames 3’ (-)	5’-CCC **CCT AGG** TCA TCA TCA GGA AGC ACG CAG GGT C -3’

Note: The symbol S, K, W, H, D and V in the sequences of the primers represents different mixture of bases. (K= G, T; S= C, G; W= A, T; H= A, C, T; D= A, G, T; V=A, C, G)

These five segments of PTE gene were overlapped by primerless PCR for 15 cycles. The whole PTE gene with six randomized sites was amplified by PCR for 55 cycles using primer 1 and primer 17. Thus, the multisite randomized PTE library, I106(6)/ F132(13)/ L271(5)/ F306(4)/ S308(10)/Y309(12), was created; the numbers in the parentheses represent the numbers of possible residues in each site. The potential size of this library is 1.87×10^5 variants. The amplified PTE library was digested with NdeI and AvrII restriction enzymes and ligated into the NdeI and AvrII digested GpdQ-pETDuet plasmid using T4 DNA ligase from Roche. The overnight ligation of the PTE library –GpdQ/pETDuet was purified by the QIAquick Kit to remove salts in the T4 DNA ligase buffer and transformed into fresh-made *E. coli* Top 10 competent cells. The transformants were incubated at 37 °C for an hour and then plated on LB-ampicilin agarose. The colony forming units (CFU) were counted and reached 3-fold of the library size. All of the CFU were collected together and grown in LB culture for 6 hours at 37 °C. The plasmids from the PTE library –GpdQ-pETDuet were extracted using the Promega Wizard® Plus Miniprep kit.

Construction of PTE Library by Error Prone PCR. Random mutagenesis PCR was performed by error-prone PCR using Mutazyme II DNA polymerase® from the Gene-Morph II system (Stratagene). The gene for the GWT-f4 mutant served as the template. The amount of template was 90 ng in each reaction for the generation of 1.5 mutations per 1,000 kb gene. The amplified PTE library and the GpdQ-pETDuet plasmids were digested by NdeI and AvrII restriction enzymes and ligated into GpdQ-pETDuet plasmid using T4 DNA ligase buffer. The library was transformed into fresh *E.*

coli Top10 competent cells. The transformants were incubated at 37 °C for an hour and plated on LB-ampicilin agarose. The colony forming units were counted to estimate the library size. Approximately 6 X 10^5 cells were collected together to grow in LB cultures for 6 hours at 37 °C. The plasmids of the PTE library/GpdQ-pETDuet were extracted using a Promega Wizard® Plus Miniprep kit.

Growth Assays. The gene for GpdQ was inserted into the first T7 promoter position of the pETDuet plasmid and the wild-type and mutants of PTE was inserted into the second T7 promoter position. The PTE/GpdQ-pETDuet plasmids were transformed into *E. coli* BL21 (DE3) competent cells and grown on LB plates containing 0.1 μg/mL ampicilin. The colonies from fresh transformations were inoculated and grown overnight in super broth medium at 30 °C. Overnight cultures were washed four times with sterile ddH_2O to remove any traces of the rich medium. A 20 mL liquid MOPS phosphate-free minimal medium culture was inoculated with 2% fresh and previously washed overnight culture. The MOPS minimal medium, pH 7.4 was supplemented with 0.1% glucose as the carbon source, and 0.1 μg/mL thiamin (XY). Various organophosphonate compounds were added to the cultures to a final concentration of 1.0 mM. As control experiments, PTE-/GpdQ- BL21 (DE3) cells were grown in the presence and absence of inorganic phosphate. PTE+/ GpdQ+ BL21 (DE3) cells were induced by 0.5 mM IPTG for protein expression. Cell growth was monitored by measuring the OD_{600} for 5-10 days at 30 °C.

Screening of the Single and Double Substitution Libraries. The products of QuikChange mutagenesis were transformed into *E. coli*. BL-21 competent cells and

inoculated in 96-deep well culture blocks containing 1 mL super broth (SB) supplemented with 0.5 mM $CoCl_2$ and 0.1 μg/mL ampicillin. Variants of the M317X library in the culture blocks were screened with paraoxon and the S_p-enantiomer of compound **5** containing 2% Bug Buster in the mixture of the assays. Variants of the C59X/S61X library in the culture blocks were screened with paraoxon and the S_p-enantiomers of compound **4** containing 2% Bug Buster in the mixture of the assays. The *para*-acetyl phenol leaving group of the S_p-enantiomers of compounds **4** and **5** was replaced with *para*-nitrophenol. The production of the hydrolysis products of paraoxon and the S_p-enantiomers of compounds **4** and **5** were measured by monitoring the formation of *para*-nitrophenol at 400 nm (ε_{400}= 17,000 M^{-1} cm^{-1}) in 50 mM CHES, pH 9.0 buffer using a SpectraMax plate reader (Molecular Devices Inc., Sunnyvale, CA) at 30 °C.

In vivo *Selection on Phosphate Free MOPS Minimal Medium Plates.* The PTE library-GpdQ-pETDuet plasmids were transformed into *E. coli* BL21 (DE3) cells and plated on LB-ampicilin agarose. The cells were collected and grown in super broth (SB) medium at 30 °C for 12 hours. The cells were washed for four times with sterile ddH_2O to remove any traces of the rich medium. The cells were plated on MOPS phosphate-free minimal medium agarose with 0.4 μg/mL ampicilin and 0.5 mM IPTG. After 7-10 days growth at 30 °C, the colonies with sizes larger than the background were selected. The first round of selection used the GWT-f2 mutant as the background and the second round used the GWT-f4 mutant as the background. Approximately 5.8 X 10^5 colonies from the multisite-randomized PTE library and approximately 6 X 10^5 colonies from the

error prone PTE library were collected and inoculated onto LB-ampicilin plates. The *in vitro* screening assays for the hydrolysis activity for paraoxon and the S_p- enantiomer of compound **5** were conducted to identify relative activities compared with wild-type PTE and the template mutant.

Expression, Growth and Preparation of Phosphotriesterase. The mutant phosphotriesterase plasmids were transformed into *E. coli* BL-21 cells. The transformed BL-21 cells were grown in Luria-Bertani (LB) broth overnight at 37 °C. The overnight cultures were used to inoculate 1L Terrific Broth (TB) containing 25 μg/mL ampicilin and 1.0 mM $CoCl_2$ at 30 °C. The expression of PTE was induced by the addition of 1.0 mM IPTG when the OD_{600} reached 0.4. The cells were harvested at 4 °C by centrifugation at 6,000 rpm after allowing the culture to reach stationary phase after 36-42 hours at 30 °C. The cells were harvested by centrifugation at 6,000 rpm for 15 minutes at 4 °C. The wet cell pellet was isolated and stored at -78 °C until needed.

Purification of Phosphotriesterase. The mutant proteins were purified from *E. coli* BL21 cells according to the previously reported protocols (*38*). The fractions were pooled based on enzymatic activity, absorbance at 280 nm and the molecular weight determined by SDS PAGE. The progress of the purification procedure was monitored by determining the specific activity and analysis with SDS-polyacrylamide gels. (Omburo *et al.*, 1992)

Kinetic Measurements and Data Analysis. The kinetic constants for each substrate were determined by monitoring the production of *para*-acetylphenol at 294 nm (ε_{294}= 7,710 M^{-1} cm^{-1}) in 50 mM CHES, pH 9.0, buffer using a SpectraMax plate reader

(Molecular Devices Inc., Sunnyvale, CA) at 30 °C. Protein concentration in crude samples was determined by measuring the absorbance at 280 nm. The kinetic constants (k_{cat} and k_{cat}/K_m) were obtained by fitting the data to equation (1), where *v* is the initial velocity, k_{cat} is the turnover rate, [A] is the concentration of substrate, E_t is the enzyme concentration, and K_m is the Michaelis constant.

$$v / E_t = k_{cat} [A] / (K_m + [A]) \quad (4.1)$$

X-ray Structure Determination and Refinement. The crystallization, structural determination and refinement of the PTE mutants, QFRN, GWT-d3 and GWT-f5 were conducted by Mr. Nicolas Fox. The works for the H254Q/H257F mutant was performed by Dr. Jungwook Kim.

Results

Expression of PTE with K185R and I274N Mutations. SDS-PAGE analysis of the soluble portions of the cell lysate for the H254G/H257W/L303T mutant and the GWT-d1 mutant (H254G/H257W/L303T/ K185R/I274N) are shown in **Figure 4.1**. The protein expression level and the soluble portion of the GWT-d1 mutant are slightly greater than the H254G/H257W/L303T (GWT) mutant. The amount of protein that has can be obtained from purification of the GWT-d1 mutant is 10-fold higher than the H254G/H257W/L303T (GWT) mutant. The addition of the K185R and I274N mutations to the wild-type PTE and other mutants help to increase the expression and protein yields by 2- to 10-fold. This suggests that the K185R and I274N mutations enhance net protein expression and solubility of PTE.

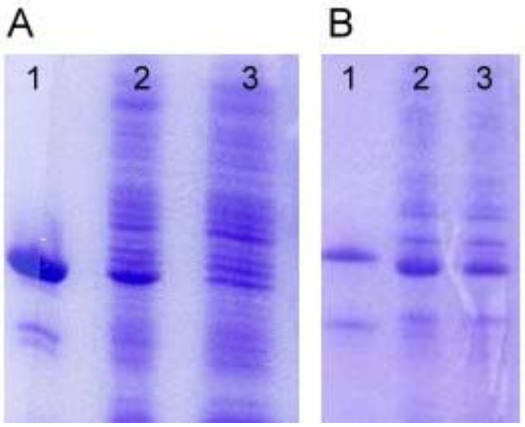

Figure 4.1 SDS-PAGE gels of crude cell lysate of the H254G/H257W/L303T mutant (A) and the GWT-d1 (H254G/H257W/L303T/K185R/I274N) mutant (B). The first lanes are standard PTE, the second lanes are cell lysate, and the third lanes are collected from the supernatant after the centrifugation of cell lysate.

Discovery of Variants towards the S_p- GF Analogue by Screening the Single and Double Substitution Libraries. The H254G/H257W/L303T mutant was previously shown to have the highest activity for the hydrolysis of the more toxic S_p- enatiomers of soman (GD) and cyclosarin (GF) analogues. The K185R and I274N mutations of PTE can increase protein expression and solubility. Hence, libraries were constructed using the GWT-d1 mutant (H254G/H257W/L303T/K185R/I274N) as the template to discover more active PTE variants for the hydrolysis of the S_p- enantiomers of compounds **4** and **5**. The 9 amino acid residues other than positions 254, 257 and 303 in the substrate binding pocket were considered as "hot spots" to be randomized for the construction of PTE libraries. The single substitution library of PTE, M317X was therefore constructed. The double substitution libraries, W131X/F132X, F306X/Y309X, S308X/Y309X, and I106X/Y308X, which have two residues randomized were also constructed. Six colonies from each library were selected randomly to confirm that the sites were randomized at the targeted positions (**Table 4.2**). Around 60 colonies from the single substitution library and around 550 colonies from the double substitution libraries were picked and grown in the super broth culture, and screened with the S_p- enantiomer of compound **5**. The variants with higher activity than the background from the first round of screening were isolated and rescreened with the same substrate. The W131X/F132X, the F306X/Y309X, the S308X/Y309X and the I106X/Y308X libraries were shown to have no any significant improvement towards the hydrolysis of the S_p- enantiomer of compound **5**. **Figure 4.2 (A)** is an example of the screening of the double substitution library**,** W131X/F132X. The first 10 samples comprise the following controls: BL21

Table 4.2 Sequence identifications of the PTE variants from the M317X, W131X/F132X, F306X/Y309X, S308X/Y309X and I106X/S308X libraries using the gene for the GWT-d2 mutant as the template.

ID of the M317X library	Mutations at the targeted sites
1	M317H
2	M317F
3	M317P

ID of the W131X/F132X library	Mutations at the targeted sites	ID of the F306X/Y309X library	Mutations at the targeted sites
1	W131P/F132Q	1	F306R/Y309Q
2	W131I/F132K	2	Y309H
3	W131A/F132E	3	F306Y/Y309A
4	W131D/F132N	4	F306W/Y309G
5	W131H/F132A	5	F306V/Y309L
6	W131N/F132P	6	F306F/Y309T

ID of the S308X/Y309X library	Mutations at the targeted sites	ID of the I106X/S308X library	Mutations at the targeted sites
1	S308L/Y309H	1	I106V/S308F
2	S308G/Y309N	2	I106S/S308Q
3	S308M/Y309G	3	I106L/S308T
4	S308T/Y309K	4	I106G
5	S308C/Y309K	5	I106A/S308L
6	S308Q/Y309S	6	S308C

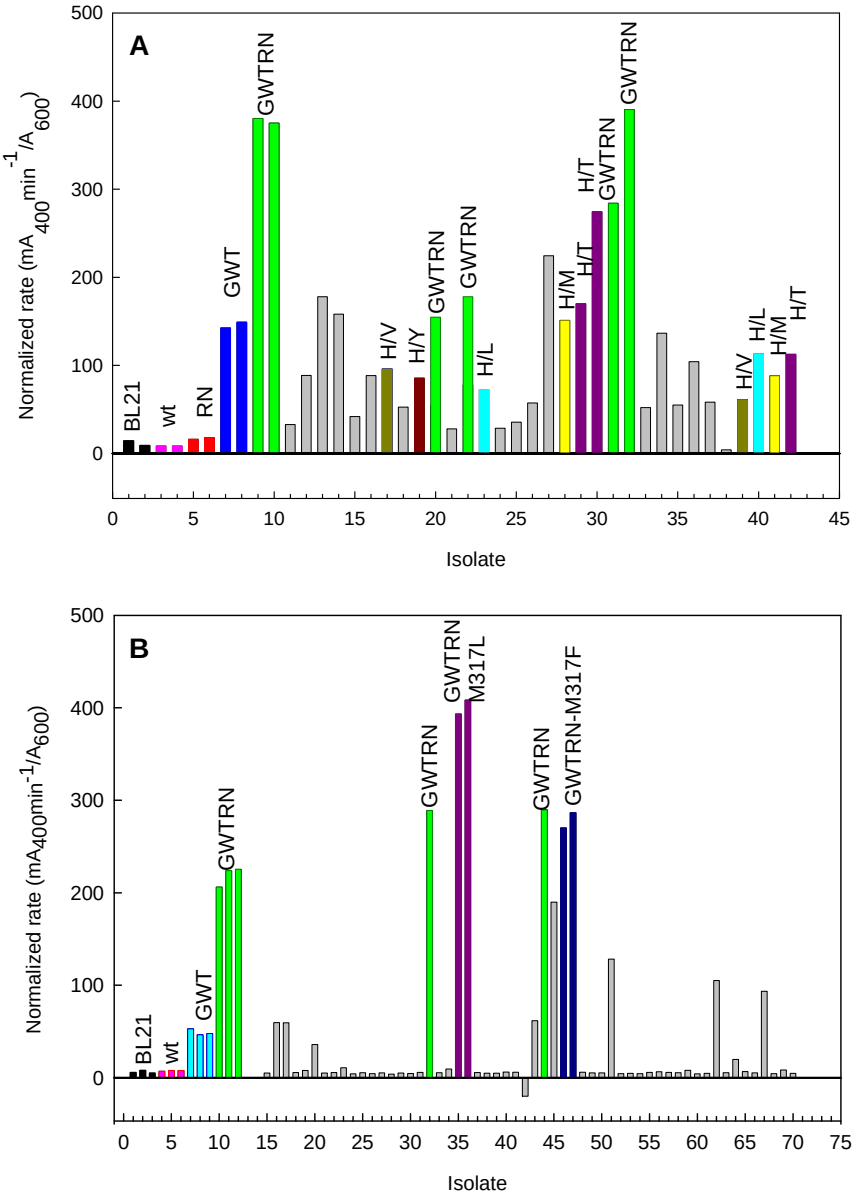

Figure 4.2 Screening of the (A) W131X/F132X and (B) M317X mutant libraries against the S_p- enantiomer of compound **5** using the GWT-d1 mutant (H254G/H257W/L303T/K185R/I274N) as the template. The W131X/F132X library in **(A)** was the second round of screening. The colonies were selected from the first round with positive results.

(DE3) containing pET20b (black), WT PTE (pink), RN PTE (red), GWT PTE (blue), and GWT-d1 PTE (GWTRN) (light green). This is the second round of screening that selected the samples with positive results from the first round. The W131X/F132X mutant library did not have beneficial variants towards the S_p- enantiomer of compound **5**. **Figure 4.2 (B)** displays the screening of the single substitution library, M317X, the first 12 samples comprise the following controls: BL21 (DE3) containing pET20b (black), WT PTE (pink), GWT PTE (cyan), and GWTRN PTE (light green). The GWT-f1 mutant (H254G/H257W/L303T/M317L/K185R/I274N) from the M317X library was isolated and shown to have a 1.5-fold enhancement in a normalized rate compared to the template GWT-d1 mutant by screening with the S_p- enantiomer of compound **5**. The colony with the background sequence for the GWT-d1 mutant was isolated. They were shown to have similar normalized rate to the GWT-d1 PTE control toward the S_p-enantiomer of compound **5**.

The purified GWT-f1 mutant was shown to have slightly better activity towards the S_p- enantiomer of compound **5** than the H254G/H257W/L303T mutant. QuikChange mutagenesis was performed to change the K185R and the I274N mutations of GWT-f1 back to lysine and isolucine, respectively. The activity for the hydrolysis of the S_p-enantiomer of compound **5** of the purified GWT-f2 mutant (H254G/H257W/L303T/M317L) is higher activity than the GWT-f1 mutant.

Discovery of Active Variants towards the S_p- GD Analogue by Screening Double Substitution Libraries. The 12 amino acid residues in the substrate binding pocket were chosen for double substitution libraries using the GWT-d1 mutant

(H254G/H257W/L303T/K185R/I274N) as the template. The W131X/F132X, F306X/Y309X, S308X/Y309X and I106X/Y308X libraries were screened with the S_p- enantiomers of compound **4**, but no beneficial variants were discovered. The A80V mutation was reported to have improved the expression of PTE in *E. coli* cells (*31*). This mutation was added to the GWT-d1 mutant using QuikChange mutagenesis. The GWT-d2 mutant (H254G/H257W/L303T/K185R/I274N/A80V) was shown to have a slightly better protein expression level and a higher activity towards the S_p- enantiomer of compound **4** than the GWT-d1 mutant. Double substitution libraries that randomize the residues close to the substrate binding pocket were created. The I255X/W302X and C59X/S61X libraries were constructed using the GWT-d2 mutant as the template. Six colonies from each library were selected to determine that the targeted positions were randomized (**Table 4.3**). For each double substitution library, around 600 colonies were picked and grown in the super broth culture and screened with the S_p- enantiomers of substrate **4**. **Figure 4.3 (A)(B)** shows the results for the second round of screening of the I255X/W302X and C59X/S61X libraries. These colonies were selected from the samples with positive results in the first round. The first 6 samples comprise the following controls: BL21 (DE3) containing pET20b (black), WT PTE (pink), and GWTRNV PTE (light green). The H254G/H257W/L303T/K185R/I274N/A80V/I255A mutant from the I255X/W302X library and the H254G/H257W/L303T/K185R/I274N/A80V/C59F mutant from the C59X/S61X library were shown to have a slightly higher normalized rate than the starting template against the S_p- enantiomers of compound **4.** However, the purified mutants,

Table 4.3 Sequence identifications of the PTE variants from the I255X/W302X and the C59X/S61X libraries using the gene for the GWT-d2 mutant as the template.

ID of the I255X/W302X library	Mutations at the targeted sites
1	I255R/W302R
2	I255L/W302A
3	I255M
4	I255S/W302Q
5	I255T/W302G
6	I255P/W302R
ID of the C59X/S61X library	**Mutations at the targeted sites**
1	C59F
2	C59L
3	C59V/S61T
4	C59Y/S61K
5	C59N/S61F
6	C59I/S61L

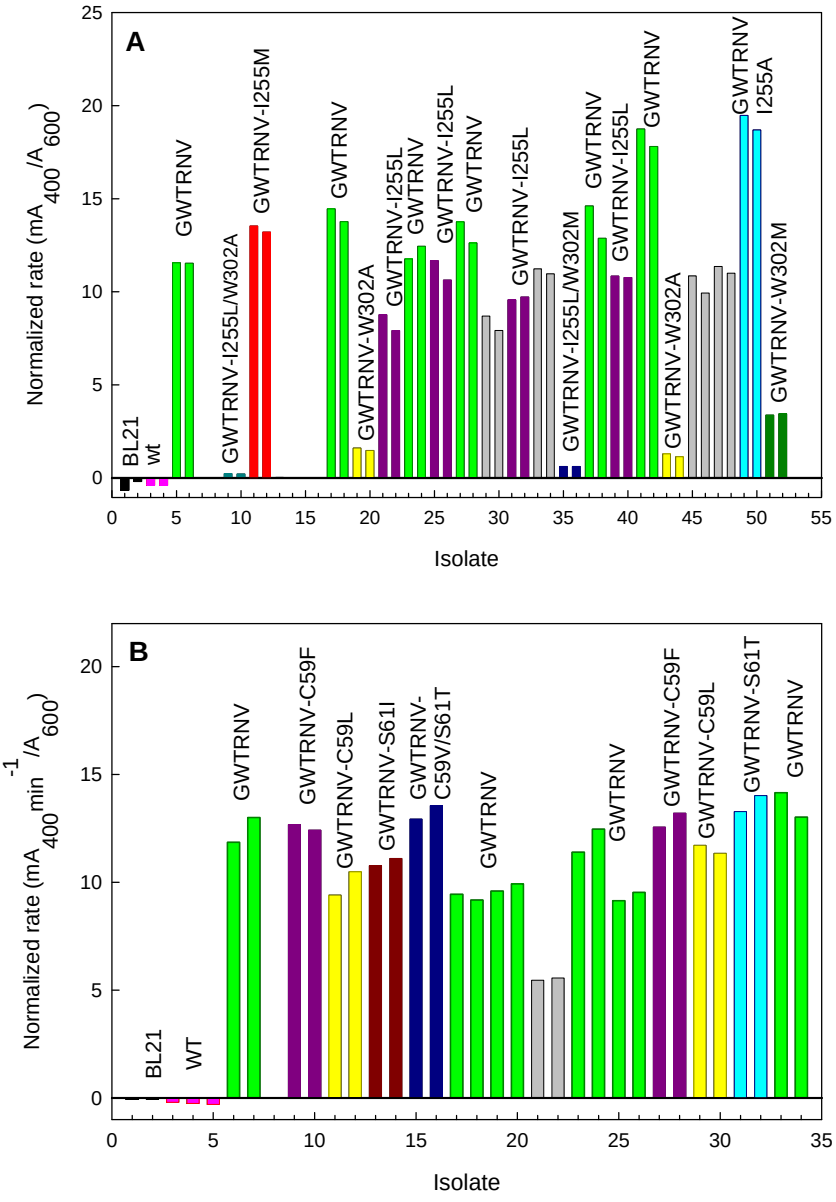

Figure 4.3 Screening of the I255X/W302X (A) and C59X/S61X (B) mutant libraries against the S_p- enantiomers of compound **4** using the GWT-d2 mutant (H254G/H257W/L303T/K185R/I274N/A80V) as the template. These are the second round of screening. The colonies were chosen from the samples with positive results in the first round of screening.

H254G/H257W/L303T/K185R/I274N/A80V/I255A and H254G/H257W/L303T/K185R/I274N/A80V/C59F, did not have an enhanced activity towards the S_p- enantiomers of compound **4**. The GWT-d3 (H254G/H257W/L303T/K185R/I274N/A80V/S61T) mutant was isolated and shown to have a 1.3-fold enhancement in the normalized rate compared to the template mutant, GWT-d2, by screening with the S_p- enantiomers of compound **4** (**Figure 4.3 (B)**). The purified GWT-d3 mutant displays the highest activity towards the S_p- enantiomers of compound **4**.

Growth of E. coli *Coexpressing PTE and GpdQ.* The growth of GpdQ+ cells in the phosphate free MOPS minimal medium in the presence of phosphonate esters was tested in previous studies. The growth rate of the cells was proportional to the catalytic efficiency of GpdQ towards the phosphonate substrates (*102*). The growth rate of the GpdQ+/PTE+ cells is related to the catalytic activities of PTE and GpdQ towards the organophosphonate diesters and methyl phosphonate monoesters, respectively. Different PTE mutants have different expression levels and thus the intracellular concentration of PTE is also associated with cell growth. In **Figure 4.4**, PTE and GpdQ coexpressed *E. coli* BL21 (DE3) cells were grown in the phosphate free MOPS minimal medium using the S_p-enantiomer of compounds **2** and **3** as the phosphorus source. The OD_{600} was measured for about 125 hours to observe cell growth. According to Chapter III and **Table 4.6** and **4.7**, the wild-type PTE has a slower hydrolysis rate towards the S_p-enantiomers of compound **2** and **3** relative to the R_p- enantiomers. The H257Y/L303T

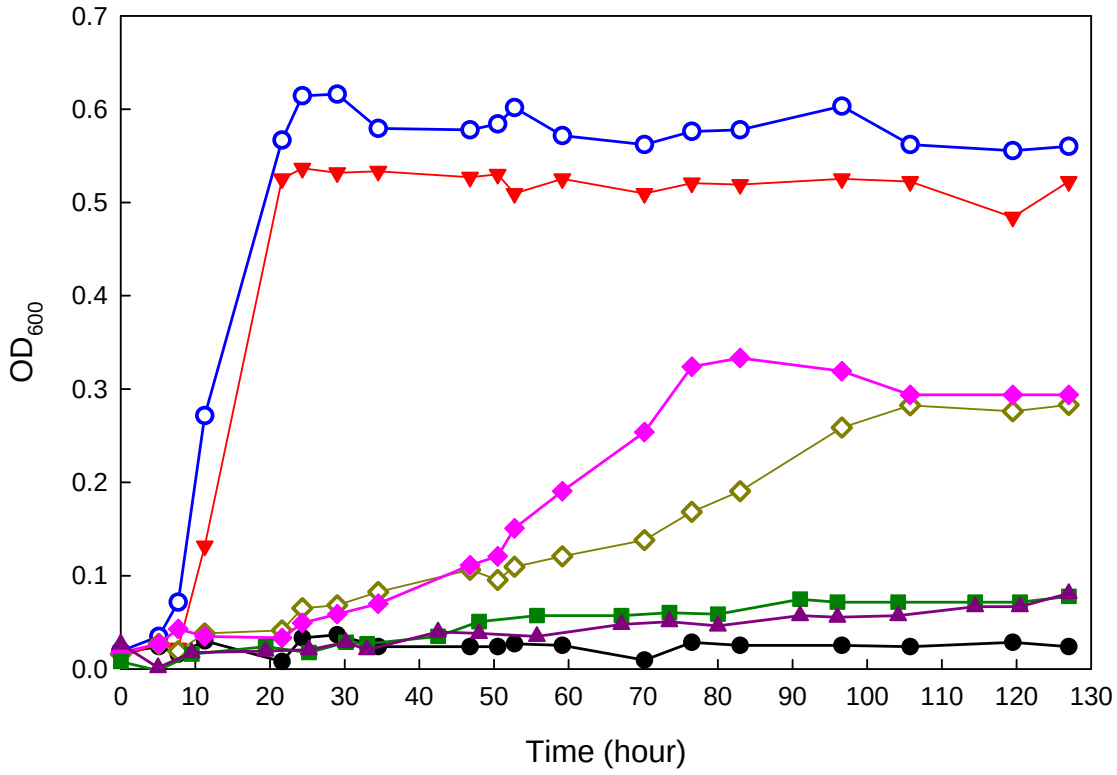

Figure 4.4 Time courses for the growth of GpdQ+/wild-type PTE in the presence of S_p-**2** (■), GpdQ+/wild-type PTE in the presence of S_p-**3** (▲), GpdQ+/ mutant PTE (H257Y/L303T) in the presence of S_p-**2** (◇), GpdQ+/ mutant PTE (I106A/H257Y/S308A) in the presence of S_p-**3** (◆), the control experiments are cells *E. coli* BL21 (DE3) in the presence of inorganic phosphate (○), methyl phosphonate(▼), and no phosphate source(●).

(YT) and the I106A/H257Y/S308A (AYA) mutants were shown to have higher activity in both k_{cat} and k_{cat}/K_m values towards the S_p-enantiomers of compound **2** and **3**, respectively. The growth curves of GpdQ+/ wild-type PTE+ cells did not show any enhancement within 125 hours. However, the cells of GpdQ+/ YT-PTE growing on the S_p-enantiomer of compound **2** show a lag phase of approximately 70 hours and the cells of GpdQ+/ AYA-PTE growing on the S_p-enantiomer of compound **3** show a lag phase of 50 hours. Previous studies have shown that the k_{cat}/K_m value of GpdQ against O-isobutyl methyl phosphonate (the hydrolysis product of compound **3**) is 66-fold higher than O-isopropyl methyl phosphonate (the hydrolysis product of compound **2**). In addition, the k_{cat}/K_m value of the I106A/H257Y/S308A (AYA) mutant towards the S_p-enantiomer of compound **3** is $3.9 \times 10^5\ M^{-1}s^{-1}$, and the k_{cat}/K_m value of the H257Y/L303T (YT) mutant towards the S_p- enantiomer of compound **2** is $1.1 \times 10^5\ M^{-1}s^{-1}$. The growth rates of GpdQ+/ YT-PTE with the S_p-enantiomer of compound **2** and GpdQ+/ AYA-PTE with the S_p-enantiomer **3** were influenced by the hydrolysis activity of mutant PTE towards the organophosphonates and GpdQ toward the phosphonates. Thus, the lag phase for GpdQ+/ YT-PTE is longer than for GpdQ+/ AYA-PTE. In control experiments, the growth curves of *E. coli* BL21 cells in the presence of inorganic phosphate are the fastest and followed by *E. coli* BL21 cells in the presence of methyl phosphonate.

The growth curves of GpdQ+/PTE+ cells in the phosphate free MOPS minimal medium in the presence of the S_p-enantiomer of compound **5** are shown in **Figure 4.5**.

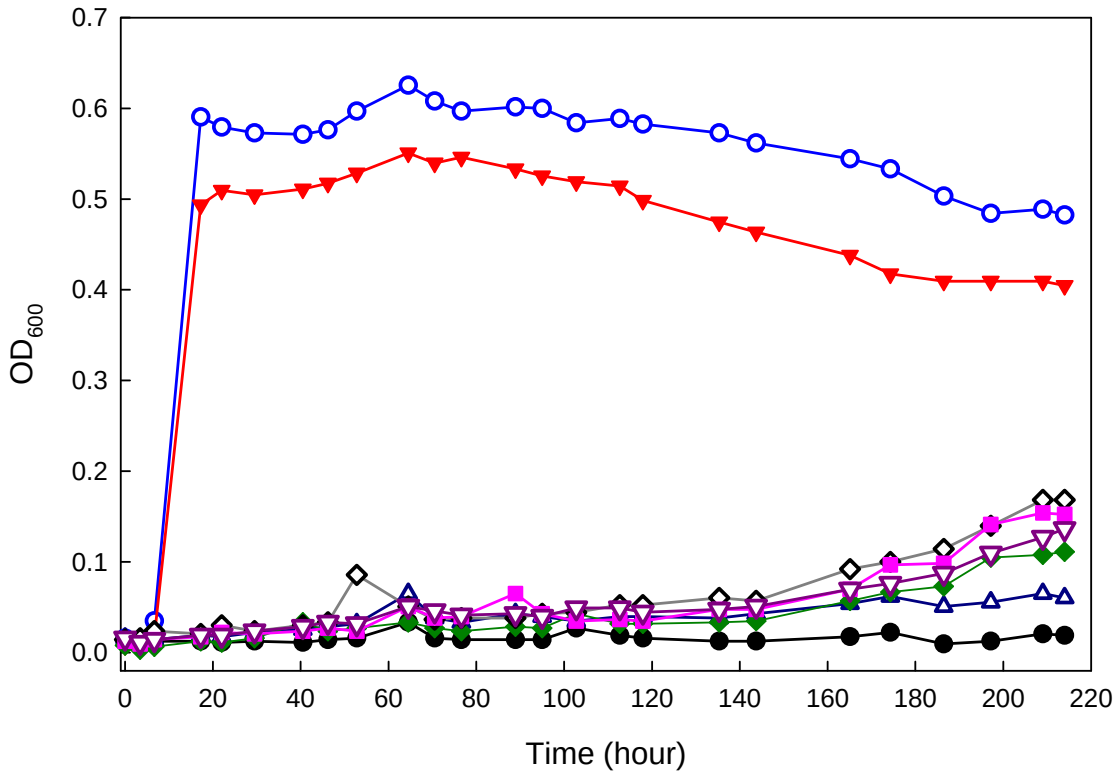

Figure 4.5 Time courses for the growth of GpdQ+/wild-type PTE in the presence of S_p-**5** (△), GpdQ+/ GWT PTE in the presence of S_p-**5** (■), GpdQ+/ mutant PTE GWT-d1 (H254G/H257W/L303T/K185R/I274N) in the presence of S_p-**5** (▽), GpdQ+/ GWT-f1 PTE (H254G/H257W/L303T/K185R/I274N/ M317L) in the presence of S_p-**5** (◆), GpdQ+/ GWT-f2 PTE (H254G/H257W/L303T/M317L) in the presence of S_p-**5**(◇), the control experiments are cells *E. coli* BL21 (DE3) in the presence of inorganic phosphate (○), methyl phosphonate(▼), and no phosphate source(●).

The cells of the GpdQ+/ PTE mutants (H254G/H257W/L303T (GWT), GWT-f1, GWT-f2, and GWT-d1) growing on the S_p-enantiomer of compound **5** display similar lag phases of approximately 165 hours, but slightly different growth rates. The GWT-f2 mutant has the best growth rate compared to the other three PTE mutants. The mutants that contain K185R/I274N were shown to have higher protein expression levels, so the intracellular concentration of PTE is higher and more substrate could be hydrolyzed to proceed the following phosphate assimilation catabolic pathway. Therefore, to be able to enhance enzyme evolution, the GWT-f1 mutant was utilized as the template to create the PTE randomized library. *In vivo* selection was performed to assess the next generation of beneficial mutants against the S_p- enantiomer of compound **5.** The results indicate that the growth rates are closely linked to the hydrolysis rate of PTE for organophosphonate diesters and GpdQ for methyl phosphonate monoesters, the expression levels of PTE is also a factor for the growth rates of the GpdQ+/PTE+ cells.

Discovery of the Active Variants towards the S_p- GF Analogue Using in vivo *Selection.* The GWT-f2 mutant (H254G/H257W/L303T/M317L) was found to be the best mutant for the hydrolysis of the S_p- GF analogue from the single substitution library. The GWT-f1 mutant (H254G/H257W/L303T/M317L/K185R/I274N) with two additional K185R and I274N substitutions is higher in protein expression level. Therefore, the library with six randomized amino acid residues in the substrate binding pocket, Ile-106, Phe-132, Leu-271, Phe-306, Ser-308 and Tyr-309, was constructed using the gene of the GWT-f1 mutant as the template. These six sites were randomized to different combinations of amino acid residues. The Ile-106 residue was randomized

to 6 amino acids, the Phe-132 residue was randomized to 13 amino acids, the Leu-271 residue was randomized to 5 amino acids, the Phe-306 residue was randomized to 4 amino acids, the Ser-308 residue was randomized to 10 amino acids and the Tyr-309 residue was randomized to 12 amino acids. This library contains 1.87×10^5 variants. Eight colonies from this library were selected to verify that the targeted sites were randomized (**Table 4.4**). The PTE library/GpdQ-pETDuet plasmid was transformed into *E. coli* BL21(DE3) cells and plated on LB agarose. Approximately 5.8×10^5 cells were selected and grown on an agarose plate containing phosphate free MOPS minimal medium and 1 mM of the S_p- enantiomer of compound **5**. The colonies that contain beneficial mutations towards the hydrolysis of the S_p- enantiomer of compound **5** were identified as being larger in size than a background colony for the GWT-f1 mutant. Around 30 large-sized colonies were selected for growth on the 96-well blocks with the super broth culture and screened with the S_p- enantiomer of compound **5**.

The screening of the multisite-randomized library with the S_p- enantiomer of compound **5** is shown in **Figure 4.6 (A)**. The first 9 samples include the following controls: BL21 (DE3) containing pETDuet (black), WT PTE (pink), the GWT-f1 mutant GWTRNL PTE (light green). The GWT-f3 mutant (H254G/H257W/L303T/M317L/I106C/F132I/L271I/K185R/I274N) was found to have a 1.2-fold enhancement in the normalized rate against the S_p- enantiomer of compound **5** compared to the GWT-f1 mutant. Another mutant with twelve mutations, H254G/H257W/L303T/M317L/I106C/F132I/L271Y/F306L/S308C/Y309C/K185R/I274N, was found to have positive result from the other screening, but the normalized rate is

Table 4.4 Sequence identifications of the PTE variants made from multisite randomized library using the gene for the GWT-f1 mutant as the template.

No.	Mutational sites from error-prone PCR
1	I106V/F132I/L271Y/F306I/S308Q/Y309N
2	I106V/F132I/L271Y/F306L/S308V/Y309S
3	I106V/F132T/L271I/F306I/S308Q/Y309A
4	I106C/F132F/L271L/F306F/S308Q/Y309V
5	I106I/F132G/L271G/F306L/S308T/Y309S
6	I106C/F132F/L271L/F306M/S308T/Y309G
7	I106V/F132A/L271Y/F306I/S308E/Y309G
8	I106M/F132I/L271L/F306M/S308L/Y309Y

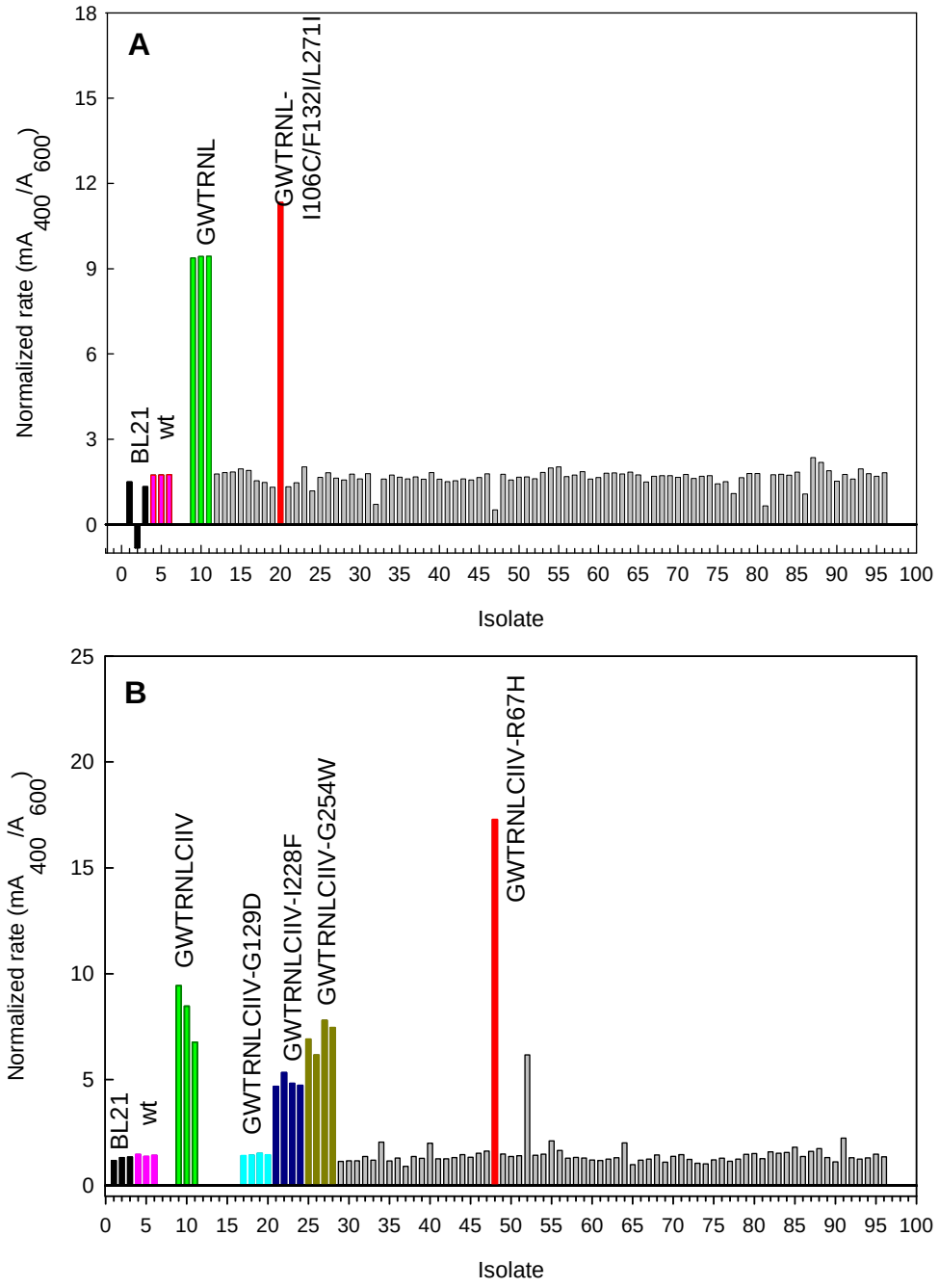

Figure 4.6 (A) Screening of 6 site randomized library from *in vivo* selection. (B) Screening of error-prone PCR library from *in vivo* selection. Both of them were the S_p-enantiomer of compound **5**.

slower than the GWT-f1control. The A80V mutation was added to the GWT-f3 mutant using QuikChange mutagenesis. The purified GWT-f4 mutant (H254G/H257W/L303T/M317L/I106C/F132I/L271I/K185R/I274N/A80V) was shown to have a higher activity towards the S_p- enantiomer of compound **5** than the purified GWT-f3 mutant by 2 fold.

The GWT-f4 mutant served as the template for error-prone PCR (epPCR). Random mutagenesis of the GWT-f4 gene was conducted using Mutazyme II DNA polymerase®. Ten colonies from this library were selected to verify the sequences, and they were shown to have ~1.5 mutations per 1000 kb gene on average. The identification of these ten colonies is shown in **Table 4.5**. The epPCR PTE library/GpdQ-pETDuet plasmids were transformed into *E. coli* BL21(DE3) cells and grown on LB agarose plates. Approximately 6×10^5 cells were selected and grown on the agarose plate containing the phosphate free MOPS minimal medium and 1 mM of the S_p- enantiomers of compound **5.** The colonies with a larger size than the background colony (the GWT-f4 mutant) were selected for growth in the super broth culture and screened with the S_p- enantiomer of compound **5**. The screening of the library created by error-prone PCR with the S_p- enantiomer of compound **5** is shown in **Figure 4.6 (B)**. The first 20 samples comprise the following controls: BL21 (DE3) containing pETDuet (black), WT PTE (pink), the GWT-f3 mutant GWTRNLCIIV PTE (light green), GWTRNLCIIV-G129D PTE (cyan), GWTRNLCIIV-I288F PTE (dark blue), WTRNLCIIV-H254W PTE (dark yellow). The GWT-f5 mutant (H254G/H257W/L303T/M317L/I106C/F132I/L271I/K185R/I274N/A80V/R67H) was

Table 4.5 Sequence identifications of the PTE variants made by error-prone PCR using the gene for the GWT-f4 mutant as the template.

No.	Mutational sites from error-prone PCR
1	L192R
2	L130Q/N353S
3	F51I/E159K
4	I228F
5	G129D
6	3 silent mutations
7	H254W
8	V40I/L192M
9	I288N/S308P
10	Background – the GWT-f4 mutant

shown to have a 2-fold enhancement in the normalized rate against the S_p- enantiomer of compound **5** compared to the template, the GWT-f4 mutant. Some positive results were found from other screening of the epPCR PTE library, however, 75% of them are the background or the GWT-f4 mutant with silent mutations.

Kinetic Properties of the PTE Mutants towards Organophosphonate Compounds. The kinetic parameters of the wild-type and mutants of PTE towards all of the organophosphonate compounds in **Scheme 4.3** are presented in **Tables 4.6** and **4.7**. The identification of the mutants in **Tables 4.6** and **4.7** are shown in **Table 4.8**. The RN mutant only contains mutations on the surface of PTE. The protein expression level and solubility of the RN mutant are higher than the wild-type. However, the catalytic efficiency is very similar to the wild-type. The H254Q/H257F (QF) mutant was shown to have a small K_m value towards the S_p-enantiomers of compounds **1**, **2** and **3** in Chapter III, which suggests that the substrate binding affinity is better, The QFRN mutant also has lower K_m values against the S_p-enantiomers of compounds **1**, **2** and **3** (less than 10 μM). In addition, the YTRN mutant also possesses similar kinetic properties with the H257Y/L303T (YT) mutant against all of the substrates. The most different point is the catalytic activity against the S_p- enantiomer of compound **3**, the k_{cat} value of the YTRN mutant is 7.5-fold higher and the k_{cat}/K_m value is 5-fold higher than the H257Y/L303T (YT) mutant.

Table 4.6 k_{cat} values (s^{-1}) for the wild-type and mutants of PTE.

	WT	RN	QFRN	YTRN	GWT	GWT-d1	GWT-d2	GWT-d3	GWT-f1	GWT-f2	GWT-f3	GWT-f4	GWT-f5
R_p/S_p-**1**	3.9e2	4.2e2	5.4e1	3.9e2	2.7e2	3.2e2	4.6e2	3.7e2	4.9e2	4.0e2	7.6e2	1.5e3	ND[a]
R_p-**1**	1.5e2	9.0e1	2.0e2	1.2e1	1.4e1	1.4e1	1.3e1	9.6e0	1.3e1	2.2e2	7.9e1	ND	ND
S_p-**1**	6.7e2	8.2e2	4.5e1	1.0e3	1.9e2	2.9e2	5.3e2	4.0e2	3.6e2	4.4e2	6.6e2	1.1e3	7.2e2
R_p/S_p-**2**	9.7e1	6.4e1	1.8e1	3.8e2	1.2e2	7.9e1	1.4e2	1.3e2	2.5e2	1.9e2	ND	9.7e2	8.1e2
R_p-**2**	1.0e2	6.6e1	6.6e1	2.0e1	ND	2.1e1	2.2e1	5.9e1	9.8e0	3.3e1	ND	ND	ND
S_p-**2**	4.0e1	2.0e1	1.1e1	7.0e2	9.2e1	8.6e1	1.3e2	2.0e2	3.0e2	2.3e2	6.2e2	1.1e3	5.9e2
R_p/S_p-**3**	5.4e1	4.4e1	1.9e1	6.7e2	4.7e1	6.3e1	6.4e1	7.5e1	9.1e1	8.7e1	1.5e2	2.5e2	1.7e2
R_p-**3**	9.3e1	4.8e1	1.3e2	4.3e1	2.0e1	8.0e0	1.3e1	2.2e1	2.9e1	3.4e1	1.3e1	1.5e1	ND
S_p-**3**	2.2e1	1.6e1	1.3e1	7.7e2	5.0e1	5.5e1	5.8e1	6.0e1	8.0e1	8.8e1	1.4e2	2.5e2	1.8e2
R_pR_c/R_pS_c $/S_pR_c/S_pS_c$-**4**	2.1e0	3.2e0	1.6e0	4.1e0	1.8e1	1.6e1	3.0e1	2.2e1	2.6e1	2.2e1	ND	ND	ND
R_pR_c/S_pR_c-**4**	2.5e0	3.3e0	1.4e0	6.6e0	1.1e1	1.8e1	2.7e1	2.6e1	4.4e1	3.8e1	ND	ND	ND
R_pS_c/S_pS_c-**4**	6.1e-1	1.0e0	7.0e-1	1.9e0	4.6e0	6.4e0	2.0e1	1.3e1	5.9e0	1.0e1	ND	8.9e0	ND
R_pR_c-**4**	3.4e0	4.5e0	1.1e0	5.8e-1	2.0e0	2.4e0	4.3e0	ND	4.0e0	ND	ND	ND	2.9e0
R_pS_c-**4**	4.5e-1	4.2e-1	3.3e-1	1.9e0	2.1e-1	1.4e0	ND	ND	8.9e-1	1.9e0	ND	ND	1.9e0
S_pR_c-**4**	7.7e-1	1.3e0	1.2e0	4.3e0	1.2e1	1.4e1	5.0e1	6.4e1	3.1e1	3.1e1	1.6e1	4.7e1	1.7e1
S_pS_c-**4**	1.6e-2	ND	5.1e-1	3.2e0	2.9e0	6.5e0	1.2e1	2.4e1	5.7e1	8.1e0	4.2e0	5.6e0	6.1e0
R_p/S_p-**5**	2.8e1	3.0e1	2.6e1	8.9e0	1.3e1	3.2e0	3.9e1	4.3e1	2.2e1	3.8e1	4.0e1	5.4e1	6.4e1
R_p-**5**	ND	2.5e1	2.2e1	1.7e1	8.1e-1	ND	9.7e-1	ND	ND	ND	2.2e0	ND	3.3e0
S_p-**5**	ND	1.3e-1	4.1e-1	7.2e0	1.9e1	3.1e0	4.7e1	4.4e1	2.6e1	3.1e1	4.4e1	1.2e2	1.2e2

[a] ND represents the enzymes were not saturated under 3mM of the substrates.

Table 4.7 k_{cat}/K_m ($M^{-1}s^{-1}$) for the wild-type and mutants of PTE.

	WT	RN	QFRN	YTRN	GWT	GWT-d1	GWT-d2	GWT-d3	GWT-f1	GWT-f2	GWT-f3	GWT-f4	GWT-f5
R_p/S_p-**1**	7.2e5	4.0e5	4.9e6	9.0e4	7.8e4	1.2e5	5.5e5	4.1e5	2.4e5	3.3e5	7.9e4	9.1e4	1.2e5
R_p-**1**	4.9e5	1.7e5	3.0e6	4.3e3	1.5e3	2.5e3	6.1e3	9.1e3	1.0e5	5.2e4	6.1e3	7.2e3	8.5e3
S_p-**1**	1.2e6	7.4e5	8.0e6	1.7e5	2.2e5	1.9e5	1.2e6	1.2e6	7.2e5	6.2e5	1.3e5	2.3e5	2.9e5
R_p/S_p-**2**	2.4e5	1.6e5	1.4e6	7.0e4	4.0e4	4.4e4	2.0e5	2.8e5	7.7e4	1.1e5	4.5e4	1.3e5	1.6e5
R_p-**2**	5.8e5	2.8e5	1.6e6	3.4e3	1.8e3	3.5e3	6.0e3	8.1e3	1.4e4	4.7e3	3.4e3	4.2e3	6.1e3
S_p-**2**	2.7e4	2.6e4	1.6e6	1.4e5	5.9e4	8.6e4	4.6e5	4.3e5	1.4e5	1.9e5	1.2e5	2.4e5	4.2e5
R_p/S_p-**3**	2.7e5	2.2e5	1.1e6	2.0e5	9.9e4	1.6e5	2.8e5	4.7e5	1.4e5	4.6e5	3.0e5	1.1e6	7.4e5
R_p-**3**	8.5e5	4.0e5	1.3e6	1.3e4	1.5e3	3.0e3	5.4e3	7.6e3	3.3e3	3.8e3	8.2e2	2.6e3	2.2e3
S_p-**3**	3.4e4	4.8e4	1.4e6	3.9e5	1.8e5	5.0e5	1.1e6	1.2e6	6.7e5	1.0e6	1.1e6	2.3e6	1.9e6
R_pR_c/R_pS_c /S_pR_c/S_pS_c-**4**	3.8e2	4.8e2	4.7e2	7.0e2	1.9e3	3.3e3	1.0e4	9.2e3	3.4e3	3.5e3	9.3e2	1.3e3	1.4e3
R_pR_c/S_pR_c-**4**	5.4e2	1.2e3	9.9e2	1.2e3	3.3e3	6.4e3	1.8e4	1.7e4	4.9e3	5.3e3	1.5e3	2.3e3	2.1e3
R_pS_c/S_pS_c-**4**	1.2e2	2.0e2	1.1e2	2.9e2	7.7e2	1.6e3	3.3e3	3.3e3	1.2e3	1.9e3	4.6e2	9.2e2	6.4e2
R_pR_c-**4**	1.3e3	3.0e3	2.8e2	3.0e2	2.2e2	6.8e2	6.4e2	5.6e2	4.2e2	4.1e2	6.3e2	7.9e2	8.5e2
R_pS_c-**4**	2.0e2	4.6e2	7.4e1	1.9e2	1.3e2	1.2e2	1.5e2	1.4e2	2.1e2	1.4 e2	1.4e2	2.0e2	1.8e2
S_pR_c-**4**	1.1e2	2.3e2	1.8e3	1.2e3	8.1e3	2.3e4	6.0e4	8.7e4	1.3e4	1.4e4	3.2e3	5.0e3	3.8e3
S_pS_c-**4**	3.2e0	1.5e1	9.6e1	4.8e2	1.7e3	4.2e3	8.1e3	1.1e4	2.6e3	2.5e3	1.5e3	1.5e3	1.2e3
R_p/S_p-**5**	7.4e3	7.1e3	4.6e3	9.1e3	1.5e4	4.7e3	7.8e4	7.2e4	2.6e4	2.1e4	3.3e4	9.2e4	9.2e4
R_p-**5**	1.6e4	1.7e4	9.0e3	3.5e3	2.5e2	3.0e2	5.4e2	5.5e2	6.0e2	8.6e2	4.5e2	5.1e2	7.7e2
S_p-**5**	2.1e1	2.8e1	3.6e2	1.4e4	2.8e4	1.0e4	5.2e4	1.5e5	3.9e4	7.7e4	1.2e5	2.5e5	3.2e5

Table 4.8 Identification of active PTE mutants.

Abbreviation of mutants	Mutational sites of mutants
RN	K185R/I274N
QFRN	H254Q/H257F/K185R/I274N
YTRN	H257Y/L303T/K185R/I274N
GWT-d1	H254G/H257W/L303T/K185R/I274N
GWT-d2	H254G /H257W/L303T/K185R/I274N/A80V
GWT-d3	H254G/H257W/L303T/K185R/I274N/A80V/S61T
GWT-f1	H254G/H257W/L303T/M317L/K185R/I274N
GWT-f2	H254G/H257W/L303T/M317L
GWT-f3	H254G/H257W/L303T/M317L/I106C/F132I/L271I/K185R/I274N
GWT-f4	H254G/H257W/L303T/M317L/I106C/F132I/L271I/K185R/I274N/ A80V
GWT-f5	H254G/H257W/L303T/M317L/I106C/F132I/L271I/K185R/I274N/ A80V/R67H

The GWT-d1, GWT-d2 and GWT-d3 mutants display an enhanced activity towards the two S_p- enantiomers of compound **4**, the analogues of the more toxic enantiomers of soman, relative to the H254G/H257W/L303T (GWT) mutant. The beneficial mutations, A80V, K185R and I274N, which are located at the surface of the protein can help protein solubility and increase the catalytic activity towards the S_p-enantiomers of compound **4**. Using the GWT-d2 mutant as a template, the GWT-d3 mutant was isolated by the screening methodology and shown to have the highest activity against the S_p- enantiomers of compound **4**. The k_{cat}/K_m values of the GWT-d3 mutant against S_pR_c- and S_pS_c- enantiomers of compound **4** are 8.7×10^4 and 1.1×10^4 $M^{-1}s^{-1}$, respectively.

The GWT-f1, GWT-f2 and GWT-f3 mutants were shown to have enhanced activity towards the S_p- enantiomer of compound **5** compared to the H254G/H257W/L303T (GWT) mutant. The M317L mutation of the GWT-f1 mutant was found by screening with the S_p- enantiomer of compound **5**. The GWT-f3 and GWT-f5 mutant were identified from the *in vivo* selection with PTE and GpdQ coexpressing *E. coli* cells on the phosphate free minimal medium agarose plate with the S_p-enantiomer of compound **5** as the sole phosphorus source. Through this selection technique, the GWT-f5 mutant is the best mutant for the hydrolysis of the S_p-enantiomer of compound **5**. The k_{cat}/K_m value is 3.2×10^5 $M^{-1}s^{-1}$. The procedure for the discovery of the PTE variants that have enhanced activity for the hydrolysis of the S_p-enantiomers of compound **4** and **5** by directed evolution is shown in **Scheme 4.5.**

Scheme 4.5 Schematic representation of the directed evolution of PTE variants that contains enhanced activity towards the S_p- enantiomers of compounds **4** and **5**.

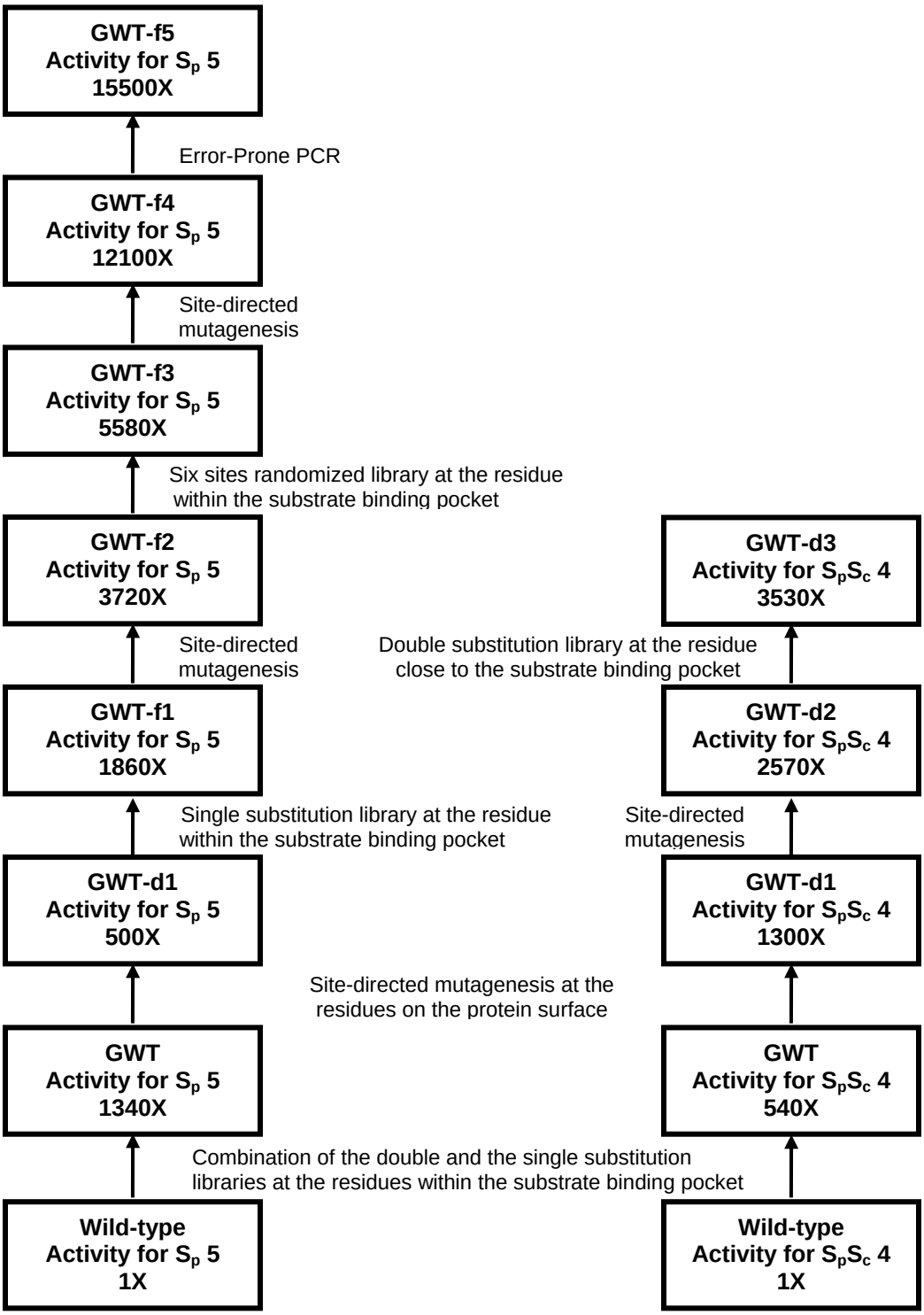

Structural Analysis of the Beneficial Mutants. The structures of the substrate binding pockets of the wild-type PTE (PDB: 1HZY) and mutants, H254Q/H257F (QF) (PDB: 2OQL), H254G/H257W/L303T (GWT) (PDB: 1P6B), QFRN, GWT-d3, GWT-f5 are shown in **Figure 4.7**. The metals in the wild-type, H254Q/H257F (QF) and H254G/H257W/L303T (GWT) structures are zinc, whereas the metals in the QFRN, GWT-d3 and GWT-f5 structures are cobalt. The backbone conformation of the residues in the substrate binding pocket and the rest of the protein are close. Superposition of QFRN, GWT-d3 and GWT-f5 mutants with the wild-type PTE (PDB: 1HZY) provides a Cα atom rmsd values of 0.37, 0.38 and 0.71 Å, respectively. The phenyl ring in Phe-132 of the H254Q/H257F (QF) mutant (**Figure 4.7(B))** rotates to a different position. The two positions of the phenyl ring of Phe-132 are observed in the H257Y/L303T structure (PDB: 2OB3) at high resolution (1.04 Å). One of the most noticeable differences from a comparison of the structures of H254G/H257W/L303T (GWT), GWT-d3 and GWT-f5 mutants is that the indole group of Trp-257 in the GWT-f5 mutant is closer to Leu-317 by 2.2 Å. This may be because the branched chain of the leucine residue in the GWT-f5 mutant provides more space for the Trp-257 residue compared to the longer chain of methionine. The I106C substitution of the GWT-f5 mutant has changed from a bulkier isoleucine group to a smaller thiol group.

The substitutions in the QFRN, GWT-d3 and GWT-f5 mutants are labeled in pink in **Figure 4.8 (A)**, **Figure 4.9(A)** and **Figure 4.10(A)**. The K185R and I274N mutations are located on the surface of the protein, Arg-185 is located on the external surface of the fourth α-helix and Asn-274 is located in loop 7. The side chain of

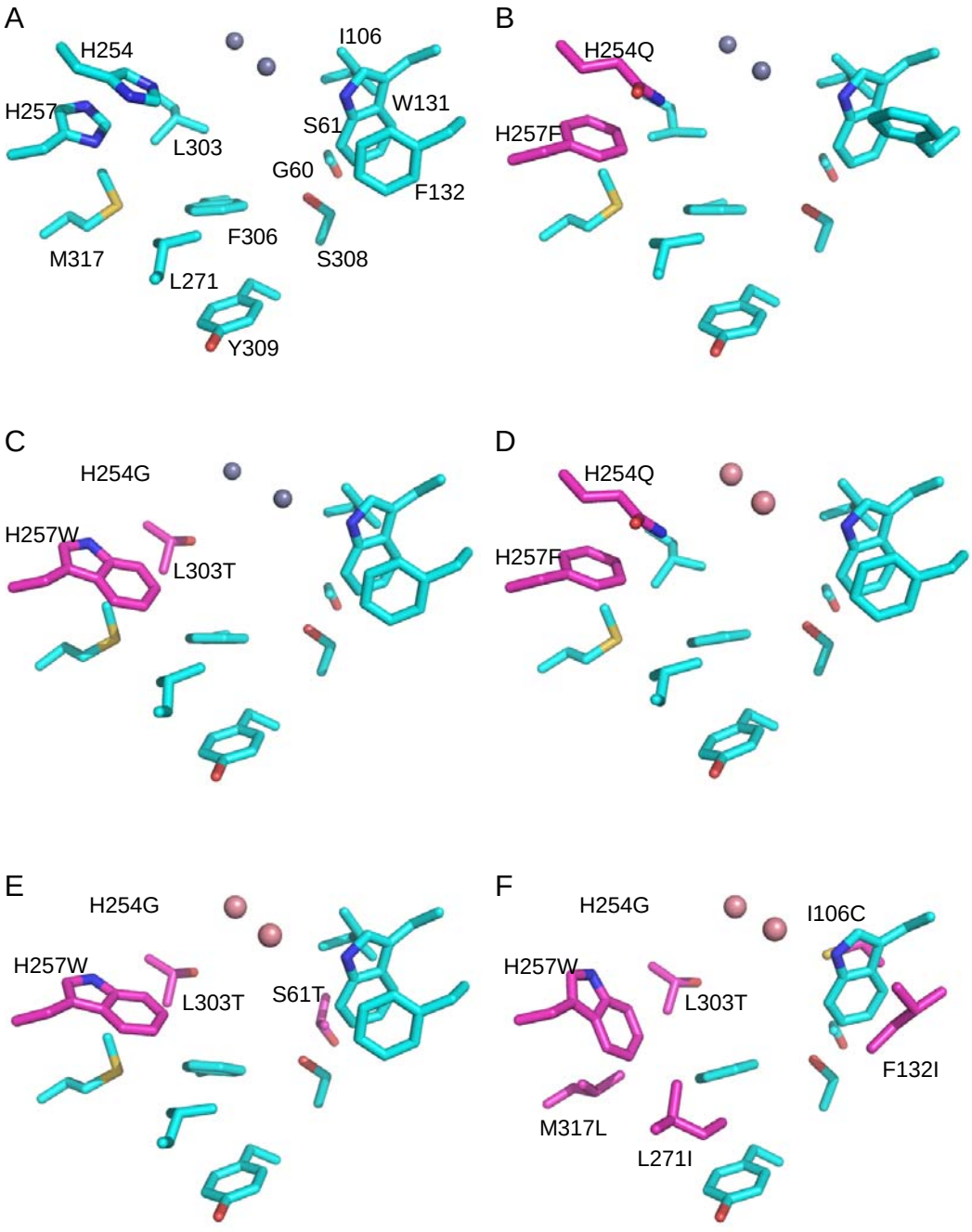

Figure 4.7 The substrate binding pocket of the wild-type and mutants of PTE. (A) wild-type (1HZY), (B) H254Q/H257F (2OQL), (C) H254G/H257W/L303T (1P6B) (D) QFRN, (E) GWT-d3 and (F) GWT-f5.

the Val-80 mutation is pointed outward at the first α-helix. The R67H mutation in the GWT-f5 mutant is located at the dimer interface (**Figure 4.10 (C)**). The two histidines at position 67 from two different subunits are stacked with an imidazole molecule, which was one of the components used for crystallization.

The K185R mutation in QFRN, GWT-d3 and GWT-f5 is shown to have hydrogen bond interactions with Ser-218 and Glu-219. The Arg-185 residue of the QFRN and GWT-f5 mutants (**Figure 4.8(B)** and **Figure 4.9(B)**) are slightly closer to Ser-218 compared to the GWT-d3 structure. However, the GWT-d5 mutant has a 3.3 Å distance between N^{ω} of Arg-185 and the carbonyl oxygen of Glu-181 on another side, this allows a hydrogen bond interaction of N^{ω} of Arg-185 and the oxygen of the carbonyl group of Glu-181. The distance between N^{δ} of Arg-185 and the oxygen of the carbonyl group of Glu-181 is 3.6 Å (**Figure 4.9(B)**). This suggests the Arg-185 residues in QFRN, GWT-d3 and GWT-f5 may be flexible on the surface of the protein to provide hydrogen bonding interaction between residues Glu-181, Ser-218 and Glu-219. However, the Lys-185 residue of the H254Q/H257F (QF) and H254G/H257W/L303T (GWT) mutants cannot form any hydrogen bonds with peripheral amino acid residues.

The I274N mutation is a change from a hydrophobic residue to a hydrophilic residue. In the case of the GWT-d3 mutant, the nitrogen and the oxygen of the side chain of Asn-274 are within the hydrogen bonding distance with the main chain amino and carbonyl groups (3.1 and 3.2 Å) (**Figure 4.9(C)**). However, the same circumstance is not shown in the QFRN mutant (**Figure 4.8(C)**). This implies the mutation of IIe-274

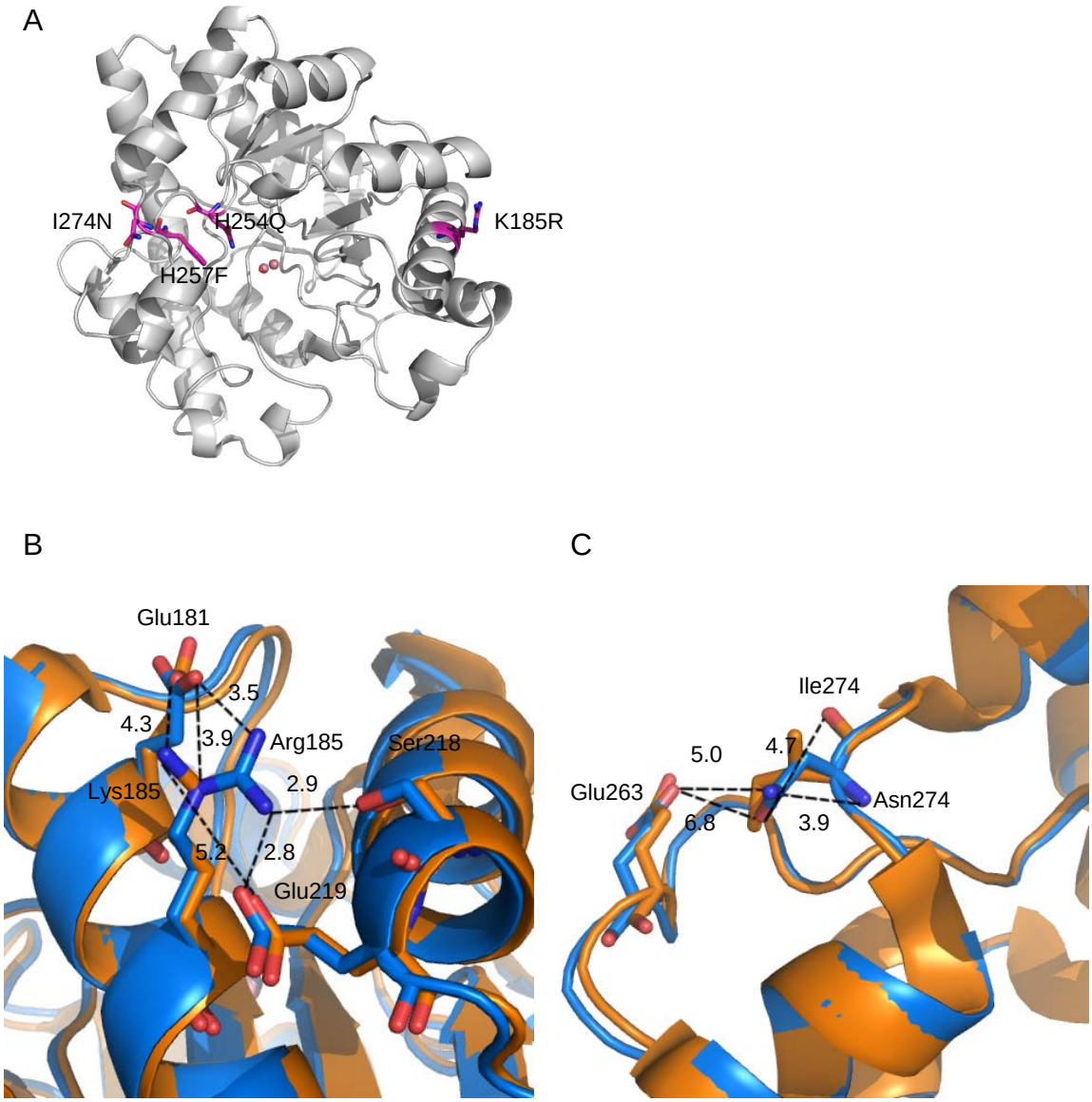

Figure 4.8 (A) The substitutions in the QFRN mutant. (B)(C) Comparisons of the QFRN (blue) and the H254Q/H257F (QF) (orange) structures

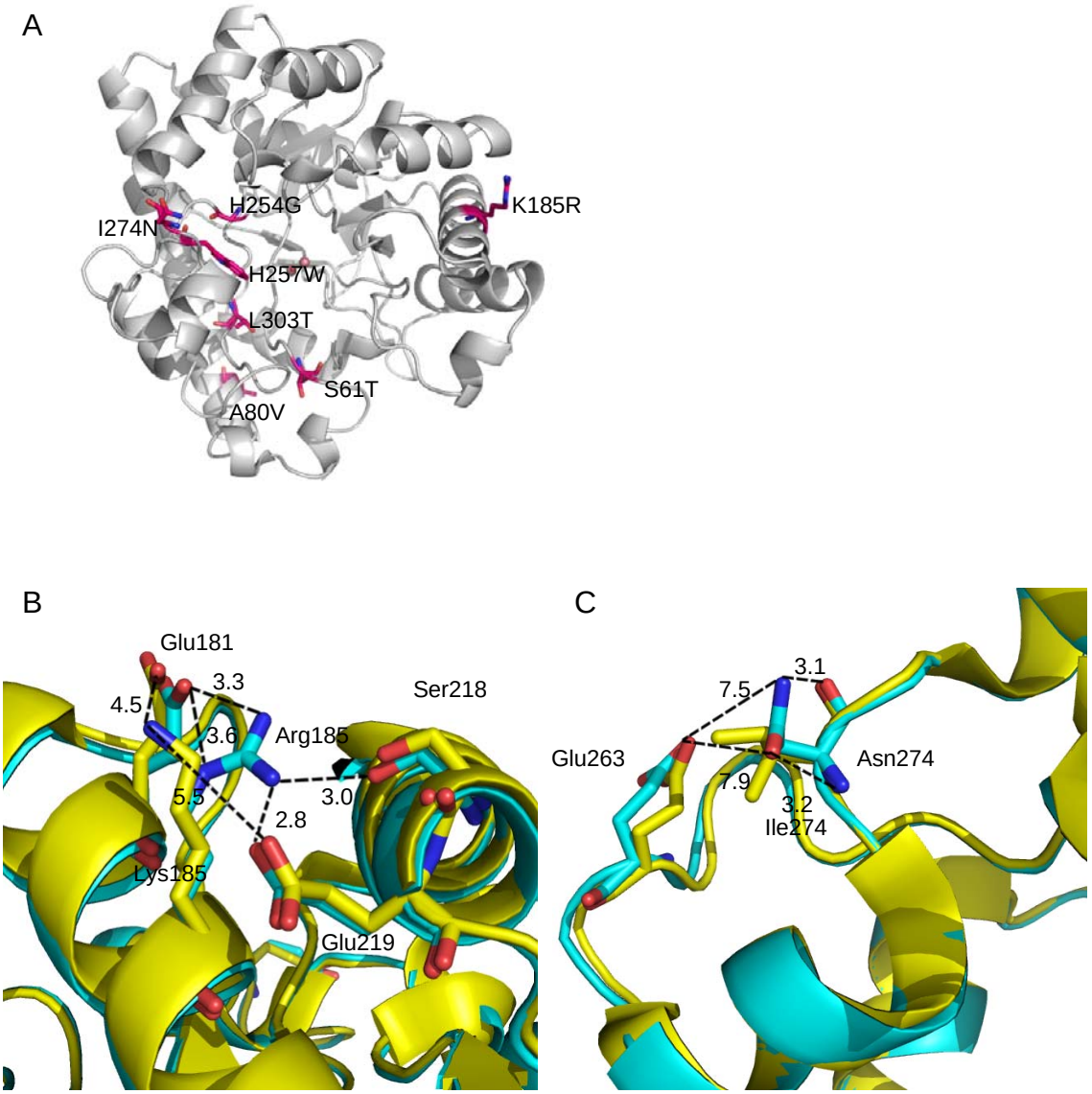

Figure 4.9 (A) The substitutions in the GWT-d3 mutant. (B)(C) Comparisons of the GWT-d3 (cyan) and the H254G/H257W/L303T (GWT) (yellow) structures.

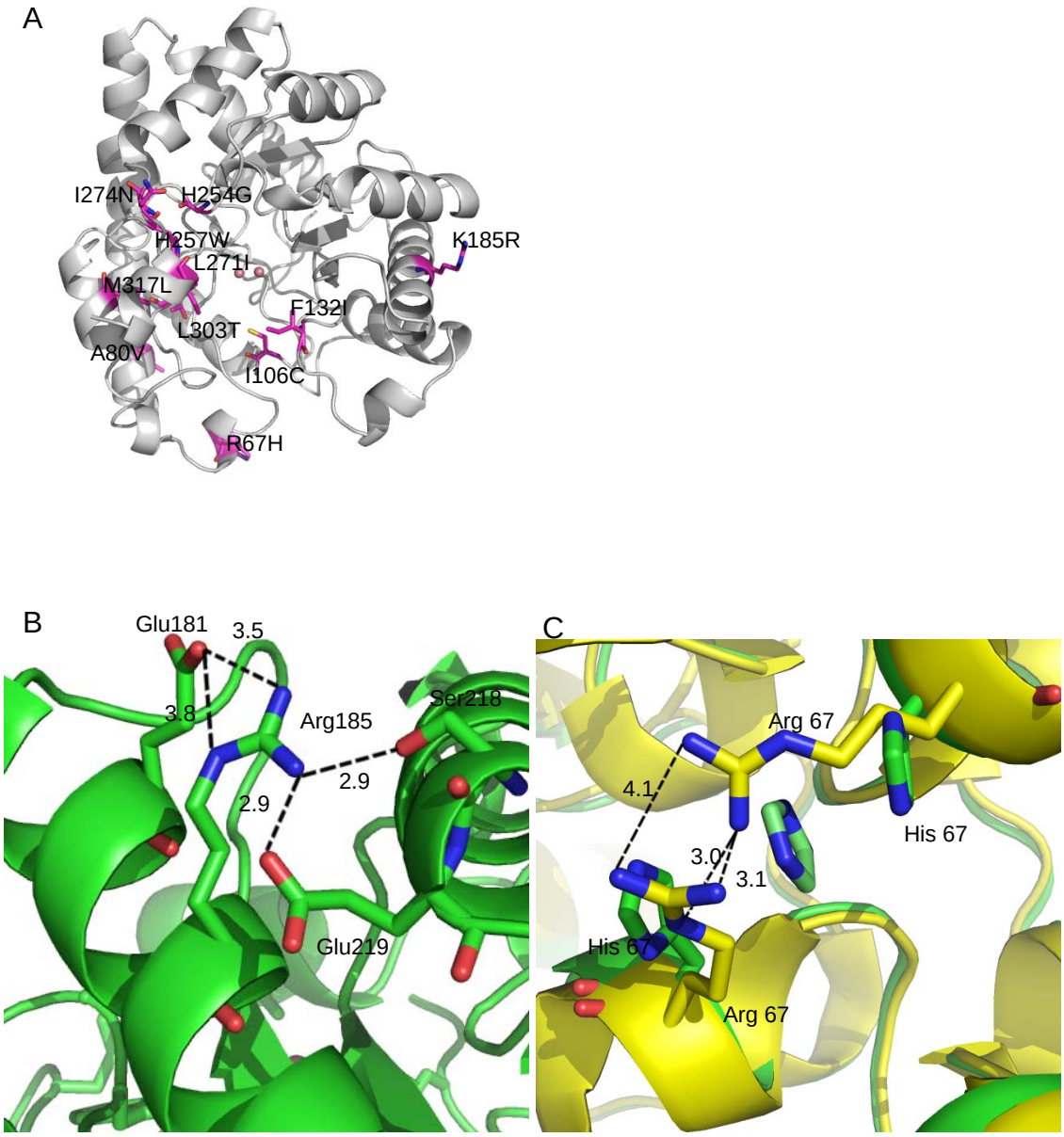

Figure 4.10 (A) The substitutions in the GWT-f5 mutant. (B) The K185R mutation of the GWT-f5. (C) Comparisons of His-67 and Arg-67 of the GWT-f5 (green) and the H254G/H257W/L303T(GWT) (yellow) structures.

to asparagine can provide more flexible movements for the residues on the surface of the protein.

Discussion

Wild-type PTE has a significant hydrolytic activity towards paraoxon. The k_{cat} value is ~ 10^4 s^{-1} and k_{cat}/K_m ~ 10^8 M^{-1} s^{-1}. However, the catalytic efficiency of the wild-type enzyme for the hydrolysis of organophosphorus nerve agents is significantly smaller, and for the hydrolysis of the more toxic S_p-enantiomers of organophosphorus nerve agents is even smaller. In Chapter III, the wild-type enzyme was shown to have a larger discrimination between the R_p and S_p-enantiomers when the substituents of the organophosphonate compounds (**Scheme 4.4**) are larger in size. The H254Q/H257F (QF) mutant was shown to have highest activity towards the more toxic S_p-enantiomers of VX, sarin and rVX analogues, compound **1**, **2** and **3**. The H254G/H257W/L303T mutant possessed the highest hydrolytic activity towards the more toxic S_p-enantiomers of soman and cyclosarin analogues, compound **4** and **5**. These mutants were selected for further modification to increase the hydrolysis activity by saturation mutagenesis and directed evolution.

The addition of K185R and I274N mutations to the wild-type and mutants of PTE increases protein expression levels and solubility. These two mutations could also enhance the hydrolytic activity for some of the compounds in **Scheme 4.3**. The QFRN mutant has higher k_{cat} and k_{cat}/K_m values towards most of the compounds compared to the H254Q/H257F (QF) mutant. Thus, the QFRN mutant is shown to have the best

activity towards the more toxic S_p-enantiomers of VX and sarin analogues, compound **1** and **2**. The enhancements are 7- and 60-fold higher than the wild-type, and the k_{cat}/K_m values are more than $10^6\ M^{-1}s^{-1}$ (**Figure 4.11**).

An *in vitro* screening technique was utilized to isolate the GWT-f1 mutant, which has a 3-fold higher activity than H254G/H257W/L303T (GWT) towards the S_p-enantiomer of the cyclosarin analogue, compound **5**. It is 3720-fold more active than the wild-type enzyme. The GWT-f1 and GWT-f2 mutants were coexpressed with GpdQ in *E. coli* cells. The cells could grow in a phosphate free minimal medium with a 165-hour lag phase using the S_p- enantiomer of compound **5** as the sole phosphorus source. Therefore, the *in vivo* selection technique is practical when using the S_p- enantiomer compound **5**. The GWT-f3 and GWT-f5 mutants were selected from the *in vivo* selection on the phosphate free MOPS minimal medium agarose plate. The GWT-f5 mutant was shown to have a 15,500-fold enhancement in k_{cat}/K_m for the hydrolysis of the more toxic S_p- enantiomer of compound **5** relative to the wild-type enzyme, and the k_{cat}/K_m value is more than $3 \times 10^5\ M^{-1}s^{-1}$ (**Figure 4.12**). Surprisingly, the GWT-f4 mutant that was found to enhance the activity against the S_p- enantiomer of compound **5** and it displays the best activity towards the of the S_p- enantiomer of compound **3**. The k_{cat}/K_m value of GWT-f4 towards the S_p- enantiomer of compound **3** is higher than $2 \times 10^6\ M^{-1}s^{-1}$ and 68 fold higher than the wild-type PTE (**Figure 4.11**). The GWT-f4 and GWT-f5 mutants comprise three distal mutations, A80V, K185R and I274N.

In a previous study, the inability of GpdQ to hydrolyze the hydrolysis product of soman, pinacolyl methyl phosphonate was demonstrated. Thus, the growth of GpdQ+

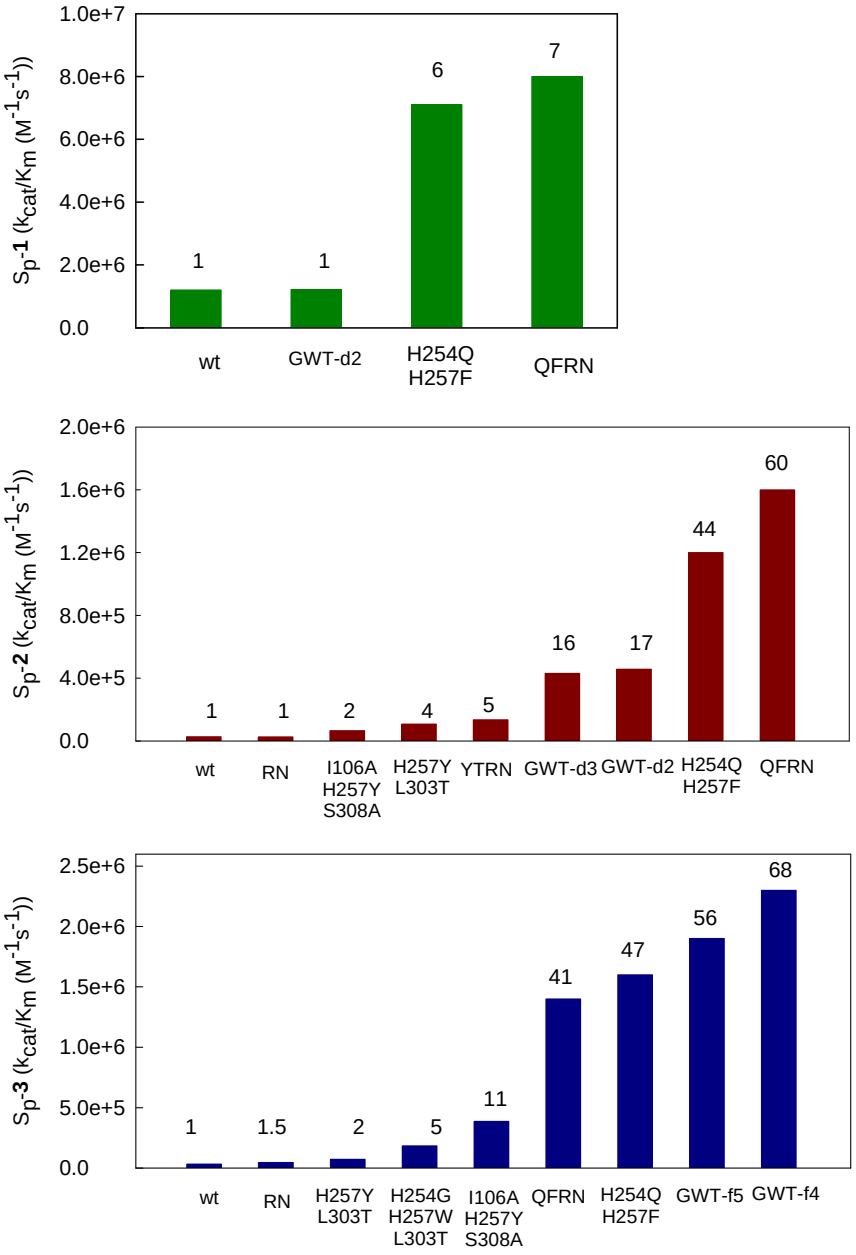

Figure 4.11 Bar graphs illustrating increased values of k_{cat}/K_m ($M^{-1}s^{-1}$)for the S_p-enantiomers of compound **1**, **2** and **3** catalyzed by the wild-type and mutants of PTE. The numbers represent the increase in activity for the mutants relative to the wild-type enzyme.

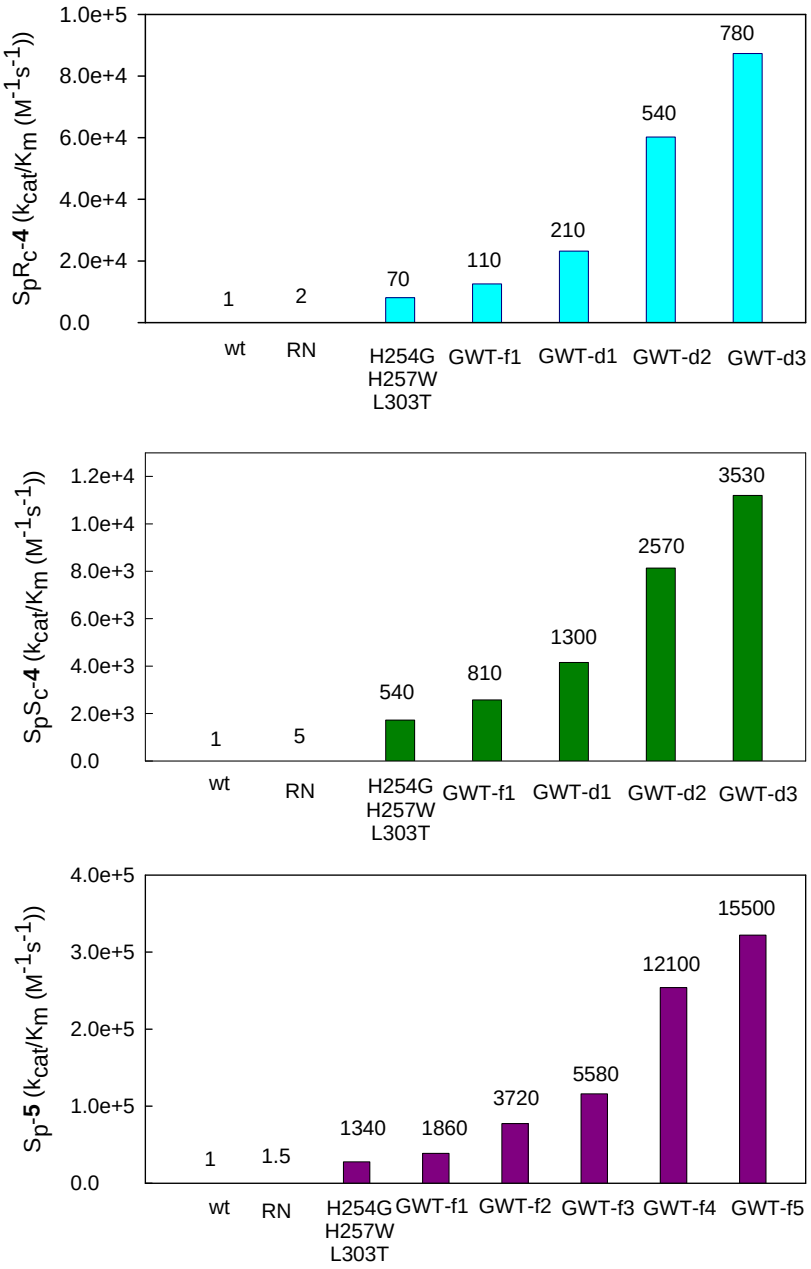

Figure 4.12 Bar graphs illustrating increased values of k_{cat}/K_m ($M^{-1}s^{-1}$) for the S_p-enantiomers of compound **4** and **5** catalyzed by the wild-type and mutants of PTE. The numbers represent the increase in activity for the mutants relative to the wild-type enzyme.

cells in a phosphorus minimal medium could not be observed in the presence of pinacolyl methyl phosphonate (XY Eman). This result shows the incapability of using *in vivo* selection for the discovery of the active mutants against the S_p- enantiomers of compound **4**. Nevertheless, the utilization of *in vitro* screening technique and the involvement of some sensitive distal mutations were able to isolate more active mutants that were based on the H254G/H257W/L303T (GWT) mutant as the template. The GWT-d3 mutant was discovered as the most active mutant to hydrolyze the more toxic S_p- enantiomers of the soman analogues, compound **4**. The k_{cat}/K_m values of the GWT-d3 mutant towards the S_pR_c and the S_pS_c - enantiomers of soman analogues are 780-and 3530-fold higher than the wild-type PTE.

The distal mutations, A80V, K185R and I274N, which are located at the surface of PTE can enhance protein expression. The R67H mutation is located at the dimer interface of PTE. These mutations are more than 17 Å away from the active site, and the sensitivity for the catalytic efficiency is not as high as the amino acid residues that reside the substrate binding pocket. However, these residues may be might be able to facilitate the entry of the substrate and increase the substrate binding affinity. The I106C, F132I and L271I mutations and the changes beyond the active site of the GWT-f5 mutant may make the protein more flexible than the H254G/H257W/L303T mutant for the entry of the S_p- enantiomer of compound **5.**

The X-ray crystal structures of the QFRN, the GWT-d3 and the GWT-f5 mutants show that the K185R and I274N mutations provide more hydrogen bonding interactions with the adjacent amino acid resides. In a previous study, the RN mutant was shown to

have 13-fold higher activity for the hydrolysis of paraoxon compared to the wild-type PTE (*28*). However, we have only observed a 2-fold enhancement (data not shown), and the other mutants with these two mutations could also increase the hydrolysis activity towards some of the organophosphonate compounds approximately 2-fold. Molecular modeling of the RN mutant showed that Glu-219 and Glu-181 can form hydrogen bonds with Arg-185. The Arg-185 residue could partition between these two glutamate residues. In addition, Glu-263 could potentially form a hydrogen bond with the Asn-274 residue (*28*). The observation from the crystal structures of the QFRN, GWT-d3 and the GWT-f5 mutants, additional residue Ser-218 can also form hydrogen bond with Arg-185. It makes the side chain of Arg-185 be closer to the side that has Ser-218 and Glu-219. Furthermore, the measurements of the I274N mutation and Glu-263 demonstrate their distances are not allowed to form hydrogen bonds. These three crystal structures indicate the K185R and I274N mutations provide more hydrogen bonding interactions with neighboring amino acid residues and water molecules which could facilitate the protein solubility and flexibility at the surface. The A80V mutation has a change to a bulkier and nonpolar side chain. It is also located at the protein surface, suggesting it may provide more efficient protein folding and contribute to protein stability. Overall, three distal mutations, A80V, K185R and I274N, could enhance protein expression level and hydrolytic activity towards most of the substrates. They might play an important role in improving the flexibility of the active site of PTE and assisting the entrance of organophosphonate compounds. A comparison with Arg- 67 of the H254G/H257W/L303T (GWT) mutant and His-67 of the GWT-f5 mutant, the two

arginines from different subunits forms hydrogen bonds to each other and the mutation to histidine at position 67 could weaken the hydrogen bond interaction between two monomers of PTE. The pi-pi stacking of two histidines with an imidazole molecule would not be present when there is no imidazole in the condition of measuring kinetic parameters. Therefore, the R67H mutation might provide more protein flexibility for the hydrolysis of the S_p- enantiomer of compound **5**.

Conclusion

The combination of saturation mutagenesis and directed evolution of PTE was able to alter stereoselectivity and enhance the catalytic activity towards unfavorable substrates. The wild-type PTE preferentially hydrolyze the R_p-enantiomers of organophosphate nerve agents and analogues relative to the S_p- enantiomers. The H254G/H257W/L303T (GWT) mutant from the first generation was shown to have reversed stereoselectivity and enhanced the catalytic activity towards the more toxic S_p-enantiomers of soman (GD) and cyclosarin (GF) analogues. The structural modification of the GWT mutant on the substrate binding pocket, surface and dimmer interface might facilitate the binding and the entrance of the S_p-enantiomers of soman and cyclosarin analogues to the active site. The second generation of mutants, the GWT-d3 and theGWT-f5, was discovered as the best mutants to catalyze hydrolysis of the S_p-enantiomers of soman and cyclosarin analogues, respectively. The k_{cat}/K_m values of the GWT-d3 mutant towards the S_pR_c and S_pS_c – enantiomers of soman analogue are 780- and 3530-fold higher than the wild-type enzyme. The k_{cat}/K_m value of the GWT-f5

mutant towards the S_p-enantiomer of cyclosarin analogue is 15500-fold higher than the wild-type enzyme.

CHAPTER V

SUMMARY AND CONCLUSIONS

Phosphotriesterase (PTE) is an enzyme isolated from soil bacteria, *Pseudomonas diminuta* MG and *Flavobcterrium sp.* strains. This enzyme is known for the ability to catalyze the detoxification of organophosphate pesticides and chemical warfare agents. The catalytic ability of PTE for the hydrolysis of paraoxon is close to the limit of diffusion of the reactant in solution. The k_{cat} and k_{cat}/K_m values are ~10^4 s^{-1} and 10^8 $M^{-1}s^{-1}$ respectively. The substrate specificity of PTE is fairly broad. It is capable of hydrolyzing organophosphorus nerve agents including tabun (GA), sarin (GB), soman (GD), cyclosarin (GF), rVX, and VX. However, the catalytic activity of PTE for the organophosphate nerve agents is lower than paraoxon. It was reported that the wild-type PTE is more efficient in catalyzing the hydrolysis of the less toxic R_p- enantiomers of organophosphate nerve agents and their analogues (GB and GD analogues) than the more toxic S_p- enantiomers (*45*). The real nerve agents are not allowed to be handled in the regular laboratories, thus the GB, GD, GF, rVX and VX analogues with *para*-acetyl phenol as the leaving group were utilized to study the kinetic properties of the wild-type and mutants of PTE.

The modification of the physical size and configuration of the binding pockets could alter the substrate stereoselectivity of PTE and increase the catalytic efficiency to hydrolyze the more toxic S_p- enantiomers of the nerve agents. The H254Q/H257F (QF) mutant of PTE modifies the configuration of the large pocket. The substrate binding

affinity of this mutant towards the S_p- enantiomers of VX, GB and rVX analogues are relatively high, with K_m values that are lower than 10 μM. The k_{cat}/K_m values for the S_p-enantiomers of VX, GB and rVX analogues are more than 10^6 $M^{-1}s^{-1}$. The H254G/H257W/L303T (GWT) mutant has an expanded small pocket and an enlarged large pocket in the substrate binding site. It is shown to have a reversed stereoselectivity for the hydrolysis of the organophosphorous nerve agent analogues. The more toxic S_p-enantiomers of organophosphonates are preferred to be hydrolyzed by this mutant. The hydrolysis of the S_pR_c- and S_pS_c-enantiomers of the GD analogues by this mutant are enhanced by 73- and 543- fold, respectively, relative to the wild-type enzyme, with k_{cat}/K_m values of 10^3 $M^{-1}s^{-1}$. The k_{cat}/K_m value of this mutant is around 10^4 $M^{-1}s^{-1}$ for the hydrolysis of the S_p-enantiomer of the GF analogues, which is 1340-fold higher than the wild-type enzyme. Therefore, mutations in the active site using the H254G/H257W/L303T (GWT) mutant as the template allow further enhancement in activity for the hydrolysis of the nerve agents and their analogues.

The mutations at the surface of PTE were introduced to several beneficial mutants. The A80V, K185R and I274N mutations were shown be important for the increase in protein expression levels, protein solubility and catalytic activity against some of the substrates. The QFRN mutant has the additional K185R and I274N mutations compared to the H254Q/H257F (QF) mutant. The k_{cat}/K_m values of the QFRN mutant towards the R_p- and S_p- enantiomers of VX and GB analogues are further enhanced. The GWT-d2 mutant has the A80V, K185R and I274N mutations that have been added to the H254G/H257W/L303T (GWT) mutant. The k_{cat}/K_m values of the

GWT-d2 mutant towards the S_pR_c- and the S_pS_c - enantiomers of the GD analogues have been further enhanced by 540- and 2570-fold relative to the wild-type enzyme, respectively.

The single and double substitution libraries of PTE, M317X and C59X/S61X, were created using QuikChange site-directed mutagenesis. The primers of QuikChange mutagenesis contain the degenerate codon, NNS, at the target positions, which was used to eliminate two stop codons, TGA and TAA (N = A, T, G, C; S= C, G). The QuikChange PCR products were transformed into *E. coli* BL-21 competent cells and inoculated into 96 deep-well culture blocks. The *in vitro* screening technique was conducted to make all possible PTE variants in the culture blocks. These variants were then screened for activity with paraoxon, and the S_p-enantiomers of the GD and GF analogues. The libraries were constructed using the sequences of the GWT-d1 and the GWT-d2 mutants as templates, which have been shown to have higher protein expression levels than the H254G/H257W/L303T (GWT) mutant. The PTE mutants that show promising activities were selected to identify their sequences. The GWT-f2 mutant was identified and isolated. The k_{cat}/K_m value of this mutant towards the hydrolysis of the S_p-enantiomer of the GF analogues is 3720-fold higher than the wild-type enzyme. In addition, the GWT-d3 mutant was identified as the best mutant towards the hydrolysis of the S_p-enantiomers of the GD analogues. The k_{cat}/K_m values for the GWT-d3 mutant with the S_pR_c- and S_pS_c-enantiomers of the GD analogues were 780- and 3530-fold higher than the wild-type enzyme, respectively.

The randomization of multiple amino acid residues in the substrate binding pockets of PTE or the incorporation of random mutations to the gene of PTE by error-prone PCR can create much larger libraries. The *in vivo* selection methodology was utilized to isolate active mutants for the library size larger than 10^3 variants, which helped to reduce time and substrate consumption. The modified PTE gene that encodes the enzyme with improved activity against the S_p-enantiomer of the GF analogue and the gene of glycerophosphodiester phosphodiesterase (GpdQ) were ligated into pET-Duet plasmid and transformed into *E. coli* (BL21) cells. The cells were grown on phosphate free minimal media plates containing the S_p-enantiomer of the GF analogues as the sole phosphorus source and the growth rates of the cells were observed. By *in vivo* selection, the GWT-f3 mutant was isolated and shown to have 5580-fold higher in activity towards the S_p-enantiomer of the GF analogues than the wild-type enzyme. The GWT-f4 mutant contains an additional A80V mutation compared to the GWT-f3 enzyme. The k_{cat}/K_m value towards the hydrolysis of the S_p-enantiomer of the GF analogue for this mutant was increased to 1.2×10^4-fold higher than the wild-type enzyme. Interestingly, the GWT-f4 mutant was determined as the most active enzyme towards the S_p-enantiomer of the rVX analogues. The random mutagenesis library was subjected to the second round of *in vivo* selection, and the GWT-f5 mutant was discovered. The k_{cat}/K_m value of the GWT-f5 towards the S_p-enantiomer of the GF analogues is 1.55×10^4-fold higher than the wild-type enzyme.

The X-ray crystal structures of the wild-type PTE and the G60A mutant were determined in the presence of the hydrolysis product diethyl phosphate and a product

analogue cacodylate, respectively. In the structure of the wild-type PTE-diethyl phosphate complex, the diethyl phosphate is symmetrically bridging between the two divalent metal cations. Cacodylate is bound between two divalent metals in the G60A mutant structure. The distance of the two metal ions in the liganded structures is approximately 4 Å compared with 3.4 Å in the unliganded complex. This result supports the reaction mechanism proposed by Aubert *et. al* that the organophosphate substrate binds to the binuclear active site and displace a water molecule that is coordinating to the β-metal ion. The interaction of the substrate with the β- metal ion weakens the coordination of the bridging hydroxide ion to the β- metal. This activates the hydroxide ion to attack the phosphorus center of the substrate. The collapse of the intermediate and the breakage of the P-O bond result in diethyl phosphate being bridged between the two divalent cations within the active site. The binuclear metal center and the active site hydroxide are regenerated after the diethyl phosphate disassociated from the active site.

REFERENCES

1. Holm, L., and Sander, C. (1997) An evolutionary treasure: unification of a broad set of amidohydrolases related to urease, *Proteins 28*, 72-82.
2. Mulbry, W. W., Karns, J. S., Kearney, P. C., Nelson, J. O., Mcdaniel, C. S., and Wild, J. R. (1986) Identification of a plasmid-borne parathion hydrolase gene from *Flavobacterium* sp. by southern hybridization with Opd from *Pseudomonas diminuta*, *Applied and Environmental Microbiology 51*, 926-930.
3. Omburo, G. A., Mullins, L. S., and Raushel, F. M. (1993) Structural characterization of the divalent-cation sites of bacterial phosphotriesterase by Cd-113 NMR-spectroscopy, *Biochemistry 32*, 9148-9155.
4. Ghanem, E., and Raushel, F. M. (2005) Detoxification of organophosphate nerve agents by bacterial phosphotriesterase, *Toxicol Appl Pharmacol 207*, 459-470.
5. Aspelin A., G. A. (1999) Pesticides industry sales and usage: 1996 and 1997 market estimates., U.S. EPA.Office of Pesticide Prog. Biological and Economic Analysis Div. Washington, D.C.733-R-799-001.
6. Johannes, T. W., and Zhao, H. M. (2006) Directed evolution of enzymes and biosynthetic pathways, *Current Opinion in Microbiology 9*, 261-267.
7. Sambrook, J., Russell, D.W. (2001) *Molecular Cloning: A Laboratory Manual,* 3rd ed. Cold Spring Harbor Laboratory Press, Cold Spring Harbor, NY.
8. Miyazaki, K., and Takenouchi, M. (2002) Creating random mutagenesis libraries using megaprimer PCR of whole plasmid, *Biotechniques 33*, 1033-1038.

9. Stemmer, W. P. C., Crameri, A., Ha, K. D., Brennan, T. M., and Heyneker, H. L. (1995) Single-step assembly of a gene and entire plasmid from large numbers of oligodeoxyribonucleotides, *Gene 164*, 49-53.

10. LinGoerke, J. L., Robbins, D. J., and Burczak, J. D. (1997) PCR-based random mutagenesis using manganese and reduced dNTP concentration, *Biotechniques 23*, 409-412.

11. Zhao H., M. J. C., Volkov A.A., Arnold F.H. (1999) Methods for optimizing industrial enzymes by directed evolution, *Manual of Industrial Microbiology and Biotechnology*, ASM Press, Washington, D.C. 597-604.

12. Stemmer, W. P. C. (1994) DNA shuffling by random fragmentation and reassembly *in vitro* recombination for molecular evolution, *Proc. Natl. Acad. Sci. U. S. A. 91,* 10747-10751.

13. Joern, J. M., Meinhold, P., and Arnold, F. H. (2002) Analysis of shuffled gene libraries, *Journal of Molecular Biology 316*, 643-656.

14. Miller, J. H. (1998) Mutators in *Escherichia coli*, *Mutation Research DNA Repair 409*, 99-106.

15. Greener, A., Callahan, M., and Jerpseth, B. (1997) An efficient random mutagenesis technique using an *E. coli* mutator strain, *Molecular Biotechnology 7*, 189-195.

16. Mayer, K. M., and Arnold, F. H. (2002) A colorimetric assay to quantify dehydrogenase activity in crude cell lysates, *Journal of Biomolecular Screening 7*, 135-140.

17. Smith, G. P., and Petrenko, V. A. (1997) Phage display, *Chemical Reviews 97*, 391-410.

18. Gold, L. (2001) mRNA display: diversity matters during *in vitro* selection, *Proc. Natl. Acad. Sci. U. S. A. 98*, 4825-4826.

19. Heinis, C., Huber, A., Demartis, S., Bertschinger, J., Melkko, S., Lozzi, L., Neri, P., and Neri, D. (2001) Selection of catalytically active biotin ligase and trypsin mutants by phage display, *Protein Engineering 14*, 1043-1052.

20. Maxwell, K. L., Mittermaier, A. K., Forman-Kay, J. D., and Davidson, A. R. (1999) A simple *in vivo* assay for increased protein solubility, *Protein Science 8*, 1908-1911.

21. Kurz, M., Gu, K., Al-Gawari, A., and Lohse, P. A. (2001) cDNA - Protein fusions: covalent protein-gene conjugates for the *in vitro* selection of peptides and proteins, *Chembiochem 2*, 666-672.

22. Sugiyama, M., Hong, Z. Y., Greenberg, W. A., and Wong, C. H. (2007) *In vivo* selection for the directed evolution of L-rhamnulose aldolase from L-rhamnulose-1-phosphate aldolase (RhaD), *Bioorganic & Medicinal Chemistry 15*, 5905-5911.

23. Seibert, C. M., and Raushel, F. M. (2005) Structural and catalytic diversity within the amidohydrolase superfamily, *Biochemistry 44*, 6383-6391.

24. Benning, M. M., Shim, H., Raushel, F. M., and Holden, H. M. (2001) High resolution X-ray structures of different metal-substituted forms of phosphotriesterase from *Pseudomonas diminuta*, *Biochemistry 40*, 2712-2722.

25. Schwarzenbacher, R., Canaves, J. M., Brinen, L. S., Dai, X. P., Deacon, A. M., Elsliger, M. A., Eshaghi, S., Floyd, R., Godzik, A., Grittini, C., Grzechnik, S. K., Guda, C., Jaroszewski, L., Karlak, C., Klock, H. E., Koesema, E., Kovarik, J. S., Kreusch, A., Kuhn, P., Lesley, S. A., McMullan, D., McPhillips, T. M., Miller, M. A., Miller, M. D., Morse, A., Moy, K., Ouyang, J., Robb, A., Rodrigues, K., Selby, T. L., Spraggon, G., Stevens, R. C., van den Bedem, H., Velasquez, J., Vincent, J., Wang, X. H., West, B., Wolf, G., Hodgson, K. O., Wooley, J., and Wilson, I. A. (2003) Crystal structure of uronate isomerase (TM0064) from *Thermotoga maritima* at 2.85 angstrom resolution, *Proteins-Structure Function and Genetics 53*, 142-145.

26. Li, T. F., Iwaki, H., Fu, R., Hasegawa, Y., Zhang, H., and Liu, A. M. (2006) alpha-amino-beta-carboxymuconic-epsilon-semialdehyde decarboxylase (ACMSD) is a new member of the amidohydrolase superfamily, *Biochemistry 45*, 6628-6634.

27. Cho, C. M. H., Mulchandani, A., and Chen, W. (2004) Altering the substrate specificity of organophosphorus hydrolase for enhanced hydrolysis of chlorpyrifos, *Applied and Environmental Microbiology 70*, 4681-4685.

28. Cho, C. M. H., Mulchandani, A., and Chen, W. (2006) Functional analysis of organophosphorus hydrolase variants with high degradation activity towards organophosphate pesticides, *Protein Engineering Design & Selection 19*, 99-105.

29. Reeves, T. E., Wales, M. E., Grimsley, J. K., Li, P., Cerasoli, D. M., and Wild, J. R. (2008) Balancing the stability and the catalytic specificities of OP hydrolases

with enhanced V-agent activities, *Protein Engineering Design & Selection 21*, 405-412.

30. diSioudi, B., Grimsley, J. K., Lai, K. H., and Wild, J. R. (1999) Modification of near active site residues in organophosphorus hydrolase reduces metal stoichiometry and alters substrate specificity, *Biochemistry 38*, 2866-2872.

31. McLoughlin, S. Y., Jackson, C., Liu, J. W., and Ollis, D. (2005) Increased expression of a bacterial phosphotriesterase in *Escherichia coli* through directed evolution, *Protein Expression and Purification 41*, 433-440.

32. Yang, H., Carr, P. D., McLoughlin, S. Y., Liu, J. W., Horne, I., Qiu, X., Jeffries, C. M. J., Russell, R. J., Oakeshott, J. G., and Ollis, D. L. (2003) Evolution of an organophosphate-degrading enzyme: a comparison of natural and directed evolution, *Protein Engineering 16*, 135-145.

33. Roodveldt, C., and Tawfik, D. S. (2005) Directed evolution of phosphotriesterase from *Pseudomonas diminuta* for heterologous expression in *Escherichia coli* results in stabilization of the metal-free state, *Protein Engineering Design & Selection 18*, 51-58.

34. Griffiths, A. D., and Tawfik, D. S. (2003) Directed evolution of an extremely fast phosphotriesterase by *in vitro* compartmentalization, *EMBO Journal 22*, 24-35.

35. May, O., Nguyen, P. T., and Arnold, F. H. (2000) Inverting enantioselectivity by directed evolution of hydantoinase for improved production of L-methionine, *Nature Biotechnology 18*, 317-320.

36. Omburo, G. A., Kuo, J. M., Mullins, L. S., and Raushel, F. M. (1992) Characterization of the zinc-binding site of bacterial phosphotriesterase, *Journal of Biological Chemistry 267*, 13278-13283.

37. Vanhooke, J. L., Benning, M. M., Raushel, F. M., and Holden, H. M. (1996) Three-dimensional structure of the zinc-containing phosphotriesterase with the bound substrate analog diethyl 4-methylbenzylphosphonate, *Biochemistry 35*, 6020-6025.

38. Benning, M. M., Kuo, J. M., Raushel, F. M., and Holden, H. M. (1994) Three-dimensional structure of phosphotriesterase: an enzyme capable of detoxifying organophosphate nerve agents, *Biochemistry 33*, 15001-15007.

39. Aubert, S. D., Li, Y. C., and Raushel, F. M. (2004) Mechanism for the hydrolysis of organophosphates by the bacterial phosphotriesterase, *Biochemistry 43*, 5707-5715.

40. Samples, C. R., Raushel, F. M., and DeRose, V. J. (2007) Activation of the binuclear metal center through formation of phosphotriesterase-inhibitor complexes, *Biochemistry 46*, 3435-3442.

41. Wong, K. Y., and Gao, J. (2007) The reaction mechanism of paraoxon hydrolysis by phosphotriesterase from combined QM/MM simulations, *Biochemistry 46*, 13352-13369.

42. Jackson, C. J., Foo, J. L., Kim, H. K., Carr, P. D., Liu, J. W., Salem, G., and Ollis, D. L. (2008) In crystallo capture of a Michaelis complex and product-

binding modes of a bacterial phosphotriesterase, *Journal of Molecular Biology 375*, 1189-1196.

43. Hong, S. B., and Raushel, F. M. (1996) Metal-substrate interactions facilitate the catalytic activity of the bacterial phosphotriesterase, *Biochemistry 35*, 10904-10912.

44. Chen-Goodspeed, M., Sogorb, M. A., Wu, F. Y., Hong, S. B., and Raushel, F. M. (2001) Structural determinants of the substrate and stereochemical specificity of phosphotriesterase, *Biochemistry 40*, 1325-1331.

45. Li, W. S., Lum, K. T., Chen-Goodspeed, M., Sogorb, M. A., and Raushel, F. M. (2001) Stereoselective detoxification of chiral sarin and soman analogues by phosphotriesterase, *Bioorganic & Medicinal Chemistry 9*, 2083-2091.

46. Borak, J., and Sidell, F. R. (1992) Agents of chemical warfare: sulfur mustard, *Annals of Emergency Medicine 21*, 303-308.

47. Millard, C. B., Kryger, G., Ordentlich, A., Greenblatt, H. M., Harel, M., Raves, M. L., Segall, Y., Barak, D., Shafferman, A., Silman, I., and Sussman, J. L. (1999) Crystal structures of aged phosphonylated acetylcholinesterase: nerve agent reaction products at the atomic level, *Biochemistry 38*, 7032-7039.

48. Benschop, H. P., and Dejong, L. P. A. (1988) Nerve agent stereoisomers - analysis, isolation, and toxicology, *Accounts of Chemical Research 21*, 368-374.

49. Hartleib, J., Geschwindner, S., Scharff, E. I., and Ruterjans, H. (2001) Role of calcium ions in the structure and function of the di-isopropylfluorophosphatase from *Loligo vulgaris*, *Biochemical Journal 353*, 579-589.

50. Hartleib, J., and Ruterjans, H. (2001) High-yield expression, purification, and characterization of the recombinant diisopropylfluorophosphatase from *Loligo vulgaris*, *Protein Expression and Purification 21*, 210-219.

51. Wang, F., Xiao, M. Z., and Mu, S. F. (1993) Purification and properties of a diisopropyl-fluorophosphatase from squid *Todarodes pacificus steenstrup*, *Journal of Biochemical Toxicology 8*, 161-166.

52. Yeung, D. T., Josse, D., Nicholson, J. D., Khanal, A., McAndrew, C. W., Bahnson, B. J., Lenz, D. E., and Cerasoli, D. M. (2004) Structure/function analyses of human serum paraoxonase (HuPON1) mutants designed from a DFPase-like homology model, *Biochimica et Biophysica Acta-Proteins and Proteomics 1702*, 67-77.

53. Hill, C. M., Li, W. S., Cheng, T. C., DeFrank, J. J., and Raushel, F. M. (2001) Stereochemical specificity of organophosphorus acid anhydrolase toward p-nitrophenyl analogs of soman and sarin, *Bioorganic Chemistry 29*, 27-35.

54. DeFrank J.J., W. W. E. (2002) Phosphofluoridates: biological activity and biodegradation, *The Handbook of Environmental Chemistry*, Part N. Organofluorines Vol. 3, Springer-Verlag, Berlin and Heidelberg, Germany (2002) pp. 295–343

55. Yeung D.T., L. D. E., Cerasoli D.M. (2008) Human paraoxonase 1: a potential bioscavenger of organophosphorus nerve agents. In: Mackness B., Mackness M., Aviram M. and Paragh G., Editors, *The Paraoxonases: their role in disease*

development and xenobiotic metabolism, Springer, pp. 151–170, Springer, Netherlands

56. Masson P., J. D., Lockridge O., Viguié N., Taupin C., Buhler C. (1998) Enzymes hydrolyzing organophosphates as potential catalytic scavengers against organophosphate poisoning, *J. Physiol. (Paris) 92*, 357-362.

57. Cheng, T. C., DeFrank, J. J., and Rastogi, V. K. (1999) Alteromonas prolidase for organophosphorus G-agent decontamination, *Chemico-Biological Interactions 120*, 455-462.

58. Dumas, D. P., Durst, H. D., Landis, W. G., Raushel, F. M., and Wild, J. R. (1990) Inactivation of organophosphorus nerve agents by the phosphotriesterase from *Pseudomonas diminuta*, *Archives of Biochemistry and Biophysics 277*, 155-159.

59. Ghanem, E. (2006) Ph.D. dissertation, Texas A&M University, Directed evolution of phosphotriesterase for detoxification of the nerve agent VX.

60. Donarski, W. J., Dumas, D. P., Heitmeyer, D. P., Lewis, V. E., and Raushel, F. M. (1989) Structure-activity relationships in the hydrolysis of substrates by the phosphotriesterase from *Pseudomonas diminuta*, *Biochemistry 28*, 4650-4655.

61. Dumas, D. P., Caldwell, S. R., Wild, J. R., and Raushel, F. M. (1989) Purification and properties of the phosphotriesterase from *Pseudomonas diminuta*, *J. Biol. Chem. 264*, 19659-19665.

62. Caldwell, S. R., Newcomb, J. R., Schlecht, K. A., and Raushel, F. M. (1991) Limits of diffusion in the hydrolysis of substrates by the phosphotriesterase from *Pseudomonas diminuta*, *Biochemistry 30*, 7438-7444.

63. Raushel, F. M., and Holden, H. M. (2000) Phosphotriesterase: an enzyme in search of its natural substrate, *Adv. Enzymol. Relat. Areas. Mol. Biol. 74*, 51-93.

64. Omburo, G. A., Kuo, J. M., Mullins, L. S., and Raushel, F. M. (1992) Characterization of the zinc binding site of bacterial phosphotriesterase, *Journal of Biological Chemistry 267*, 13278-13283.

65. Omburo, G., Kuo, J., and Raushel, F. M. (1992) Metalloenzyme derivatives of the bacterial phosphotriesterase, *FASEB Journal 6*, A461-A461.

66. Chen, S. L., Fang, W. H., and Himo, F. (2007) Theoretical study of the phosphotriesterase reaction mechanism, *Journal of Physical Chemistry B 111*, 1253-1255.

67. Jackson, C., Kim, H. K., Carr, P. D., Liu, J. W., and Ollis, D. L. (2005) The structure of an enzyme-product complex reveals the critical role of a terminal hydroxide nucleophile in the bacterial phosphotriesterase mechanism, *Biochimica Et Biophysica Acta-Proteins and Proteomics 1752*, 56-64.

68. Kuiper, J. M., Hulst, R., and Engberts, J. B. F. N. (2003) A selective and mild synthetic route to dialkyl phosphates, *Synthesis-Stuttgart, 34*, 695-698.

69. Otwinowski, Z., and Minor, W. (1997) Macromolecular crystallography, In: A. Carter, C. W., Jr., and Sweet, R. M., Editors, In *Methods in Enzymology*, pp 307-326, Academic Press, New York.

70. Vagin, A., and Teplyakov, A. (1997) MOLREP: an automated program for molecular replacement, *J. Appl. Crystallogr. 30*, 1022-1025.

71. Lamzin, V. S., Wilson, K. S., and Perrakis, A. (2001) Crystallography of biological macromolecules, Rossmann, M. G., and Arnold, E., Editors, *International Tables for Crystallography*, pp 720-722 Kluwer Academic Publishers, Dordrecht, Netherlands.

72. Emsley, P., and Cowtan, K. (2004) Coot: model-building tools for molecular graphics, *Acta Crystallogr D Biol Crystallogr 60*, 2126-2132.

73. Murshudov, G. N., Vagin, A. A., and Dodson, E. J. (1997) Refinement of macromolecular structures by the maximum-likelihood method, *Acta Crystallogr D Biol Crystallogr 53*, 240-255.

74. Becke, A. D. (1993) A new mixing of Hartree-Fock and local density-functional theories, *Journal of Chemical Physics 98*, 1372-1377.

75. Becke, A. D. (1997) Density-functional thermochemistry .5. Systematic optimization of exchange-correlation functionals, *Journal of Chemical Physics 107*, 8554-8560.

76. Lee, C. T., Yang, W. T., and Parr, R. G. (1988) Development of the Colle-Salvetti correlation-energy formula into a functional of the electron-density, *Physical Review B 37*, 785-789.

77. Barone, V., and Cossi, M. (1998) Quantum calculation of molecular energies and energy gradients in solution by a conductor solvent model, *Journal of Physical Chemistry A 102*, 1995-2001.

78. Cammi, R., Mennucci, B., and Tomasi, J. (1999) Second-order Møller-Plesset analytical derivatives for the polarizable continuum model using the relaxed density approach, *Journal of Physical Chemistry A 103*, 9100-9108.

79. Klamt, A., and Schuurmann, G. (1993) COSMO - a new approach to dielectric screening in solvents with explicit expressions for the screening energy and its gradient, *Journal of the Chemical Society-Perkin Transactions 2*, 799-805.

80. Tomasi, J., Mennucci, B., and Cammi, R. (2005) Quantum mechanical continuum solvation models, *Chemical Reviews 105*, 2999-3093.

81. Frisch, M. J., Trucks, G. W., Schlegel, H. B., Scuseria G. E., *et al.* (2004) *Gaussian 03, revision D.01*, Gaussian, Inc., Wallingford, CT.

82. Hong, S. B., and Raushel, F. M. (1999) Stereochemical constraints on the substrate specificity of phosphotriesterase, *Biochemistry 38*, 1159-1165.

83. Wu, F. Y., Li, W. S., Chen-Goodspeed, M., Sogorb, M. A., and Raushel, F. M. (2000) Rationally engineered mutants of phosphotriesterase for preparative scale isolation of chiral organophosphates, *Journal of the American Chemical Society 122*, 10206-10207.

84. Li, Y. C., Aubert, S. D., Maes, E. G., and Raushel, F. M. (2004) Enzymatic resolution of chiral phosphinate esters, *Journal of the American Chemical Society 126*, 8888-8889.

85. Marti-Arbona, R., Fresquet, V., Thoden, J. B., Davis, M. L., Holden, H. M., and Raushel, F. M. (2005) Mechanism of the reaction catalyzed by isoaspartyl dipeptidase from Escherichia coli, *Biochemistry 44*, 7115-7124.

86. Thoden, J. B., Marti-Arbona, R., Raushel, F. M., and Holden, H. M. (2003) High-resolution X-ray structure of isoaspartyl dipeptidase from *Escherichia coli*, *Biochemistry 42*, 4874-4882.

87. Liaw, S. H., Chen, S. J., Ko, T. P., Hsu, C. S., Chen, C. J., Wang, A. H. J., and Tsai, Y. C. (2003) Crystal structure of D-aminoacylase from *Alcaligenes faecalis* DA1 - A novel subset of amidohydrolases and insights into the enzyme mechanism, *Journal of Biological Chemistry 278*, 4957-4962.

88. Lai, W. L., Chou, L. Y., Ting, C. Y., Kirby, R., Tsai, Y. C., Wang, A. H. J., and Liaw, S. H. (2004) The functional role of the binuclear metal center in D-aminoacylase: one-metal activation and second-metal attenuation, *Journal of Biological Chemistry 279*, 13962-13967.

89. Thoden, J. B., Phillips, G. N., Neal, T. M., Raushel, F. M., and Holden, H. M. (2001) Molecular structure of dihydroorotase: a paradigm for catalysis through the use of a binuclear metal center, *Biochemistry 40*, 6989-6997.

90. Zheng, F., Zhan, C. G., and Ornstein, R. L. (2002) Theoretical determination of two structural forms of the active site in cadmium-containing phosphotriesterases, *Journal of Physical Chemistry B 106*, 717-722.

91. Ecobichon, D. J. (2001) *Casarett and Doull's Toxicology: The Basic Science of Poisons,* 6th ed. McGraw-Hill, New York, pp. 763- 810.

92. Worek, F., Szinicz, L., Eyer, P., and Thiermann, H. (2005) Evaluation of oxime efficacy in nerve agent poisoning: development of a kinetic-based dynamic model, *Toxicology and Applied Pharmacology 209*, 193-202.

93. Harper, L. L., Mcdaniel, C. S., Miller, C. E., and Wild, J. R. (1988) Dissimilar plasmids isolated from *Pseudomonas diminuta* Mg and a *Flavobacterium* sp. (Atcc-27551) contain identical Opd genes, *Applied and Environmental Microbiology 54*, 2586-2589.

94. Kolakowski, J. E., DeFrank, J. J., Harvey, S. P., Szafraniec, L. L., Beaudry, W. T., Lai, K. H., and Wild, J. R. (1997) Enzymatic hydrolysis of the chemical warfare agent VX and its neurotoxic analogues by organophosphorus hydrolase, *Biocatalysis and Biotransformation 15*, 297-312.

95. Chen-Goodspeed, M., Sogorb, M. A., Wu, F. Y., and Raushel, F. M. (2001) Enhancement, relaxation, and reversal of the stereoselectivity for phosphotriesterase by rational evolution of active site residues, *Biochemistry 40*, 1332-1339.

96. Nowlan, C., Li, Y. C., Hermann, J. C., Evans, T., Carpenter, J., Ghanem, E., Shoichet, B. K., and Raushel, F. M. (2006) Resolution of chiral phosphate, phosphonate, and phosphinate esters by an enantioselective enzyme library, *Journal of the American Chemical Society 128*, 15892-15902.

97. Hill, C. M., Li, W. S., Thoden, J. B., Holden, H. M., and Raushel, F. M. (2003) Enhanced degradation of chemical warfare agents through molecular engineering of the phosphotriesterase active site, *Journal of the American Chemical Society 125*, 8990-8991.

98. Lum, K. T. (2004) Ph.D. dissertation, Texas A&M University, Directed evolution of phosphotriesterase: towards the efficient detoxification of sarin and soman.

99. May, O., Nguyen, P. T., and Arnold, F. H. (2000) Inverting enantioselectivity by directed evolution of hydantoinase for improved production of L-methionine, *Nat Biotechnol 18*, 317-320.

100. Hsu, C. C., Hong, Z., Wada, M., Franke, D., and Wong, C. H. (2005) Directed evolution of D-sialic acid aldolase to L-3-deoxy-manno-2-octulosonic acid (L-KDO) aldolase, *Proc. Natl. Acad. Sci. U. S. A. 102*, 9122-9126.

101. Cho, C. M., Mulchandani, A., and Chen, W. (2002) Bacterial cell surface display of organophosphorus hydrolase for selective screening of improved hydrolysis of organophosphate nerve agents, *Applied Environmental Microbiology 68*, 2026-2030.

102. Ghanem, E., Li, Y. C., Xu, C. F., and Raushel, F. M. (2007) Characterization of a phosphodiesterase capable of hydrolyzing EA 2192, the most toxic degradation product of the nerve agent VX, *Biochemistry 46*, 9032-9040.

103. Wanner, B. L. (1994) Molecular genetics of carbon-phosphorus bond cleavage in bacteria, *Biodegradation 5*, 175-184.

104. Kononova, S. V., and Nesmeyanova, M. A. (2002) Phosphonates and their degradation by microorganisms, *Biochemistry (Mosc) 67*, 184-195.

VITA

Name: Ping-Chuan Tsai

Address: Department of Chemistry
Texas A&M University
PO Box 30012
College Station, TX 77842-3012

Email Address: pctsai@mail.chem.tamu.edu

Education: Ph.D. Chemistry
December 2009
Texas A&M University
College Station, Texas

B.S. Chemistry
May 2003
National Tsing-Hua University
Hsinchu, Taiwan